



Fossil chemical-physical (dis)equilibria between paleofluids and host rocks and their relationship to the seismic cycle and earthquakes

M. Curzi^{a,*}, L. Aldega^a, A. Billi^b, C. Boschi^c, E. Carminati^a, G. Vignaroli^d, G. Viola^d, S. M. Bernasconi^e

^a Dipartimento di Scienze della Terra, Sapienza Università di Roma, P.le Aldo Moro 5, 00185 Roma, Italy

^b Consiglio Nazionale delle Ricerche, IGAG, Rome, Italy

^c Istituto di Geoscienze e Georisorse, Consiglio Nazionale delle Ricerche, Via Moruzzi 1, Pisa 56124, Italy

^d Dipartimento di Scienze Biologiche, Geologiche ed Ambientali – BiGeA, Università degli studi di Bologna, Via Zamboni 67, Bologna 40126, Italy

^e Geological Institute, ETH Zürich, Sonneggstrasse 5, 8092 Zürich, Switzerland

ARTICLE INFO

Keywords:

Fluid-rock interaction
Seismic cycles
Paleofluid
Chemical-physical (dis)equilibrium
Earthquake
Mineralizations
Faulting

ABSTRACT

Understanding the behavior of fluids in seismically active faults and their chemical-physical (dis)equilibrium with the host rock is important to understand the role of fluids upon seismicity and their possible potential for forecasting earthquakes. The small number of case studies where seismic and geochemical data are available and the lack of accessibility to fault zones at seismogenic depth for recent earthquakes limit our understanding of fluid circulation and its relationship to seismicity. The study of fault-fluid relationships in exhumed faults can broaden the number of case histories and improve our understanding of the role of fluids in the seismic cycle in different tectonic settings. Here we use new geochemical and thermal data and a review of published studies from the Apennines fold-and-thrust belt (Italy) to provide a model of fluid circulation during the seismic cycle related to either the local orogenic compressional or post-orogenic extensional tectonics. We also suggest a workflow based upon different methods to identify tectonic-related chemical-physical (isotopic and thermal) (dis)equilibria in fluid-rock systems during the seismic cycle. The proposed workflow involves multiscale structural and isotope geochemical analyses, radiometric dating, and burial-thermal modeling. It is applied to carbonate-hosted faults exhumed from a depth shallower than 4 km (temperature $\leq \sim 130$ °C and pressure $\leq \sim 130$ MPa). We show that in the Apennines, during syn-orogenic shortening, thrusting is mostly assisted by fluid circulation in an effectively closed system where fluid and host rock remain close to chemical and thermal equilibrium. In contrast, post-orogenic normal faulting occurs in association with upward and/or downward open fluid circulation systems leading to chemical-physical disequilibria between the host rock and the circulating fluids. Isotopic and thermal fluid-rock disequilibria are particularly evident during pre- and co-seismic extensional deformation. Mineralizing fluids, whose temperature can vary between 30 °C warmer and 16 °C colder than the host rock, result from the mixing of fluids derived from both the deforming host rock and external sources (meteoric or deep crustal). The proposed workflow offers the potential to track past seismic cycles and provide indications on actual fluid-earthquake relationships including the identification of potential seismic precursors and modes of triggered seismicity that might be different in extensional and compressional tectonic settings.

1. Introduction

Earthquakes can mobilize and transfer mineralizing fluids from deep to shallow structural levels during high strain-rate and short-lived deformation episodes. Ascending fluids may be in chemical-physical (dis)equilibrium with the surrounding rock and transport exotic

chemical elements (e.g., Skelton et al., 2019; Barbieri et al., 2021; Zhao et al., 2021; Boschetti et al., 2022; Caracausi et al., 2022). Such (dis) equilibria in chemistry, temperature, and pressure between fluids and host rocks have been recently investigated and used as possible earthquake precursors (e.g., Skelton et al., 2014; Barberio et al., 2017; Chiarabba et al., 2022). Fluid ingress and circulation during fault

* Corresponding author:

E-mail address: manuel.curzi@uniroma1.it (M. Curzi).

<https://doi.org/10.1016/j.earscirev.2024.104801>

Received 9 August 2023; Received in revised form 27 April 2024; Accepted 2 May 2024

Available online 8 May 2024

0012-8252/© 2024 Published by Elsevier B.V.

activity is documented by the presence of tectonic mineralizations, such as cements, veins, and slickenfibers (Sibson, 1981, 2000; Roure et al., 2005), which precipitate during different phases of the seismic cycle (e.g., Müller, 2003; Micklethwaite and Cox, 2004; Cox, 2010; Uysal et al., 2011; Smeraglia et al., 2016; Ünal-Imer et al., 2016; Coppola et al., 2021). These tectonic mineralizations can be used to determine the origin of the fluids circulating within fault zones and the deforming crust and, thus, to constrain fluid-rock interaction during seismic cycles (e.g., Barker and Cox, 2011; Nuriel et al., 2011; Beaudoin et al., 2014, 2022; Lacroix et al., 2014; Sturrock et al., 2017; Hoareau et al., 2021; Wang et al., 2022). Some studies on tectonic mineralizations in northern Iceland (Andrén et al., 2016) and the central Apennines (Coppola et al., 2021) recently contributed to validate a set of hydrogeochemical anomalies detected in groundwaters (Skelton et al., 2014; Barberio et al., 2017) and recognized them as usable as potential seismic precursors shortly before $M_w > 5.5$ earthquakes.

The identification of chemical-physical (dis)equilibrium between a fluid and its host rock is the focus concept of this paper and is of paramount importance to constrain the fluid evolution in time and space. In particular, it allows us to identify the modes of fluid ingress and flow within active fault zones, and fossil seismic cycles and earthquakes (Uysal et al., 2007, 2011; Menzies et al., 2014; Ring et al., 2016; Lacroix et al., 2018a, 2018b; Cerchiari et al., 2020; Wang et al., 2022; Washburn et al., 2023).

The seismically active Central Apennines fold-and-thrust belt is an ideal study area to investigate the physical-chemical properties of fluid-rock systems during syn-orogenic compression and post-orogenic extension. Moreover, the obtained models can be compared and validated with the observed seismic events and their related fluid movements and may thus be used to define and refine methods of earthquake forecasting (e.g., Miller et al., 2004; Barberio et al., 2017, 2021). As in the case of many orogenic belts, the Central Apennines have undergone orogenic shortening followed by extension (e.g., Mareschal, 1994; Wang et al., 2012; Asti et al., 2022). Shortening is active in the external portion

of the belt. Post-orogenic extension is still active in the axial sector of the belt, as testified by several instrumental and historical $M_w \leq 7$ earthquakes.

The aim of this paper is to provide a model of fluid circulation during compressive and extensional seismic cycles, and to derive a workflow for identifying tectonic- and seismic cycle-related chemical-physical (dis)equilibria in fluid-rock systems. We limit our review mostly, but not exclusively, to carbonate-hosted fault zones, which were exhumed from depths shallower than ~ 4 km corresponding to temperatures cooler than ~ 130 °C and pressures lower than ~ 130 MPa. In addition, we consider studies from other fold-and-thrust belts to develop an integrated method for the identification of fossil fluid (dis)equilibria.

Our results may find further applications in seismology to better understand fluid-related pre-seismic V_p/V_s anomalies (the ratio of P to S wave velocities; e.g., Lucente et al., 2010; Chiarabba et al., 2020) or earthquakes connected with fluid injections and hydrofracturing (e.g., Hajati et al., 2015; Shapiro, 2015; Zhu et al., 2021). Further applications are foreseen in hydrogeochemistry, to better understand pre-seismic chemical-physical anomalies of groundwater (e.g., Barbieri et al., 2021; Gori and Barberio, 2022), in experimental seismology to design laboratory and numerical experiments of fluid-assisted seismic cycles (e.g., Cappa et al., 2019; Snell et al., 2020), and in ore geology to better understand the relationships between ore deposits and fault activity (e.g., Cox, 2005, 2020).

2. Background: identification of indicators of fossil seismic cycles in the rock record

2.1. Rationale

A seismic cycle encompasses the following four stages of cyclical stress accumulation and release which steer the overall seismic style of a fault zone (Fig. 1): (i) inter-seismic phase, lasting tens or thousands of years or more, consisting of a tectonically quiescent period of stress

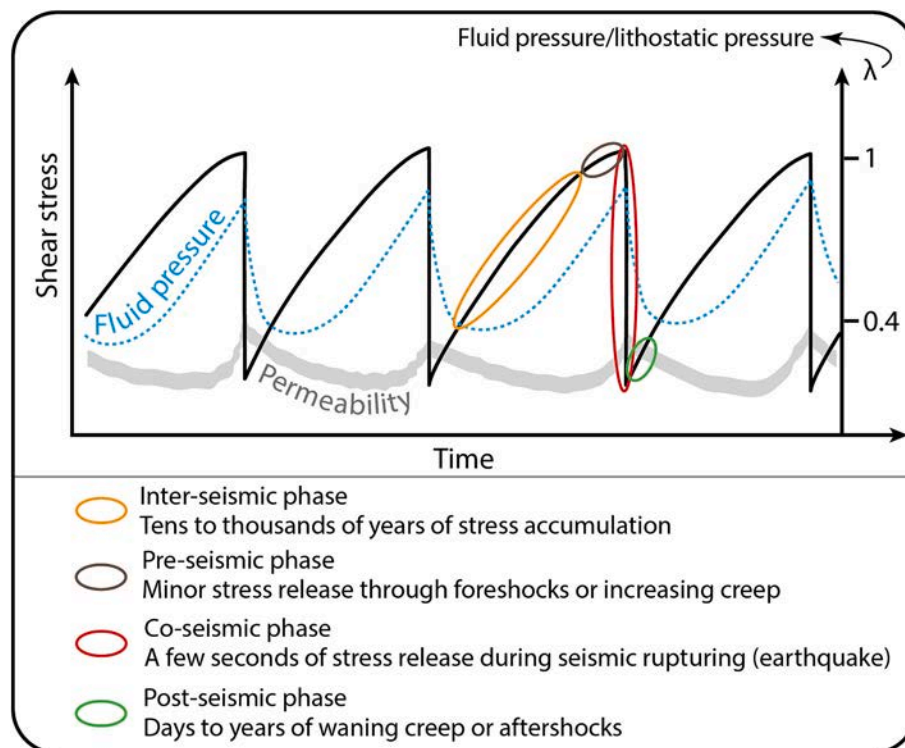


Fig. 1. Conceptual representation of seismic cycles showing the variation of shear stress and the ratio between fluid pressure and lithostatic pressure along a fault plane, the first order behavior of fluid pressure, and the bulk structural permeability of a fault zone (from Curzi et al., 2023). Each phase of the seismic cycle is also shown.

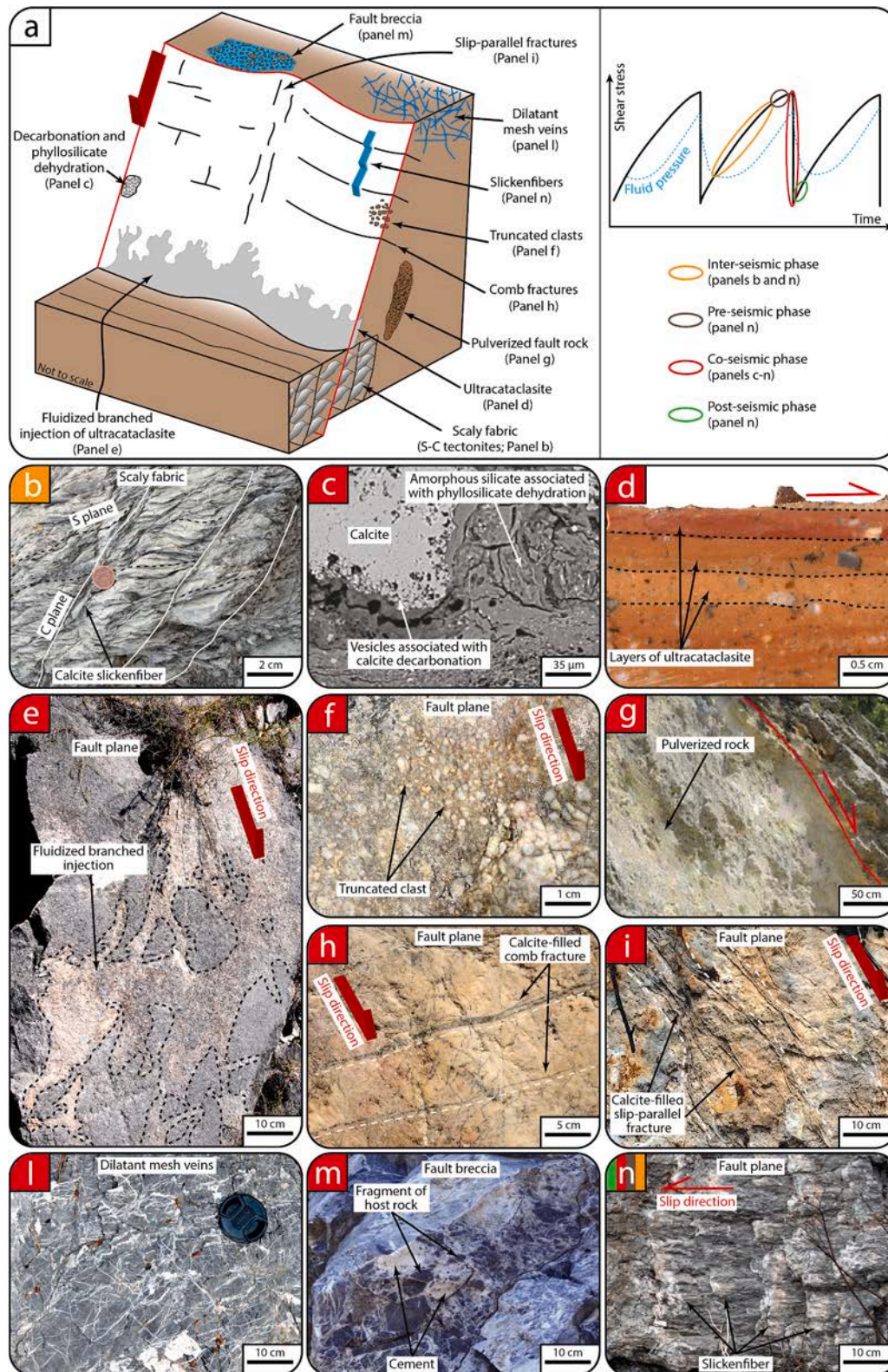


Fig. 2. (a) Conceptual cartoon showing meso- and microstructural indicators of fossil seismic cycles, earthquakes (modified from Stewart and Hancock, 1990). Conceptual representation of seismic cycles and phases during which the structures shown in panels b-n develop. (b) Scaly fabrics (S–C tectonites). (c) Scanning electron microphotograph of calcite crystals with vesicles associated with decarbonation and amorphous silicate associated with phyllosilicate dehydration (modified after Collettini et al., 2013). (d) High-resolution scan of hand specimen of ultracataclasite layers developed along the fault plane (modified after Coppola et al., 2021). (e) Fluidized branched injection of ultracataclasite on the fault plane (modified after Coppola et al., 2021). (f) Clasts truncated by a fault plane. (g) Pulverized rocks (modified after Ferraro et al., 2019). (h) Calcite-filled comb fractures (modified after Smeraglia et al., 2018). (i) Calcite-filled slip-parallel fractures (modified after Smeraglia et al., 2018). (l) Dilatant mesh veins. (m) Fault breccia. (n) Calcite slickenfibers (modified from Goodfellow et al., 2017).

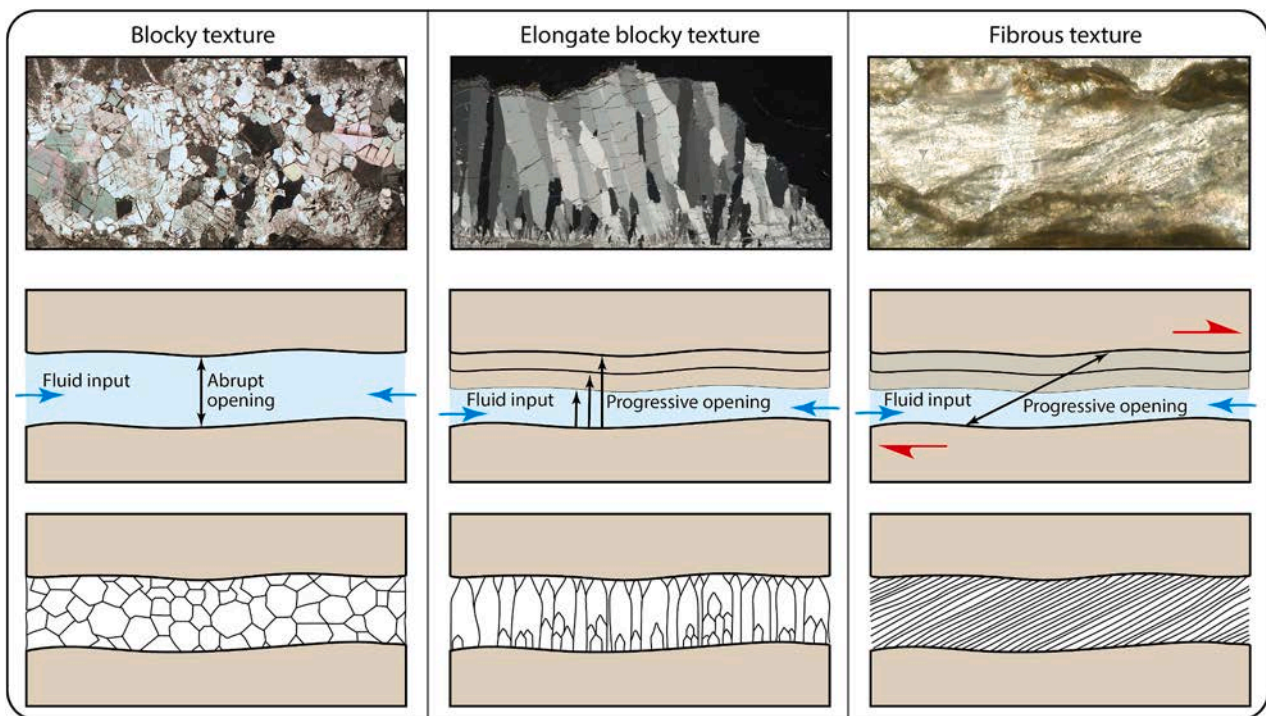


Fig. 3. Microphotograph of blocky, elongate blocky, and fibrous textures of calcite crystals and scheme for their development and precipitation. The shape of crystals, their aspect ratio, and their growth direction indicate rapid or slow deformation-precipitation events which therefore can be associated with distinct phases of the seismic cycle. Blocky textures imply rapid crack opening related to fluid overpressure possibly associated with co-seismic rupture. Elongate blocky textures imply repeated increments of fracture opening and progressive incremental precipitation. This texture does not directly provide information on the phases of seismic cycles. Fibrous textures form by progressive small increments of opening/shear and precipitation likely during inter-seismic phases.

Table 1

Synthesis of meso- and micro-structures of fault rocks and carbonate mineralizations representative of phases of seismic cycles in carbonate-hosted faults in the upper brittle crust.

Structure	Description	Presumed phase of the seismic cycle
Scaly fabric (Figs. 2a and b)	Anastomosing network of tectonic foliations containing veins and slickenfibers precipitated from fluids mobilized from the host rocks during pressure-solution	Inter-seismic phase
Fading grain boundaries, void and vesicles (Figs. 2a and c)	Develop along fault planes and in response to frictional heating which induces decarbonation and/or phyllosilicate dehydration and clay mineral transformation	Co-seismic phase
Ultracataclite layers (Figs. 2a, d, and e)	Particles <10 μm in diameter, localized along the fault plane and commonly displaying fluidized injecting layers	Co-seismic phase
Truncated clasts (Figs. 2a and f)	Clasts truncated by fault planes	Co-seismic phase
Pulverized rocks (Figs. 2a and g)	Comminuted rocks characterized by a myriad of pervading dilational microfractures developing during (high strain rate) slip	Co-seismic phase
Comb veins and slip-parallel veins (Figs. 2a, h, and i)	Veins perpendicular and parallel to the normal fault surface, associated with tension crack opening and rapid filling of pressured fluids during down-dip stretching of the footwall block due to local stress release	Co-seismic phase
Mesh veins (Figs. 2a and l)	Sets of dilatant mesh veins associated with high fluid pressure (hydrofracturing) during seismic events	Pre-/co-seismic phase
Cement-supported fault breccias (Figs. 2a and m)	Associated with episodic events of fluid overpressure, co-seismic dilatancy, and implosive brecciation	Co-seismic phase
Slickenfibers (Figs. 2a and n)	Associated with fault planes (and surfaces along which slip localizes) during (i) shear during slow inter-seismic or post-seismic deformation and/or (ii) rapid co-seismic deformation. Microtextures allowing the identification of slow vs. rapid fluid-assisted deformation	Inter- co- and- post-seismic phase
Blocky texture (Fig. 3)	Roughly equidimensional and randomly oriented crystals associated with fluid overpressure, crack opening, and fast precipitation in fluid-filled open crack	Co-seismic phase (?)
Elongate blocky texture (Fig. 3)	Rod-shaped crystals with high length/width ratio imply opening of a vein by small increments and progressive incremental fluid precipitation during slow deformation	(?)
Fibrous texture (Fig. 3)	Presence of stretched or rod-shaped crystals with a much higher length/width ratio than in the elongate blocky textures; response to opening and shear by small increments and progressive incremental precipitation	Inter-seismic phase (?)

Table 2
Geochemical methods to identify fluid-rock (dis)equilibrium and infer evidence of fossil seismic cycles in the rock record.

Method	Description	Information on the involved paleofluids	Chemical fluid-rock equilibrium	Chemical fluid-rock disequilibrium	Presumed phase of the seismic cycle
C stable isotopes	The $\delta^{13}\text{C}$ of tectonic carbonates reflects the composition of the dissolved inorganic carbon in the fluid	The $\delta^{13}\text{C}$ of tectonic carbonates directly reflects specific fluid sources allowing to derive fluid origin (e.g., CO_2 -rich deep fluids or fluids interacting with light C-enriched soils)	Tectonic carbonate and host rock with overlapping $\delta^{13}\text{C}$ values	Tectonic carbonate and host rock with distinct $\delta^{13}\text{C}$ values	Possible co-seismic phase
O stable isotopes	The $\delta^{18}\text{O}$ of tectonic carbonates reflects fractionation processes and depends on the $\delta^{18}\text{O}$, and temperature of the fluid	The $\delta^{18}\text{O}$ of tectonic carbonates provide an overall view of the fluid source, although the temperature-dependent fractionation requires to constrain the fluid temperature	Tectonic carbonate and host rock with overlapping $\delta^{18}\text{O}$ values	Tectonic carbonate and host rock with distinct $\delta^{18}\text{O}$ values	(?)
Clumped isotopes	Abundance of $^{13}\text{C}-^{18}\text{O}$ isotope bonds in the carbonate ions above a theoretical random distribution	Temperature of mineralizing fluid. Coupled with $\delta^{18}\text{O}$ of tectonic mineralization, clumped isotopes allow to calculate the fluid $\delta^{18}\text{O}$ isotopic composition	When compared with the host rock temperature at the time of tectonic carbonate precipitation, clumped isotopes-based temperature permits to identify thermal (dis)equilibrium		Possible co-seismic phase
Cathodoluminescence (CL)	Based on the content of Mn^{2+} and trivalent REE-ions (Dy^{3+} , Sm^{3+} , and Tb^{3+}) that are the most important activators of extrinsic CL, while Fe^{2+} is a quencher of CL	Redox conditions during mineral precipitation and different generations of mineralizations	(?)	(?)	(?)
REEs	Marine carbonates are characterized by (i) slight light rare Earth elements (LREEs) depletion with respect to the heavy rare Earth elements (HREEs), (ii) negative Ce anomaly, and (iii) positive La anomaly	LREEs depletion and HREEs enrichment in tectonic carbonates may testify the involvement of CO_2 -rich fluids	Tectonic carbonates and carbonate host rocks characterized by diagnostic negative Ce anomaly and REE concentrations	Tectonic carbonates with enrichment/depletion of REE concentrations with respect to the carbonate host rocks	Possible co-seismic phase
He isotopes	He in natural fluids is sourced from the atmosphere, mantle, and crust and the $^3\text{He}/^4\text{He}$ ratios of these three sources are significantly different	The $^3\text{He}/^4\text{He}$ isotopic ratios of tectonic carbonates reflect the source of mineralizing fluids	$^3\text{He}/^4\text{He}$ isotopic ratio with crustal affinity	$^3\text{He}/^4\text{He}$ isotopic ratio with exotic (e.g., mantle, magmatic) affinity	Possible co-seismic phase
Sr isotopes	^{87}Sr and ^{86}Sr isotopes hardly undergo any significant fractionation. Hence, tectonic mineralizations directly preserve $^{87}\text{Sr}/^{86}\text{Sr}$ isotopic ratio of the mineralizing fluid	The $^{87}\text{Sr}/^{86}\text{Sr}$ isotopic ratios of tectonic carbonates reflect the source of mineralizing fluids and the extent of fluid-rock interaction	Similar $^{87}\text{Sr}/^{86}\text{Sr}$ isotopic ratios between tectonic carbonates and host rocks	Distinct $^{87}\text{Sr}/^{86}\text{Sr}$ isotopic ratios between tectonic carbonates and host rocks	Possible co-seismic phase
Fluid inclusions	Microscopic pockets of liquids trapped within minerals during crystal growth that contain information on the original chemical and physical conditions of mineralizing paleofluids	Microthermometry and Raman spectroscopy permit to (i) calculate the temperature (and derive the pressure) and (ii) define the chemical composition and salinity of fluids at the time of precipitation	Fluid inclusions constraining temperature and chemistry similar to the host rock	Fluid inclusions constraining high temperature, high salinity, and exotic elements	Possible co-seismic phase

accumulation, (ii) pre-seismic phase, when minor stress releases occur through increasing creep or foreshocks, (iii) co-seismic phase, lasting from a few to tens of seconds, releasing the accumulated stress during an earthquake and the associated rupturing, and (iv) post-seismic phase, lasting from days to years depending on the size of the rupture and the strength and permeability of the rock mass when aftershocks or a phase of waning creep occur (e.g., Power and Tullis, 1989; Lindh, 1990; Scholz, 1991; Sibson, 1994; Ellsworth et al., 2013).

In the study of fault-related mineralizations, it is crucial to identify the part of the seismic cycle when they formed and to constrain the fluid pressure conditions. To this end, we review the main meso- and micro-structures with the potential to make such an identification in carbonate rocks (Figs. 2 and 3 and Table 1). Pseudotachylytes, commonly acknowledged as tracers of past earthquakes within crystalline rocks (e.g., Cowan, 1999; Rowe and Griffith, 2015), form at depths >3 km and mostly in non-carbonate lithotypes and are not reviewed in here. The indicators and geochemical methods useful to identify the origin of mineralizing fluids and fluid-rock (dis)equilibria during phases of the

seismic cycles (inferred from the meso- and micro-structures) are also reviewed (Table 2).

2.2. Meso- and micro-structures as indicators of the seismic cycle

The following meso- and microstructures are indicative of the mechanisms, strain rate, hydraulic features, and fluid pressure associated with deformation. They allow us to infer the phase of the seismic cycle in which they develop (Fig. 2 and Table 1): when indicative of high strain rate they might be representative of a co-seismic phase whereas low strain rate might represent an inter-seismic phase.

- Scaly fabrics

Scaly fabrics, including S—C fabrics (Figs. 2a, b), accommodate a combination of pressure solution and frictional sliding associated with fluid pressure fluctuations (e.g., Berthé et al., 1979; Tesei et al., 2014; Fisher et al., 2021). They commonly form in suitable lithotypes and

during inter-seismic phases, when slow aseismic (creep) deformation occurs in response to elastic strain accumulation (e.g., [Sibson, 1986](#); [Meneghini and Moore, 2007](#); [Rowe et al., 2011](#)). Pressure solution mobilizes pore fluids from the host rock (likely in isotopic and thermal equilibrium with it) and leads to precipitation of tectonic veins and slickenfibers, enhancing the healing of the fault zone and promoting elastic strain accumulation (e.g., [Dietrich et al., 1983](#); [Gratier et al., 2011](#)).

- Fading grain boundaries, voids and/or vesicles

Such structures ([Figs. 2a, c](#); e.g., [De Paola et al., 2011](#); [Collettini et al., 2013](#); [Bullock et al., 2015](#)) occur along fault planes and form in response to high strain rates (co-seismic slip) and associated frictional heating, which may induce decarbonation and/or phyllosilicate dehydration and transformation via mixed layer minerals ([Balsamo et al., 2014](#)) in the first few millimeters off the fault planes. Hence, these micrometric scale structures are diagnostic of fossil earthquakes.

- Ultracataclasite layers

Ultracataclasite layers commonly occur along the fault plane and consist of matrix and clasts <10 μm in diameter. Locally, they contain fluidized injectites that localize displacement during repeated co-seismic slips ([Figs. 2a, d](#); [Chester and Chester, 1998](#); [Lin, 2011](#); [Smith et al., 2011](#); [Nuriel et al., 2012](#); [Rowe and Griffith, 2015](#); [Karabacak et al., 2022](#)).

- Truncated clasts

They are locally found along discrete fault planes where they are believed to undergo sharp truncation during co-seismic fault slip ([Figs. 2a, f](#); [Billi and Di Toro, 2008](#); [Fondriest et al., 2013](#); [Delle Piane et al., 2017](#)).

- Pulverized rocks

They are extremely comminuted damage zone rocks characterized by numerous dilational microfractures and are indicative of high strain rate and earthquakes (co-seismic phase; [Billi and Di Toro, 2008](#); [Doan and Billi, 2011](#); [Incel et al., 2017](#); [Zwiessler et al., 2017](#); [Billi et al., 2023](#); [Fig. 2a, g](#)). They are commonly associated with physical processes, including dynamic unloading ([Ben-Zion and Shi, 2005](#); [Dor et al., 2006](#); [Payne and Duan, 2017](#)), dynamic fragmentation ([Doan and Gary, 2009](#); [Doan and Billi, 2011](#); [Wechsler et al., 2011](#); [Yuan et al., 2011](#); [Doan and d'Hour, 2012](#)), transient tensile pulses ([Xu and Ben-Zion, 2017](#); [Griffith et al., 2018](#); [Smith and Griffith, 2022](#)). However, they have been recently associated with accumulation and rapid decompression of pressurized CO₂-rich gasses ([Billi et al., 2023](#)), suggesting the involvement of deep and/or exotic fluids likely in chemical-physical disequilibrium with the host rock.

- Comb and slip-parallel veins

Comb and slip-parallel veins are oriented perpendicular and parallel to the faults, respectively ([Hancock and Barka, 1987](#); [Stewart and Hancock, 1990](#); [Doblas et al., 1997](#); [Collettini et al., 2014](#); [Figs. 2a, h, and i](#)). The development of comb veins during fracture opening is apparently not compatible with the stress field associated with normal faults (in which σ_1 and σ_3 are vertical and horizontal, respectively). They were initially interpreted as “tension cracks reflecting down-dip stretching during localized post-slip stress reorientation” ([Hancock and Barka, 1987](#); [Stewart and Hancock, 1990](#)). However, it has more recently been proposed that comb and slip-parallel veins can also form during co-seismic down-dip displacement of the footwall block and co-seismic stress release localizing deep overpressured fluids ingress and

flow ([Smeraglia et al., 2018](#)).

- Mesh (or stockwork) veins

Mesh veins are defined as sets of dilatant randomly-oriented veins ([Figs. 2a, and l](#)) that document hydraulic fracturing (hydrofractures) under low or even null differential stress and fluid overpressure conditions associated with pre-/co-seismic phases ([Sibson, 2000, 2004](#); [Cox et al., 2001](#); [Meneghini and Moore, 2007](#); [Fagereng and Harris, 2014](#)). The development of hydrofractures, genetically associated with crack opening and rapid infilling by pressurized fluids, can potentially account for the rapid ascent of deep fluids in chemical-physical disequilibrium with the host rock during earthquakes ([Curzi et al., 2021](#)).

- Crackle and chaotic cement-supported fault breccias

These breccias ([Fig. 2a, and m](#)) develop during co-seismic implosive brecciation with episodic fluid overpressure and subsequent rapid depressurization during fluid venting ([Sibson, 2000](#); [Mort and Woodcock, 2008](#); [Woodcock and Mort, 2008](#)) and may represent evidence of dilatancy and involvement of possibly exotic pressurized fluids.

- Slickenfibers

Slickenfibers develop along fault planes and surfaces along which slip localizes ([Figs. 2a, and n](#)) and track the displacement direction. They form during shear associated with (i) slow inter-seismic or post-seismic deformation, during which fluid pressure fluctuations can be associated with slow shear events (ii) and/or rapid co-seismic deformation occurring under repeated fluid overpressure and associated rapid shear events (e.g., [Power and Tullis, 1989](#); [Gratier and Gamond, 1990](#); [Fagereng et al., 2010, 2011](#)). The association of slickenfibers with specific deformation-precipitation processes, and with a specific phase of the seismic cycle, requires the identification of their internal textures.

As expanded below, the internal texture of slickenfiber mineralizations ([Fig. 3](#)) allows one (i) discriminating high vs. low fluid pressure, (ii) constraining the deformation mechanisms and strain rate, and (iii) inferring the phase of the seismic cycle when shear occurs.

- Blocky textures

Blocky textures ([Fig. 3](#)) are characterized by roughly equidimensional and randomly oriented crystals and imply rapid crack opening, possibly mediated by fluid overpressure, and fast precipitation in fluid-filled open cracks (e.g., [Hilgers et al., 2001, 2004](#); [Passchier and Trouw, 2005](#); [Bons et al., 2012](#)). Blocky textures indicate rapid deformation, possibly associated with co-seismic phases, and fracture filling likely associated with the involvement of overpressured fluids. However, blocky textures do not directly provide evidence of fossil earthquakes and can be also associated with fluid overpressures during pre- and post-seismic phases.

- Elongate blocky textures

Elongate blocky textures ([Fig. 3](#)) contain rod-shaped crystals characterized by high length/width ratio and imply repeated increments of fracture opening and progressive incremental precipitation (e.g., [Hilgers et al., 2001](#); [Hilgers and Urai, 2002](#); [Passchier and Trouw, 2005](#); [Bons et al., 2012](#)). This type of texture is not directly associated with fluid overpressure and does not directly provide information on the phases of seismic cycles.

- Fibrous textures

Fibrous textures ([Fig. 3](#)) are characterized by stretched or rod-shaped crystals with a much higher length/width ratio than in elongate blocky

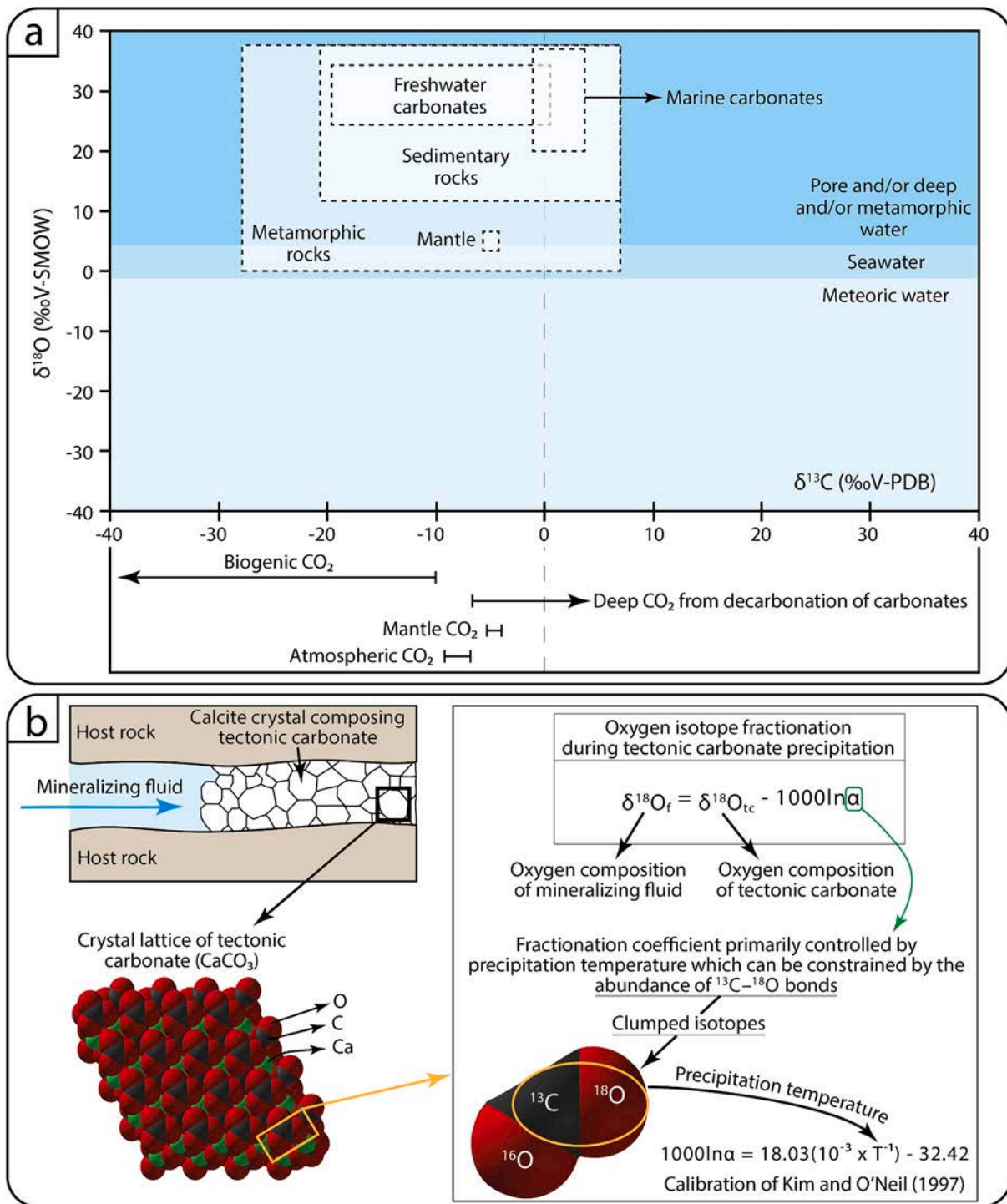


Fig. 4. (a) Reference $\delta^{18}\text{O}$ (V-SMOW) vs. $\delta^{13}\text{C}$ (V-PDB) diagram showing the main isotopic field for representative fluids and rock types. Data from Rollinson and Pease (1993), Nelson and Smith (1996), Hoefs (1997), Hayes et al. (2001), Valley et al. (2005), Misra (2012), and Sharp (2017). (b) Schematic representation of a tectonic carbonate and its crystal lattice. The formula of O isotope fractionation, the calibration of the temperature-dependent O isotopes fractionation by Kim and O'Neil (1997), and schematic ¹³C-¹⁸O isotope bond within CO₃²⁻ ions, on which clumped isotope geothermometer is based, are shown.

textures and form by progressive small increments of opening/shear and precipitation (e.g., Gratier and Gamond, 1990; Passchier and Trouw, 2005). These textures do not provide evidence of fluid overpressure and indicate slow deformation associated with low strain rate during slow aseismic slip (e.g., Bons et al., 2012; Tessei et al., 2013).

2.3. Geochemical methods to identify fluid-rock (dis)equilibria and fossil indicators of seismic cycles

- Stable Carbon isotopes

The carbon isotope composition ($\delta^{13}\text{C}$) of carbonates reflects the composition and origin of the dissolved inorganic carbon in the fluids because carbon isotope fractionation at low temperatures is only

minimally temperature-dependent (Hoefs, 1997). Marine carbonates are characterized by $\delta^{13}\text{C}$ values close to 0 ‰ (V-PDB). Carbonates of tectonic origin characterized by negative $\delta^{13}\text{C}$ values and hosted in marine carbonates indicate a contribution of carbon derived from organic carbon respiration in soils and/or from the interaction of fluids with organic matter-rich rocks (e.g., Sharp, 2017).

Deep CO_2 arising from the mantle is characterized by $\delta^{13}\text{C}$ values between $\sim -5\text{‰}$ and $\sim -3\text{‰}$ (e.g., Chiodini et al., 2000). Deep CO_2 arising from decarbonation of carbonate-rich rocks at depth is instead enriched in the heavy carbon isotope ^{13}C with respect to the parental carbonate (e.g., Sharp, 2017). Deep CO_2 produced by decarbonation can be characterized by $\delta^{13}\text{C}$ comprised between $\sim 4\text{‰}$ and, when produced from organic-rich carbonates, $\sim -7\text{‰}$ (e.g., Rielli et al., 2022; Fig. 4a). In tectonically active regions, such as the Apennines, deep CO_2 -rich fluids can flow upward especially during pre- to co-seismic phases (e.g., Caracausi and Paternoster, 2015; Di Luccio et al., 2018) and lead to tectonic carbonate precipitation during co-seismic rapid CO_2 degassing (e.g., Billi et al., 2023). Tectonic carbonates precipitating from such a rapid degassing of deep CO_2 -rich fluids show $\delta^{13}\text{C}$ values $> \sim 6\text{--}8\text{‰}$, thus clearly accounting for an isotopic fluid-rock disequilibrium associated with the involvement of deep CO_2 -rich fluids (Di Luccio et al., 2018; Baldermann et al., 2020; Billi et al., 2023).

- Stable Oxygen isotopes

The stable oxygen isotope composition ($\delta^{18}\text{O}$) of carbonates depends on the $\delta^{18}\text{O}$ and the temperature of the fluid from which they precipitate (e.g., Sharp, 2017). Different fluids and rock types have different ranges of $\delta^{18}\text{O}$ values (Fig. 4a) but when fluids interact with rocks for a long time they can equilibrate and reach isotopic equilibrium (Nelson and Smith, 1996; Hoefs, 1997). By comparing the $\delta^{18}\text{O}$ of tectonic carbonates and host rocks, it is possible to deduce whether mineralizing fluids were in isotopic (dis)equilibrium with the host rocks provided that the temperature of precipitation of the carbonates can be constrained (Fig. 4b).

- Carbonate Clumped isotope thermometry

Carbonate clumped isotope thermometry exploits the tendency of heavy isotopes (^{13}C and ^{18}O) to bond together (hence the term “clumped isotopes”) in the carbonate lattice with decreasing temperature (Ghosh et al., 2006; Schauble et al., 2006; Fig. 4b). By measuring the temperature-dependent abundance of $^{13}\text{C}\text{--}^{18}\text{O}$ isotope bonds above a theoretical random distribution in carbonate minerals, it is possible to constrain the temperature of carbonate precipitation, without knowing the fluid composition, as in conventional stable isotope geochemistry. The clumped isotope composition of carbonates is expressed with the parameter Δ_{47} (Ghosh et al., 2006).

With the temperature determined by clumped isotopes and using the temperature-dependent oxygen isotope fractionation between carbonate and fluid, it is possible to calculate the $\delta^{18}\text{O}$ of the fluid from which the carbonate precipitated (Fig. 4b). While for clumped isotopes in the last few years there has been a convergence to one calibration that appears valid at least for all non-biogenic carbonates (Anderson et al., 2021; Jautzy et al., 2020; Fiebig et al., 2021), carbonate-water oxygen isotope calibrations still have significant differences (e.g., O’Neil et al., 1969; Kim and O’Neil, 1997; Daëron et al., 2019). This leads to uncertainties in the reconstruction of paleofluid oxygen isotope compositions but still provides robust information on the source and allows identifying the involvement of exotic fluids in chemical-physical (dis)equilibrium with the host rock.

- Cathodoluminescence (CL)

Cathodoluminescence in carbonate minerals is mainly controlled by the content of Mn^{2+} and trivalent REE-ions (Dy^{3+} , Sm^{3+} , and Tb^{3+}),

which are the most significant activators of extrinsic CL, with Fe^{2+} being a quencher of luminescence (Machel, 2000). Their concentration in carbonate minerals depends on fluid composition and redox conditions during mineral precipitation (e.g., Sommer, 1972; Machel, 1985, 1997, 2000). Similar or different CL signatures between tectonic mineralizations and host rock cannot be used to directly identify an unambiguous fluid-rock chemical (dis)equilibrium. However, CL on tectonic carbonates allows: (i) identifying multiple events of precipitation and/or different generations of mineralizations from CL zonation patterns of crystals, (ii) detecting mineralizations that are not visible with normal optical microscopy, (iii) recognizing recrystallization or diagenetic alteration (iv), identifying distinct events of precipitation, and (v) correlating minerals belonging to the same generation in different samples (e.g., Dromgoole and Walter, 1990). Thus, CL is a key analytical technique to any robust geochemical analysis of tectonic carbonates.

- Rare Earth Elements (REEs)

Marine carbonates are characterized by a diagnostic slight depletion of light rare earth elements (LREEs) relative to the heavy rare earth elements (HREEs), a negative Ce anomaly, and positive La anomaly (Webb and Kamber, 2000; Özyurt et al., 2020). Hence, tectonic carbonates exhibiting negative Ce anomaly and REE concentrations (PASS-normalized) in the range of those from carbonate host rocks indicate low fluid-rock ratios and/or a long residence time of fluids within the carbonate host rock and therefore attest to a chemical equilibrium in the fluid-rock system (e.g., Bolhar et al., 2004; Nuriel et al., 2011; Uysal et al., 2011). On the contrary, tectonic carbonates characterized by enrichment/depletion of REE concentrations with respect to the carbonate host rocks may document the involvement of exotic fluids and/or different degrees of fluid-rock interaction (Nuriel et al., 2011; Uysal et al., 2011; Coppola et al., 2021; Curzi et al., 2021). LREE and HREE enrichments or depletions in tectonic carbonates depend on distinct partition coefficients for the REEs, which depend on their cationic radius. LREEs are preferentially assimilated in the crystal lattice compared to HREE (Braun et al., 1990; Bau, 1991; Bau and Moller, 1992; Négrel et al., 2000). Instead, LREE depletion and HREE enrichment in tectonic carbonates commonly occur when CO_2 -rich fluids interact with carbonate rocks. Indeed, CO_2 -rich circulating fluids form stronger complexes with HREE than with LREE (Négrel et al., 2000; Cerchiari et al., 2020). For this reason, REE concentrations in tectonic carbonates provide constraints on the origin of fluids (host rock residential vs. external source) and the extent of fluid-rock interaction, and they may also be used as indicators for the occurrence of earthquake-related CO_2 release (Nuriel et al., 2011; Uysal et al., 2011; Cerchiari et al., 2020; Coppola et al., 2021).

- Helium isotopes

He in natural fluids derives from three sources with significantly different $^3\text{He}/^4\text{He}$: atmosphere, mantle, and crust (e.g., Ballentine et al., 2002; Graham, 2002; Gautheron et al., 2005). Hence, this tracer is a powerful proxy for recognizing the origin of fluids in tectonic mineralizations (e.g., Pili et al., 2011; Czuppon et al., 2014; Curzi et al., 2022; Marchesini et al., 2022). The He isotopic signature of fluids and gases in seismically active regions is higher (between 0.7 and 1 Ra) than typical crustal fluids (0.01–0.03 Ra) from cratons and sedimentary basins far from tectonically active regions (e.g., Caracausi and Paternoster, 2015). While He is highly mobile, it remains trapped within low permeability rocks and cannot escape without the occurrence of fracture networks. Hence, He produced from the crust or mantle can efficiently flow upward through dilatancy processes associated with earthquakes (e.g., Scholz et al., 1973; Caracausi and Paternoster, 2015; Ring et al., 2016; Caracausi et al., 2022). Studies on He isotopes extracted from tectonic carbonates in the Apennines, documented the involvement of crustal fluids with a clear mantle contribution also during fossil earthquakes

(Smeraglia et al., 2018). He isotopes studies of gas emissions, mud volcanoes, springs, and wells along seismically active areas in the Apennines clearly document that deep and/or mantle derived fluids were released during earthquakes (e.g., Italiano et al., 2001; Chiodini et al., 2011; Caracausi and Paternoster, 2015; Caracausi et al., 2022). He isotope studies in springs showed an association with increased upflow of deep CO₂-rich fluids recognized as seismic precursors (e.g., Barbieri et al., 2020; Boschetti et al., 2022; Gori and Barberio, 2022). Thus, He isotope analysis of tectonic mineralizations can yield a diagnostic fingerprint of fossil earthquakes involving CO₂-rich fluids.

- Strontium isotopes

Sr isotopes in tectonic mineralizations directly reflect the ⁸⁷Sr/⁸⁶Sr isotopic ratio of the mineralizing fluid (Palmer and Edmond, 1989; Avigour et al., 1990; Horton et al., 2003; Drake et al., 2020). On this ground, tectonic carbonates precipitated from fluids that extensively interacted with the host rock, are characterized by a ⁸⁷Sr/⁸⁶Sr isotopic ratio similar to that of the host rock (e.g., Åberg, 1995; Dielforder et al., 2022). In contrast, carbonates precipitated from exotic fluids, with limited interaction with the host rocks may be characterized by a Sr isotopic composition similar to that of the fluid source (e.g., Machel and Cavell, 1999; Uysal et al., 2007; Dielforder et al., 2022). Hence, Sr isotopes are a powerful tracer of the source, extent of fluid-rock interaction, and ascent/descent of exotic fluids which can be involved during co-seismic slip (e.g., Uysal et al., 2007; Beaudoin et al., 2014).

- Fluid inclusions

Fluid inclusions are microscopic pockets of liquid trapped within the minerals during crystal growth and contain information on the original chemical and physical conditions of the mineralizing fluids (e.g., Roedder and Bodnar, 1980; Roedder, 1984; Invernizzi et al., 1998; Ceriani et al., 2011; Bodnar et al., 2013; Mangenot et al., 2017). Microthermometry, Raman spectroscopy, and chemical analysis of crushed fluid inclusions, allow us to calculate the temperature of fluids and define the chemical composition and salinity (as NaCl equivalents) of fluids from which the carbonate precipitated (e.g., Hanks et al., 2006; Beaudoin et al., 2014; Hoareau et al., 2021). Fluid inclusions allow the detection of exotic fluids bringing exotic elements or compounds such as CO₂ or hydrocarbons and transported during earthquakes and co-seismic phases.

3. Geological setting of the study area

3.1. Tectonic setting of the Central Apennines

The Central Apennines are a NW-SE trending, late Oligocene-to-Present fold-and-thrust belt developed in response to the W-directed subduction of the Adriatic lithosphere beneath the European plate (Carminati et al., 2010; Malinverno and Ryan, 1986). The structure of the Central Apennines is the result of the superimposition of orogenic and post-orogenic extensional deformation progressively migrated and still migrating toward E and NE (Faccenna et al., 2001; Carminati et al., 2012; Fig. 5a, b). Orogenic shortening, which began in the internal (western) sector of the belt in late Oligocene-early Miocene time, was mainly accommodated by NE-verging folds and thrusts, which deformed pre- and syn-orogenic deposits (Patacca et al., 1990; Cosentino et al., 2010; Curzi et al., 2020b; Fig. 5a, b). The eastward migration of the belt was accompanied by extension at its rear (west), associated with normal faulting and the formation of the Tyrrhenian back-arc basin. Extension initiated during the late Miocene in the internal sector and progressively migrated toward the axial zone of the Apennines (Malinverno and Ryan, 1986; Faccenna et al., 1997; Cavinato and De Celles, 1999; Billi et al., 2006; Fig. 5a, b) where it is still active. In the central Apennines, it is preempted and accompanied by upflow of deep fluids and is responsible

for major (Mw ≥ 6.0) earthquakes (e.g., Chiarabba et al., 2009; Chiaraluce et al., 2017; Fig. 5a). Extension was also associated with 3–4 km exhumation of syn- and pre-orogenic deposits in the internal and external portion of the belt and < 2 km along the whole Apennines (Fig. 5b; Corrado et al., 2010; Fellin et al., 2022). At present, thrusting is inactive in the inner and axial portions of the chain whereas it is active in the external Adriatic and Po plain domains (e.g., Carminati et al., 2010; Turrini et al., 2015).

3.2. Stratigraphic setting of the Central Apennines

A detailed knowledge of the deforming stratigraphic succession is of fundamental importance to infer the fluid origin and possible fluid-rock interaction during the seismic cycle. The Mesozoic-Cenozoic stratigraphic successions of the Central Apennines are represented by the Umbria-Marche-Sabina Pelagic Basin (UMSB) and Latium-Abruzzi Carbonate Platform (LAP) sedimentary successions of the Adria passive margin (e.g., Cosentino et al., 2010; Fig. 5a). Such basin and platform environments developed in response to the Middle Triassic-Early Jurassic rifting of the Adria Plate that dissected the succession in fault-bounded structural highs and pelagic basins (e.g., Santantonio, 1993; Cipriani, 2016). Rifting dismembered an Upper Triassic-Lower Jurassic carbonate platform, on which, above the Paleozoic basement, Triassic evaporites and Jurassic shallow water carbonates deposited (e.g., Cosentino et al., 2010; Fig. 5a). The UMSB succession consists of Upper Triassic evaporites followed by Lower Jurassic shallow water carbonates, which evolve upward to deep water marly limestone and cherty limestone deposited in pelagic settings between the Early Jurassic and the Oligocene (e.g., Cosentino et al., 2010; Fig. 5a). Starting from Oligocene times, the terrigenous input progressively increased, while carbonate sedimentation diminished. Middle-upper Miocene siliciclastic turbidites represent the foredeep stage associated with flexural subsidence resulting from the subduction of the Adriatic plate (e.g., Cosentino et al., 2010; Fig. 5a). The LAP succession consists of Upper Triassic evaporites and dolostones followed by shallow-water Jurassic-to-middle-upper Miocene carbonates (Fig. 5a). During the middle to late Miocene, carbonate sedimentation was interrupted by drowning and coeval input of terrigenous sediments followed by siliciclastic turbidites deposited in foredeep basins (Cipollari and Cosentino, 1995; Cosentino et al., 2010; Fig. 5a). During post-orogenic extensional faulting, Plio-Pleistocene continental deposits filled intramountain basins (e.g., Cosentino et al., 2010, 2017). The main Mesozoic-Cenozoic stratigraphic successions of the Central Apennines are shown in Fig. 5a. Our samples are mainly taken from Jurassic-Paleogene limestones and marly limestones and from Messinian sandstones and marls (Fig. 5 and Table S1).

3.3. Previous studies on paleofluid-faulting relationships in the Apennines

The first regional-scale studies of fluid circulation along thrusts and normal faults in the Central Apennines documented, by means of C and O isotopes on tectonic calcite mineralizations, the change of fluid circulation from an orogenic compressional deformation stage to post-compressive extension (Maiorani et al., 1992; Conti et al., 2001; Ghisetti et al., 2001; Fig. S1). In particular, Ghisetti et al. (2001) proposed that compressional deformation occurred in “semi-closed” fluid systems in which host-rock derived fluids were mobilized during compressional deformation. Subsequently, post-compressive extensional faulting was accompanied by “semi-open to open” fluid systems in which meteoric fluids penetrated downward along normal fault damage zones. Similarly, Agosta and Kirschner (2003), who focused on extension-related fluid-rock systems, confirmed that meteoric fluids are invariably involved during normal faulting-related exhumation and excluded the involvement of deep (e.g., mantle, crustal magmas, and/or devolatilizing carbonate rocks) fluids. Recent works in the Apennines demonstrated that local fluid-rock-fault systems are indeed rather complex and

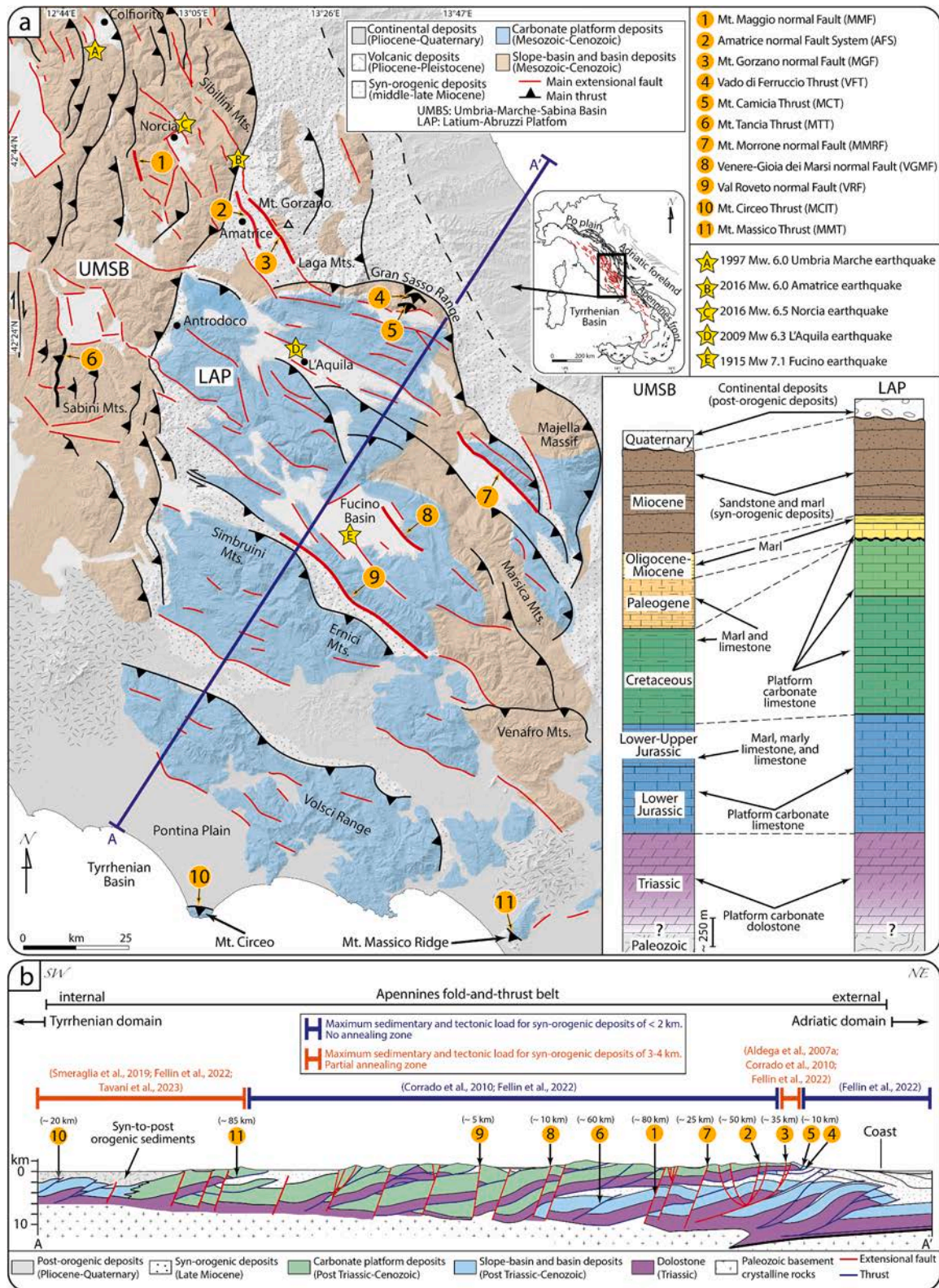


Fig. 5. (a) Simplified geological map of the central Apennines showing the location of main extensional and thrust faults (modified after Curzi et al., 2020b). Location of fault zones (1–11) considered in this study and epicenters of historical earthquakes are shown in the map. Representative stratigraphic columns of the Umbria-Marche-Sabina pelagic Basin (UMSB; modified after Cipriani, 2016) and Latium-Abruzzi Carbonate Platform (LAP; modified after Parotto and Praturlon, 1975) are also shown in (a). Inset in (a) shows a schematic tectonic setting for the Apennines. (b) Conceptual geological cross-section through the central Apennines (modified after Cosentino et al., 2010). The structural position of the eleven fault zones considered in this study is projected. For reasons of synthesis and visualization, each fault considered in this study is projected for many kilometers (values shown in b) along the same cross-section. For this reason, the structural position of projected faults can be poorly accurate. Note that the structures n. 1 (Mt. Maggio normal Fault) and n. 6 (Mt. Tancia Thrust) are actually exposed above the Mesozoic-Cenozoic carbonate platform deposits (to the north of the cross-section trace).

can involve both shallow and deep fluids during distinct phases of the seismic cycle. These studies are reviewed below.

4. Materials and methods

In this study, we compare structural, isotopic, and thermal data from eleven thrust/extensional/inverted faults (Fig. 5, Table 3 and Table S1) in the Central Apennines. We present new data from the Monte Maggio normal Fault (MMF), Venere-Gioia dei Marsi normal Fault (VGMF), and published data from the Amatrice normal Fault System (AFS), Mt. Gorzano normal Fault (MGF) cutting through a reverse fault, Vado di Ferruccio Thrust (VFT) and Mt. Circeo Thrust (MCIT) cut by later extensional faults, extensionally-inverted Mt. Camicia Thrust (MCT) and Mt. Tancia Thrust (MTT), Mt. Morrone normal Fault (MMRF), Val Roveto normal Fault (VRF), and Mt. Massico Thrust (MMT; Tables 3 and S1).

The analytical methods for the new data are described in the following:

- Stable C and O isotopes

Measurements were carried out at the Stable Isotope Laboratory of IGG, CNR of Pisa (Italy), and at the Stable Isotope Laboratory of the Geological Institute of ETH, Zürich (Swiss). Powders of tectonic calcite mineralizations were prepared using a microdrill equipped with drill bits down to 0.3 mm in diameter. Carbon and oxygen isotopic composition of the bulk carbonate was measured using a GasBench II coupled to a Delta V mass spectrometer (both ThermoFischer Scientific, Bremen, Germany) as described in Breitenbach and Bernasconi (2011). Briefly, about 100 µg of powdered sample were placed in vacutainers, flushed with helium and were reacted with 5 drops of 104% phosphoric acid at 70 °C. In batch of 70 samples instrument was calibrated with the internal standards MS2 ($\delta^{13}\text{C} = +2.13\text{‰}$, $\delta^{18}\text{O} = -1.81\text{‰}$) and ETH-4 ($\delta^{13}\text{C} = -10.19\text{‰}$, $\delta^{18}\text{O} = -18.71\text{‰}$) which are calibrated to the international reference materials NBS 19 ($\delta^{13}\text{C} = +1.95\text{‰}$, $\delta^{18}\text{O} = -2.2\text{‰}$) and NBS 18 ($\delta^{13}\text{C} = -5.01\text{‰}$, $\delta^{18}\text{O} = -23.00\text{‰}$; Bernasconi et al., 2018). The standard for C isotopes abundance measurements is based on a Cretaceous belemnite sample from the Pee Dee Formation in South Carolina, USA and is reported in V-PDB (where V is the abbreviation for “Vienna”, the headquarters for the International Atomic Energy Agency that distributes standards). The standard for O isotopes abundance measurements is

Table 3

Summary of main attributes of selected fault zones in the Central Apennines. For further details see Table S1 in the Supplementary Material.

Tectonic regime	Fault	Location	Age of compressional tectonic mineralization	Age of extensional tectonic mineralization	Δ_{47} Temperature	Temperature of the host rocks at the time of tectonic mineralization precipitation		References	
Compressional	Mt. Massico Thrust (MMT)	Central-southern Apennines	U-Pb age ~ 5.1 Ma	U-Pb age ~ 2.8 Ma	106–147 °C	125 ± 5 °C		Smeraglia et al. (2019, 2020)	
	Mt. Maggio normal Fault (MMF)	Central-northern Apennines			48–58 °C			This study	
	Amatrice normal Fault System (AFS)	Central Apennines		U-Th age between ~355 and 108 ka				Vignaroli et al. (2020)	
Extensional	Venere-Gioia dei Marsi normal Fault (VGMF)	Central Apennines			18–23 °C			This study	
	Val Roveto normal Fault (VRF)	Central Apennines		U-Th age between ~317 and ~ 121 ka	32–64 °C			Smeraglia et al. (2018)	
	Mt. Morrone normal Fault (MMRF)	Central Apennines		U-Th age Between ~268 and ~189 ka	23–41 °C			Vignaroli et al. (2022)	
Both compressional and extensional	Mt. Tancia Thrust (MTT)	Central Apennines	K-Ar age ~ 9.5 Ma and ~ 7.5 Ma	K-Ar age ~ 2.9 Ma	Compression 55–78 °C	Extension 26–28 °C	Compression 65 ± 2 °C	Extension 62 ± 2 °C	Curzi et al. (2020a)
	Mt. Gorzano normal Fault (MGF)	Central Apennines	Messinian (Milli et al., 2007)	U-Pb age of ~2.5 Ma and ~ 1.6 Ma	67–77 °C	72–85 °C inter-seismic extension	74 ± 2 °C (this work)	82 ± 2 °C during pre-/co-seismic deformation	Curzi et al. (2021)
	Mt. Circeo Thrust (MCIT)	Central-southern Apennines	U-Pb age ~ 15.6 Ma and ~ 12.7 Ma	U-Pb age ~ 9 Ma	102–117 °C	99–135 °C	100 ± 10 °C	115 ± 5 °C	Tavani et al. (2023)
	Mt. Camicia Thrust (MCT)	Central Apennines							Lucca et al. (2019)
	Vado di Ferruccio Thrust (VFT)	Central Apennines							Lucca et al. (2019)

based on the Vienna Standard Mean Ocean Water and is reported in V-SMOW.

- Clumped isotopes

The clumped isotope composition of tectonic calcite mineralizations was determined at the ETH Zurich using a Thermo Fisher Scientific 253Plus mass spectrometer which is coupled to a Kiel IV carbonate preparation device, following the method described by Schmid and Bernasconi (2010), Meckler et al. (2014), and Müller et al. (2017). The Kiel IV device includes a custom built PoraPakQ trap held a $-40\text{ }^{\circ}\text{C}$ to eliminate potential organic contaminants. Prior to each sample run, the pressure-dependent backgrounds are determined on all beams to correct for non-linearity effects in the mass spectrometer. During each run, 18 replicates of 90–110 μg of different samples and 5 replicates of each of the three carbonate standards, ETH-1, ETH-2 and 10 replicates ETH-3 (Bernasconi et al., 2018), are analyzed for data normalization. One replicate of the international standard IAEA C2 is analyzed to monitor the long-term reproducibility of the method. All instrumental and data corrections are carried out with the software Easotope (John and Bowen, 2016) using the revised IUPAC parameters for ^{17}O correction (Bernasconi et al., 2018). Results from stable isotope analyses (Table S1) are reported in the conventional δ notation with respect to the Vienna Pee Dee Belemnite (V-PDB) for $\delta^{13}\text{C}$ and Vienna Standard Mean Ocean Water (V-SMOW) for $\delta^{18}\text{O}$.

The new clumped isotope data are presented in the I-CDES scale (Bernasconi et al., 2021) and temperatures are calculated using the Anderson et al. (2021) calibration. Clumped isotope compositions from the older studies compiled in this review were reported in the CDES scale and Δ_{47} -temperatures were calculated using the Kele et al. (2015) calibration. As discussed in Bernasconi et al. (2021), the Δ_{47} values expressed on the CDES scale and calculated with the former accepted values of the ETH standards, which is the case for all pre 2021 publications, are not directly comparable with the newest I-CDES scale.

However, the temperatures can be directly compared with an uncertainty of a few degrees, because all measurements presented in this review and the Kele et al. (2015) calibration used for temperature calculations in older publications were carried out at the ETH laboratory using the ETH Standards (Bernasconi et al., 2018, 2021).

- Burial-thermal modeling

The burial-thermal models have been constrained by organic (vitrinite reflectance) and inorganic (mixed layer illite-smectite) thermal indicators, using Basin Mod® 1-D software (Burnham and Sweeney, 1989; Sweeney and Burnham, 1990). The main assumptions for modeling were: (1) rock decompaction factors apply only to clastic deposits (Sclater and Christie, 1980), (2) variations of seawater depth in time are assumed not to be relevant, because thermal evolution is mainly affected by sediment thickness rather than by water depth (Butler, 1992), (3) thrusting and/or normal faulting ages is constrained by U–Pb dating of tectonic carbonates and/or when available K–Ar dating of *syn*-kinematic clay minerals, (4) thermal modeling is performed using LLNL Easy %R₀ method based on Burnham and Sweeney (1989) and Sweeney and Burnham (1990), (5) exhumation is considered linear for given time intervals and is constrained by thermochronological data when available, (6) geothermal gradient of $25\text{ }^{\circ}\text{C}/\text{km}$ to $30\text{ }^{\circ}\text{C}/\text{km}$ is used for the orogenic buildup and up to $50\text{ }^{\circ}\text{C}/\text{km}$ is used for the extensional faulting with associated Quaternary magmatic/hydrothermal activity in the peri-Tyrrhenian margin, (7) thrusting is considered instantaneous when compared with the duration of deposition of stratigraphic successions, as indicated by theoretical models (Endignoux et al., 1990), and (8) burial rate for distinct sedimentary layers is constrained by their stratigraphic ages and thicknesses.

4.1. Chemical and thermal (dis)equilibria states

In the following, we define the thermal and chemical (dis)equilibria

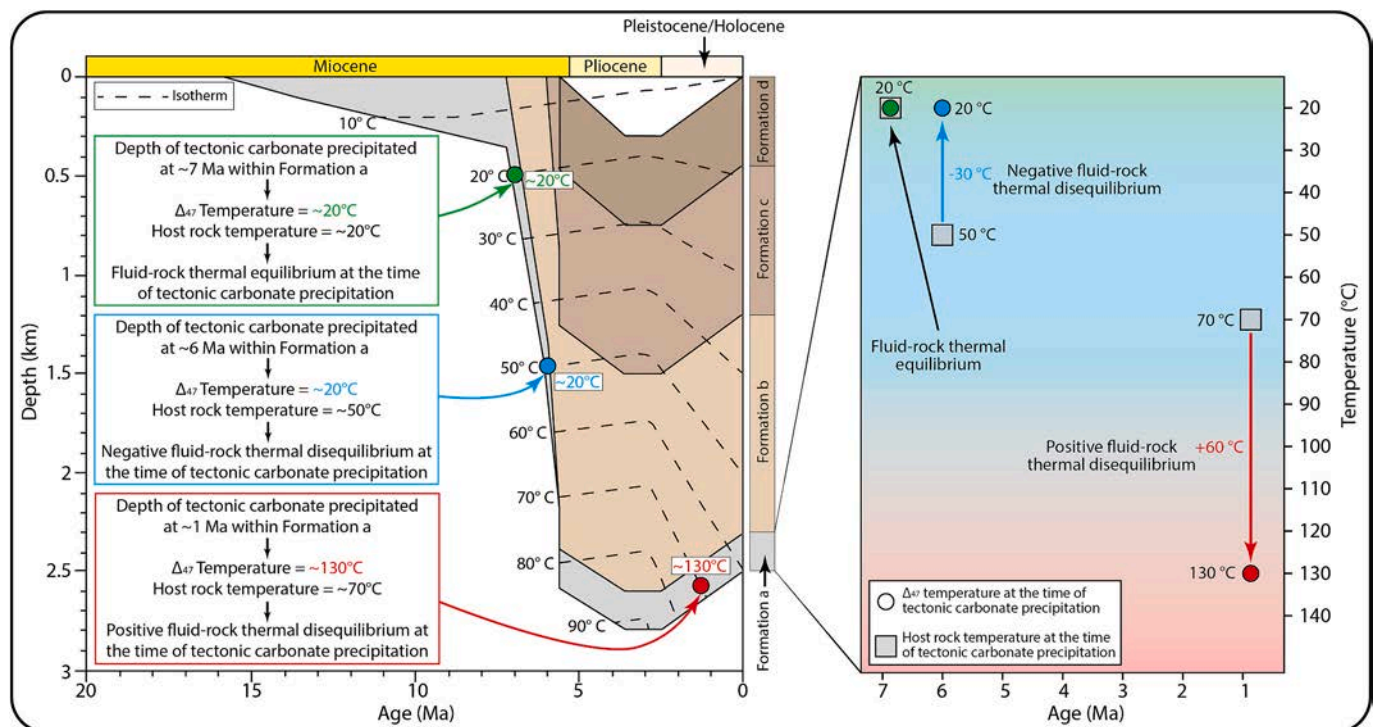


Fig. 6. Conceptual cartoon showing how to calculate the temperature difference between paleofluid and host rock at the time of tectonic carbonate precipitation. The thermal (dis)equilibrium is calculated by subtracting the host rock temperature at the time of tectonic calcite precipitation, which is calculated by the burial-thermal modeling and constrained by U–Pb dating of tectonic calcite mineralizations or by K–Ar dating of *syn*-kinematic clay minerals (see text), to the Δ_{47} temperature of tectonic calcite. Positive or negative thermal disequilibrium indicates fluid warmer or colder than the host rock, respectively.

states detectable for the investigated mineralizing fluid-host rock couplets. We consider a difference of ± 3 ‰ between the mean $\delta^{13}\text{C}$ and mean $\delta^{18}\text{O}$ of host rock and tectonic mineralization as a threshold for isotopic (dis)equilibrium in the fluid-rock system. This value is based on the analytical uncertainties of the methods and on the local and broad range of isotopic composition of host rocks described in Section 5.2. As this threshold is an arbitrary minimum value based on our dataset, this same threshold must be tested and validated in future studies with different datasets and may therefore be modified or adapted to specific cases.

The thermal disequilibrium is evaluated considering the difference between the temperature of the host rock at the time of tectonic calcite precipitation and that of the paleofluid from which the mineralization precipitated (Δ_{47} temperature of tectonic calcite; Fig. 6). The temperature of the host rock at the time of tectonic calcite precipitation is extracted from burial-thermal modeling and constrained by U—Pb or K—Ar dating of the mineralization (Fig. 6). To determine the related uncertainty on temperature value at the time of tectonic carbonate precipitation, we varied the adopted geothermal gradient value by ± 1 °C/km. Any greater variation of the geothermal gradient value produced thermal maturity curves that did not match the paleothermal data and therefore the resulting modeling solution was not acceptable and was ignored. We consider a minimum difference of ± 15 °C between fluid and host rock as the threshold to identify a thermal disequilibrium in the fluid-rock system. This value is representative of significative thermal variations and includes the uncertainties (from 1° to 10 °C) calculated for the host rock temperature. However, the identification of thermal disequilibria may suffer from uncertainties associated with the analytical methods described above. For this reason, we treated and carefully discussed the calculated thermal (dis)equilibria in the context of microstructural and isotopic constraints, and we provide a detailed discussion regarding the uncertainties of thermal data in the Section 5.7.

5. Results and discussion: workflow for detecting chemical and thermal (dis)equilibria

The following workflow (Figs. 7 and S2) provides an ideal methodological approach for the identification of (dis)equilibria in fluid-rock systems and to relate them to a distinct phase of the seismic cycle. The workflow is presented to assist the reader while reading the following sections, while limits, potential, and future perspectives are discussed in Sections 5.7 and 5.8.

5.1. Meso- and micro-structures

After constraining fault geometry and kinematics with field work and sampling, the first step of the workflow is the meso- to micro-structural characterization of tectonic mineralizations, also supported by CL microscopy, to associate them with specific phases of the seismic cycle (Fig. 7), by using the criteria described in Section 2.2.

- Inter-seismic mineralizations

- (i) Calcite veins and slickenfibers with blocky, elongate, and/or fibrous textures are associated with S—C fabrics developed during reverse faulting along the MMT, MTT, VFT, MCT, MGF and MCIT thrusts, and during the tectonic inversion of the MTT. Their association with S—C fabrics is interpreted as the result of inter-seismic pressure-solution processes and associated precipitation under fluid pressure fluctuation, in analogy with similar structures described elsewhere (e.g., Kolb et al., 2005; Meneghini and Moore, 2007; Gratier et al., 2011; Vannucchi, 2019).

Calcite mineralizations along the MTT and MCIT are dull and homogeneously red under CL, respectively, and do not show any zonation. This indicates the absence of significant changes in fluid trace element

composition during precipitation events associated with S—C fabric development (Curzi et al., 2020a; Tavani et al., 2023). Calcite mineralizations along the VFT and MCT are characterized by variable CL colors, indicating that fluids of different origin circulated within the fault zones and mixed during deformation (Lucca et al., 2019).

- (ii) Extensional calcite slickenfibers that decorate bedding-parallel shear planes along the MG fault are characterized by blocky and fibrous textures (Curzi et al., 2021), which, in analogy with structures described in other studies (e.g., Power and Tullis, 1989), are interpreted as the result of fluid overpressure events during inter-seismic flexural slip.

- Pre-/co-seismic mineralizations

- (iii) Meshed calcite veins (hydrofractures) with a blocky texture along the MG have been interpreted as the result of pre-/co-seismic deformations associated with fluid overpressure events and associated hydrofracturing (Curzi et al., 2021). Such an interpretation is corroborated by meso- and microstructural evidence from other studies (e.g., Woodcock et al., 2007).

- Co-seismic mineralizations

- (iv) Comb veins and slip-parallel veins with blocky and elongate blocky textures along the VRF, are interpreted as co-seismic structures (Smeraglia et al., 2018). By analogy, we interpret comb veins on the MMF and comb veins and cement in fault breccias organized in bands orthogonal to the VGFMF as the result of possible co-seismic opening and fluid input and post-seismic sealing. Observations in CL on the elongate blocky mineralizations from the VRF document the presence of different generations of zoned calcite crystals characterized by different CL colors. This is consistent with a change in fluid chemistry from one crystallization event to another and within each event (Smeraglia et al., 2018).
- (v) Sub-vertical veins characterized by internal blocky textures and developed during fault segmentation of the AFS have been interpreted as co-seismic structures (Vignaroli et al., 2020), consistently with structural evidence of active tectonics derived from other studies (e.g., Peacock and Parfitt, 2002). These dilatant structures resulted from the last structural increments at the tips of isolated fault strands, where local stress perturbation controlled the structural permeability of the AFS to pulses of vertical infiltration of surficial/shallow derived fluids.
- (vi) Veins and slickenfibers arranged along the fault strands of the MMRF are the products of channelized, fault-parallel fluid circulation in response to co-seismic events of reactivation and dilatancy of the main slip surface (Vignaroli et al., 2022), consistently with other studies (e.g., Fondriest et al., 2012; Delle Piane et al., 2017; Coppola et al., 2021). The Authors proposed a scenario of cyclic fault-fluid interactions in the MMRF within a recurrence time of 10–15 ka between successive co-seismic events. Different CL signatures were observed in mineralizations sampled along the MMRF, suggesting that meteoric-dominated fluids were contaminated by different fluids during multiple fault reactivations (Vignaroli et al., 2022).

5.2. Carbon and oxygen isotope (dis)equilibria

As a second step, to identify isotopic (dis)equilibria in the fluid-rock system (Figs. 7 and S2c), we analyze $\delta^{18}\text{O}$ and $\delta^{13}\text{C}$ of the host rock and mineralizations (Fig. 8) plotting $\delta^{18}\text{O}$ and $\delta^{13}\text{C}$ (Figs. 9 and 10) as well as $\delta^{18}\text{O}$ vs. $\delta^{13}\text{C}$ (Figs. 11 and 12) data. The analysis is conducted separately for compressional (MTT, MGF, MMT, VFT, MCT, MCIT) and extensional (VRF, VGFMF, MMF, AFS, and MMRF) faults.

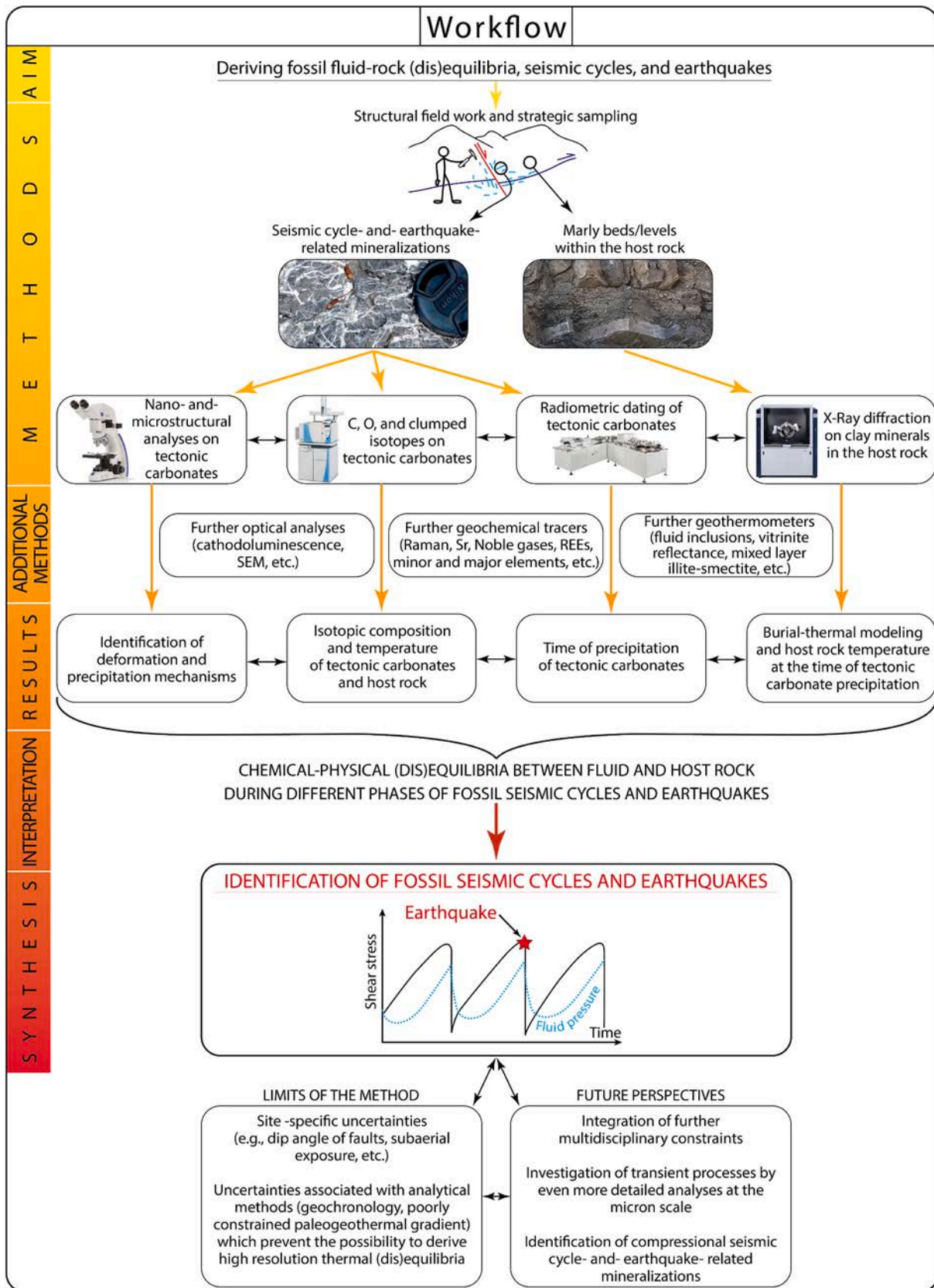


Fig. 7. Workflow for reconstructing the fluid-rock (dis)equilibria during fault activity to identify phases of the seismic cycle and fossil earthquakes. The workflow integrated field observations and sampling of seismic cycle-related mineralization and host rock with microstructural, geochemical, mineralogical, and geochronological analyses to identify chemical-physical (dis)equilibria in fluid-rock systems and retrieve fossil earthquakes.

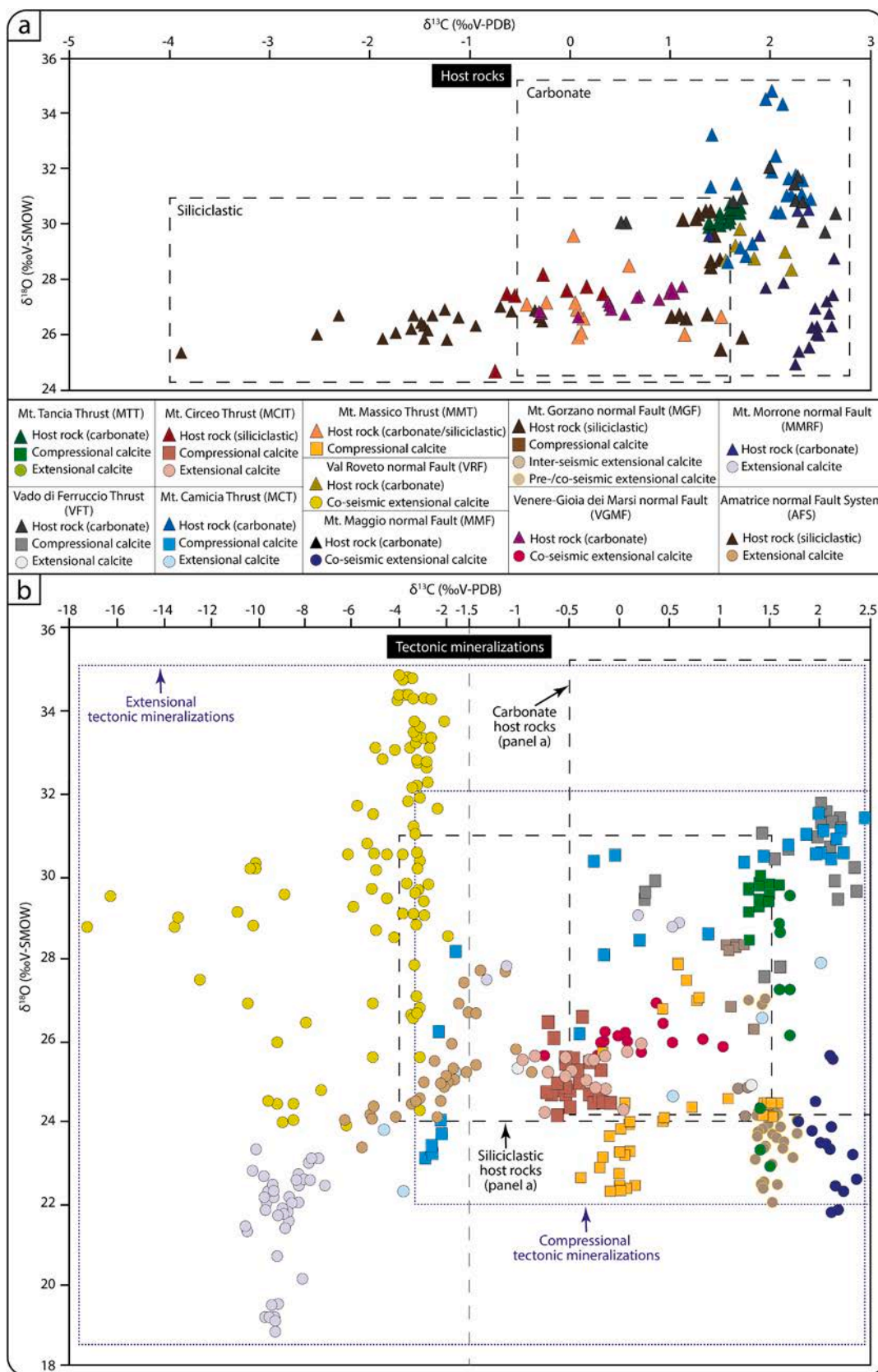


Fig. 8. (a) $\delta^{18}\text{O}$ ‰ (V-SMOW) vs. $\delta^{13}\text{C}$ ‰ (V-PDB) diagram for the host rocks of the different faults. (b) $\delta^{18}\text{O}$ ‰ (V-SMOW) vs. $\delta^{13}\text{C}$ ‰ (V-PDB) diagram for tectonic calcite mineralizations (compressional and extensional). The $\delta^{13}\text{C}$ scale in (b) is enlarged for values lower than -2‰. The whole isotopic composition of carbonate and siliciclastic host rocks are shown by the dotted black rectangles. The whole isotopic composition of compressional and extensional tectonic calcite mineralizations are shown by the dotted blue rectangles.

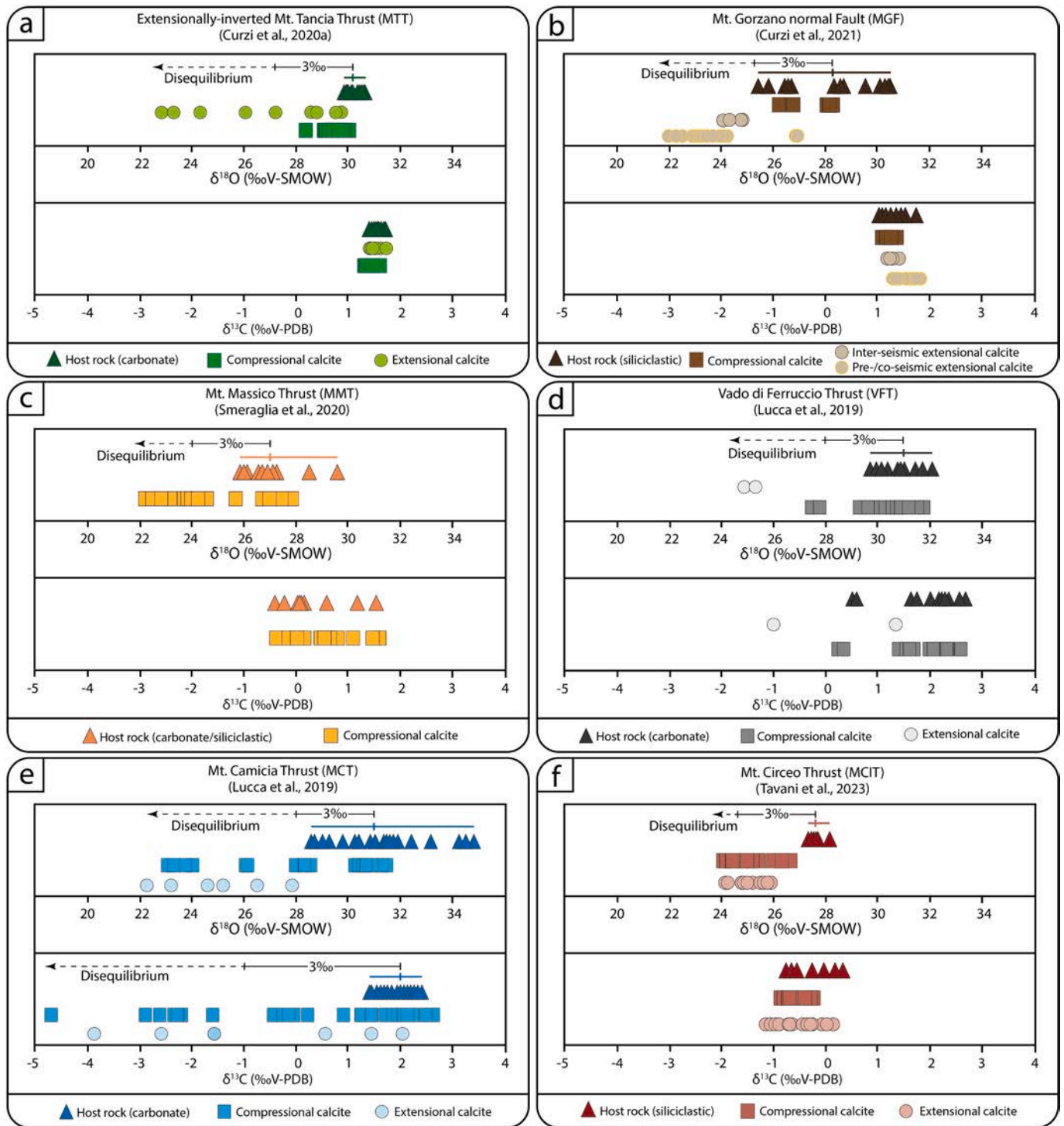


Fig. 9. $\delta^{18}\text{O}$ ‰ (V-SMOW) and $\delta^{13}\text{C}$ ‰ (V-PDB) diagram for tectonic calcite mineralizations and host rock along different thrusts in the Apennines (for the location of each structure see Fig. 1a). Lines and ticks indicate the host rock isotopic range and average. (a) Along the MTT, the $\delta^{18}\text{O}$ composition of extension-related mineralizations and host rock indicate an isotopic disequilibrium. (b) In the MGF, extension-related calcite mineralizations are characterized by an isotopic (in terms of $\delta^{18}\text{O}$) disequilibrium with respect to the host rock. (c) Along the MMT, compressional calcite mineralizations and host rocks are characterized by an isotopic disequilibrium in terms of $\delta^{18}\text{O}$ composition. (d) Compressional calcite mineralizations along the VFT show an overall isotopic equilibrium with host rocks. Calcite mineralizations associated with later extensional faults cutting across the VFT show an isotopic ($\delta^{18}\text{O}$) disequilibrium with the host rock. (e) Compressional and extensional calcite mineralizations along the MCT show a clear $\delta^{18}\text{O}$ and $\delta^{13}\text{C}$ isotopic disequilibrium with respect to host rocks. (f) Compressional and extensional calcite mineralizations along the Mt. Circeo Thrust (MCIT) show slight $\delta^{18}\text{O}$ isotopic disequilibrium with the host rock.

The $\delta^{13}\text{C}$ and $\delta^{18}\text{O}$ values of the carbonate host rocks vary between -0.5‰ to $+3\text{‰}$ and between $+24\text{‰}$ to $+35\text{‰}$, respectively (Figs. 8–12). Carbonate cements within siliciclastic host rocks show a broader range of $\delta^{13}\text{C}$ values between -4‰ and $+2\text{‰}$, and of $\delta^{18}\text{O}$ values between 24‰

and 30‰ (Figs. 8–12). Compressional calcite mineralizations are characterized by $\delta^{13}\text{C}$ varying from 0‰ to $+3\text{‰}$ and $\delta^{18}\text{O}$ from 22‰ to $+34\text{‰}$, in the range of their respective host rocks (Figs. 9 and 11), indicating isotopic equilibrium between fluids and host rock at the time of

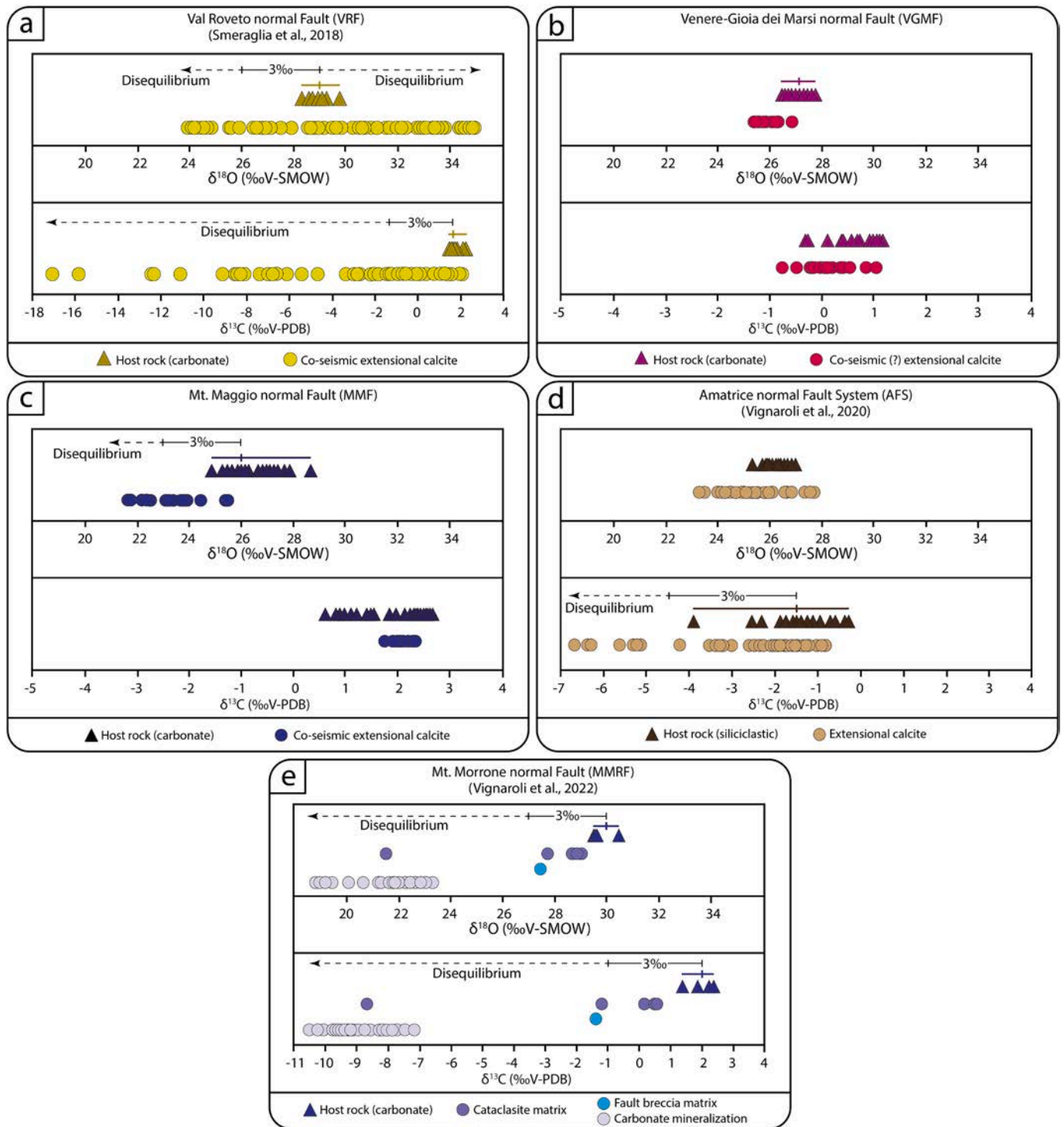


Fig. 10. $\delta^{18}\text{O}$ ‰ (V-SMOW) and $\delta^{13}\text{C}$ ‰ (V-PDB) diagram for tectonic calcite mineralization and host rock along different normal faults in the Apennines (for the location of each structure see Fig. 1a). Lines and ticks indicate the host rock isotopic range and average. Along each structure, except for the VGMF, a clear isotopic disequilibrium between tectonic calcite mineralization and host rock is evident.

precipitation. Limited isotopic disequilibria are observed for compressional structures and are marked by tectonic calcite mineralization characterized by $\delta^{18}\text{O}$ and/or $\delta^{13}\text{C}$ values lower than the host rock (Figs. 8b, 9c, d and f, and 11c, d and f). Moreover, calcite mineralizations associated with the out-of-sequence activity of the MCT displays a marked isotopic disequilibrium with $\delta^{13}\text{C}$ and $\delta^{18}\text{O}$ values lower than those observed for the host rock (Figs. 9e and 11e).

Calcite mineralizations associated with extensional deformations

typically exhibit isotopic disequilibrium with respect to the host rock (Figs. 9–12) as they are characterized by lower $\delta^{13}\text{C}$ and $\delta^{18}\text{O}$ values. The most evident disequilibrium is observed along the VRF, with a decrease of $\delta^{13}\text{C}$ values from +3‰ to -5‰ (Figs. 10a and 12a) and along the MMRF with a decrease of $\delta^{13}\text{C}$ values from 0‰ to -11‰; (Figs. 10e and 12e), where co-seismic comb veins and mineralizations have been collected (Smeraglia et al., 2018; Vignaroli et al., 2022). A clear isotopic disequilibrium is also observed for pre-/co-seismic extensional calcite

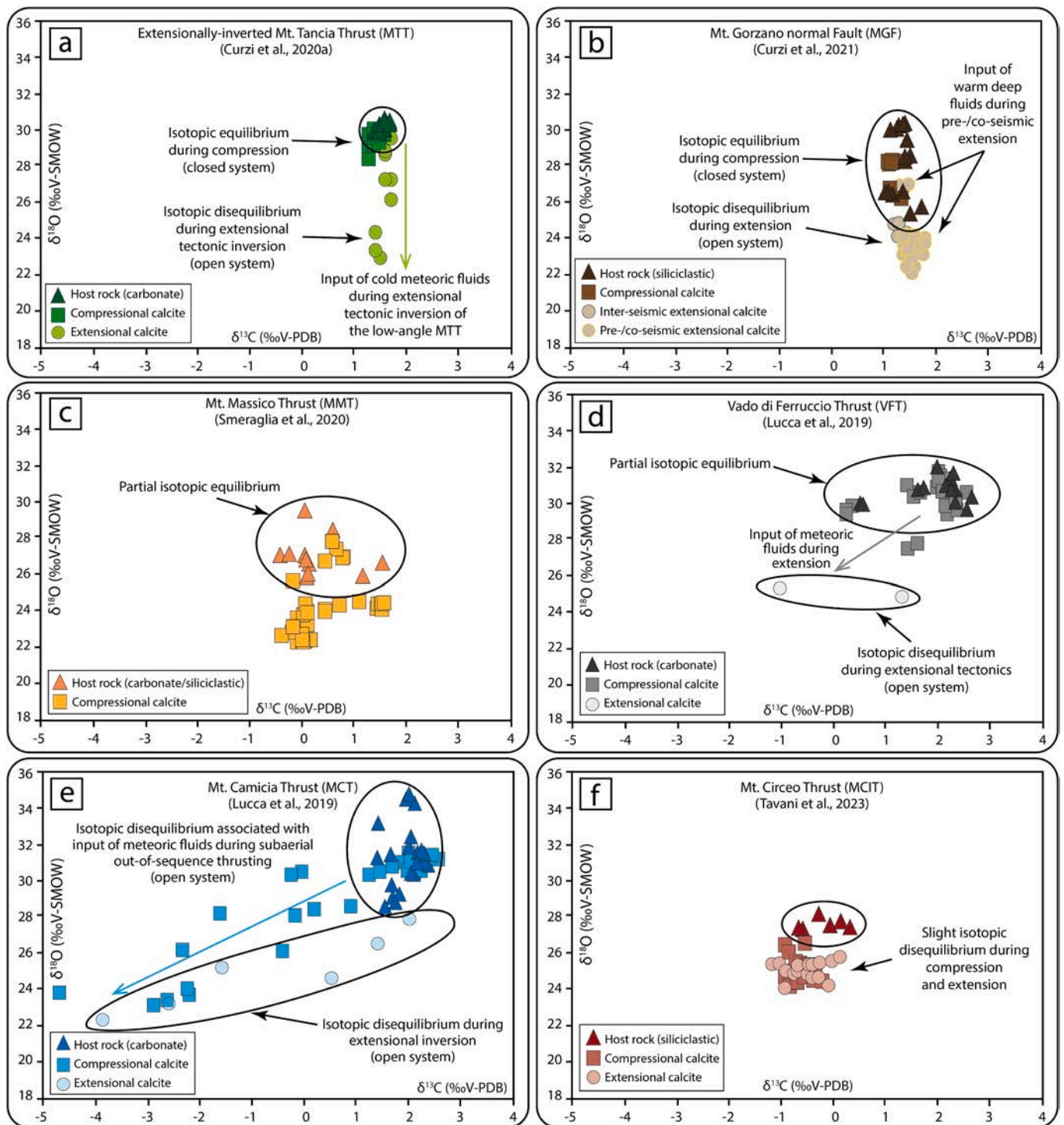


Fig. 11. $\delta^{18}\text{O}$ ‰ (V-SMOW) vs. $\delta^{13}\text{C}$ ‰ (V-PDB) diagram for tectonic calcite mineralizations and host rock along different thrusts in the Apennines (for the location of each structure see Fig. 1a). (a) Along the MTT, calcite mineralizations associated with S–C compressional fabric display a clear isotopic equilibrium with respect to the host rocks. Extension-related calcite mineralizations are characterized by a decrease of $\delta^{18}\text{O}$ ‰ values indicating an opening of the fluid system during post-compressive extensional tectonics. (b) In the MGF, calcite mineralizations associated with S–C compressional fabric display a clear isotopic equilibrium with respect to the host rocks. Extension-related calcite mineralizations are instead characterized by decreasing $\delta^{18}\text{O}$ ‰ values indicating an opening of the fluid system during the post-compressive extensional tectonics. (c) Along the MMT, calcite mineralizations associated with S–C compressional fabric show a partial isotopic equilibrium with respect to the host rocks. Most calcite mineralizations display $\delta^{18}\text{O}$ ‰ values lower than those from the host rocks. (d) Calcite mineralizations associated with S–C compressional fabric along the VFT show a substantial isotopic equilibrium with the host rocks. Calcite mineralizations associated with later extensional faults cutting across the VFT show an isotopic disequilibrium with the host rock. (e) Calcite mineralizations associated with S–C compressional fabric along the MCT (out-of-sequence thrust) show a clear isotopic disequilibrium with respect to the host rocks highlighted by lower $\delta^{18}\text{O}$ and $\delta^{13}\text{C}$ values. The isotopic disequilibrium is also shown for calcite mineralizations associated with the extensional inversion of the MCT. (f) Compressional calcite mineralizations within S–C fabrics and extensional slickenfibers along normal faults along the Mt. Circeo Thrust (MCIT) showing slight isotopic disequilibrium with the host rock during compression and extension.

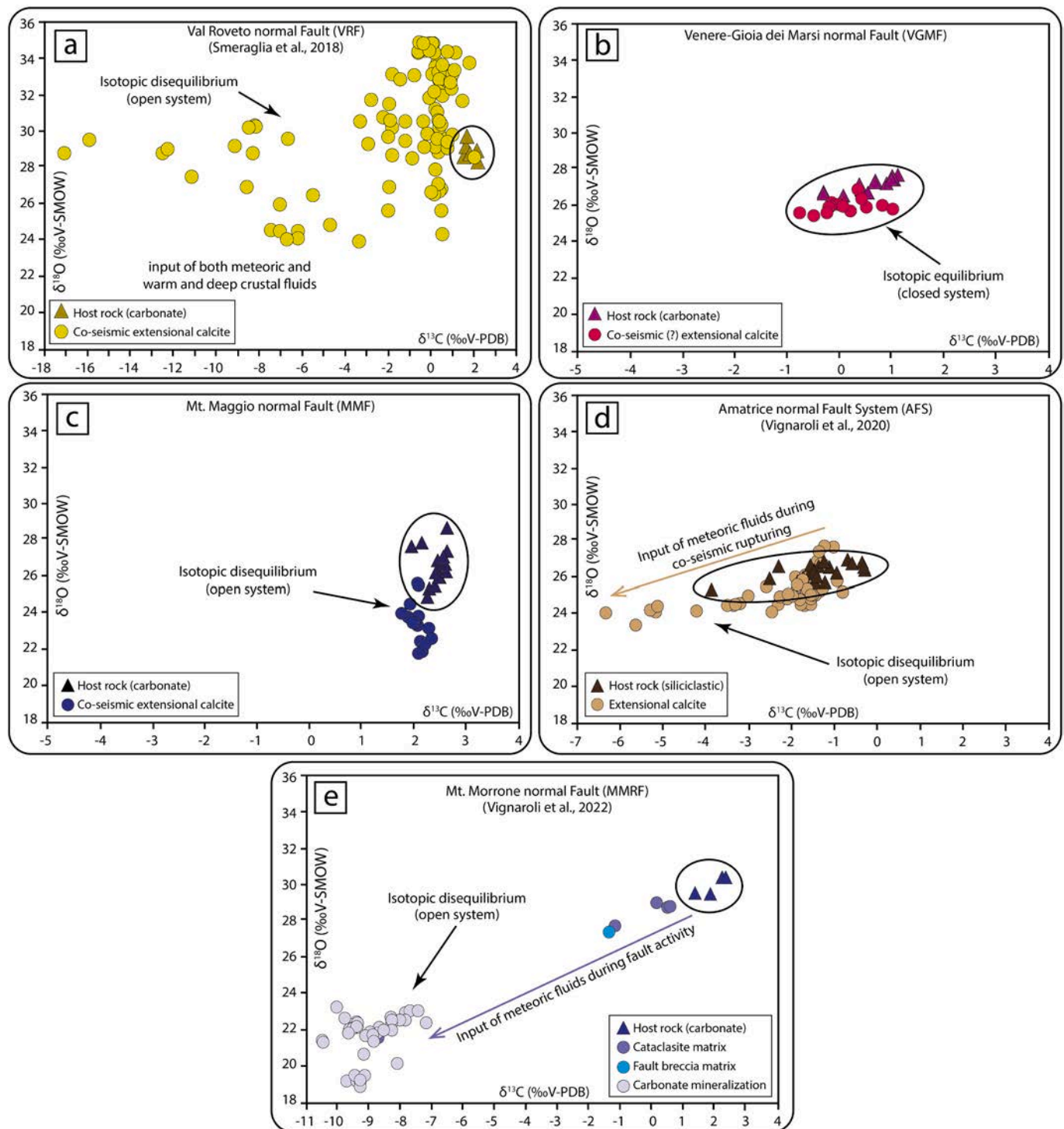


Fig. 12. $\delta^{18}\text{O}$ ‰ (V-SMOW) vs. $\delta^{13}\text{C}$ ‰ (V-PDB) diagram for tectonic calcite mineralization and host rocks along different normal faults in the Apennines (for the location of each structure see Fig. 1a). Along each structure, isotopic disequilibrium between tectonic calcite mineralization and host rock is evident. Along the VGMF a very limited disequilibrium is observed, and a higher number of data is necessary to better identify the isotopic (dis)equilibrium state in the fluid-rock system.

mineralization along the MGF, which are characterized by $\delta^{18}\text{O}$ values up to 9‰ lower (from +31‰ to +22‰) than the host rock (Figs. 9b and 11b). Along inverted structures (VFT, MCT, MTT and MGF; Figs. 9b, d, and e and 11b, d, and e), extensional mineralizations display $\delta^{18}\text{O}$ and/or $\delta^{13}\text{C}$ that are markedly lower than host rock and compressional mineralizations. Mineralizations from the VGMF show $\delta^{18}\text{O}$ isotopic equilibrium (Figs. 10b and 12b).

5.3. Thermal (dis)equilibria

In the third step of our workflow (Figs. 7 and S2d-e), we calculate the temperature difference between paleofluid and host rock by subtracting the host rock temperature at the time of tectonic calcite precipitation from the Δ_{47} temperature of calcite mineralizations.

Fig. 13 shows the 1D burial-thermal modeling of the faulted successions along the MGF (Fig. 13a), MTT (Fig. 13b), MMT (Fig. 13c), and

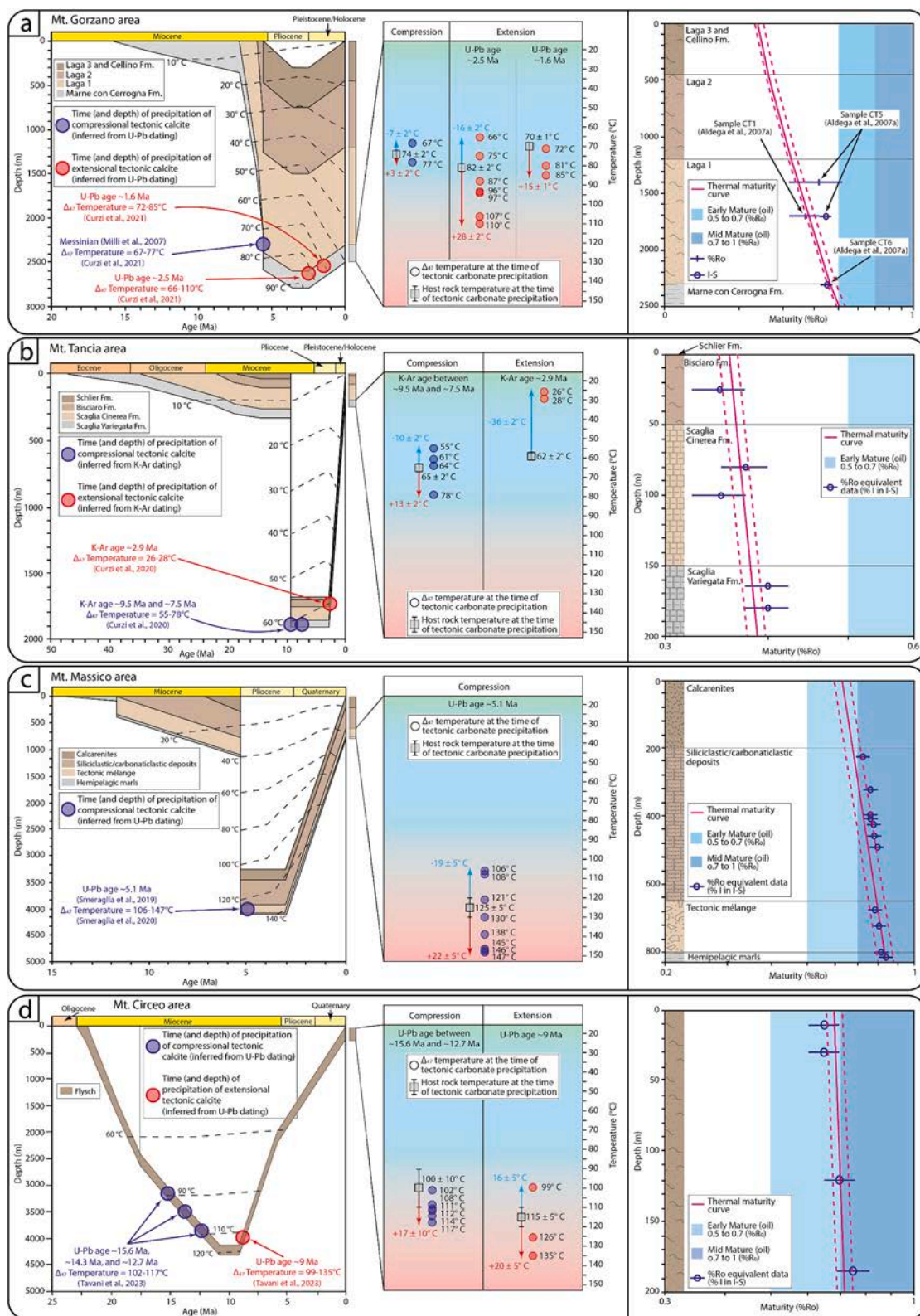


Fig. 13. (a) Burial-exhumation history of the sedimentary succession deformed in the Mt. Gorzano area, with thrusting constrained by stratigraphic and biostratigraphic constraints from Milli et al. (2007) and exhumation constrained by U–Pb ages from Curzi et al. (2021). The thermal maturity curve calibrated against illite content in mixed layers I–S and vitrinite reflectance data from Aldega et al. (2007a) is shown. (b) Burial-exhumation history and thermal maturity curve (calibrated against illite content in mixed layers I–S converted into Ro% equivalent values) of the sedimentary succession deformed in the Mt. Tancia area (from Curzi et al., 2020a). (c) Burial-exhumation history and thermal maturity curve (calibrated against illite content in mixed layers I–S converted into Ro% equivalent values) of the sedimentary succession deformed in the Mt. Massico area (from Smeraglia et al., 2019). (d) Burial-exhumation history and thermal maturity curve (calibrated against illite content in mixed layers I–S converted into Ro% equivalent values) of the sedimentary succession deformed in the Mt. Circeo (MCIT; modified after Tavani et al., 2023). The ages and Δ_{47} temperatures of tectonic calcite mineralizations and the temperature difference between fluid and host rock at the time of tectonic calcite precipitation are shown.

MCIT (Fig. 13d), in which the depth at which tectonic carbonates precipitated and the temperature of the host rocks at the time of tectonic carbonate precipitation are highlighted (Section 4 and Fig. 6). Fig. 14 is derived from Fig. 13 and summarizes paleofluid and host rock temperatures.

The MTT and MGF display a thermal equilibrium, with a temperature difference between paleofluid and host rock of -10 °C and +13 °C and of -7 °C and +3 °C, respectively, during compression (Figs. 13a, b, and 14). The thermal difference between paleofluid and host rock during compression along the MCIT indicates a slight disequilibrium, with fluids up to 17 °C warmer than the host rock (Figs. 13d and 14). The MMT display a thermal disequilibrium with fluids up to 19 °C colder and 22 °C warmer than the host rock (Figs. 13c and 14).

The most evident thermal disequilibria are calculated for extensional

faulting, with paleofluid temperatures 36 °C colder than the host rock along the MTT (Figs. 13b and 14), and colder and warmer along the MCIT (from -16 °C to +20 °C; Figs. 13d and 14) and MGF (from -16 °C to +28 °C; Figs. 13a and 14). Along the MGF, pre-/co-seismic extensional deformations (and precipitation of blocky mesh veins) occurred with thermal disequilibrium (with fluids -16 °C colder and +28 °C warmer than the host rocks) larger than that calculated in the same area during inter-seismic extensional deformations (with fluids +15 °C warmer than the host rocks and responsible for precipitation of slickenfibers; Figs. 13a and 14). As a whole, even considering the errors associated with the host rock temperatures, thermal disequilibria during extensional deformations are evident.

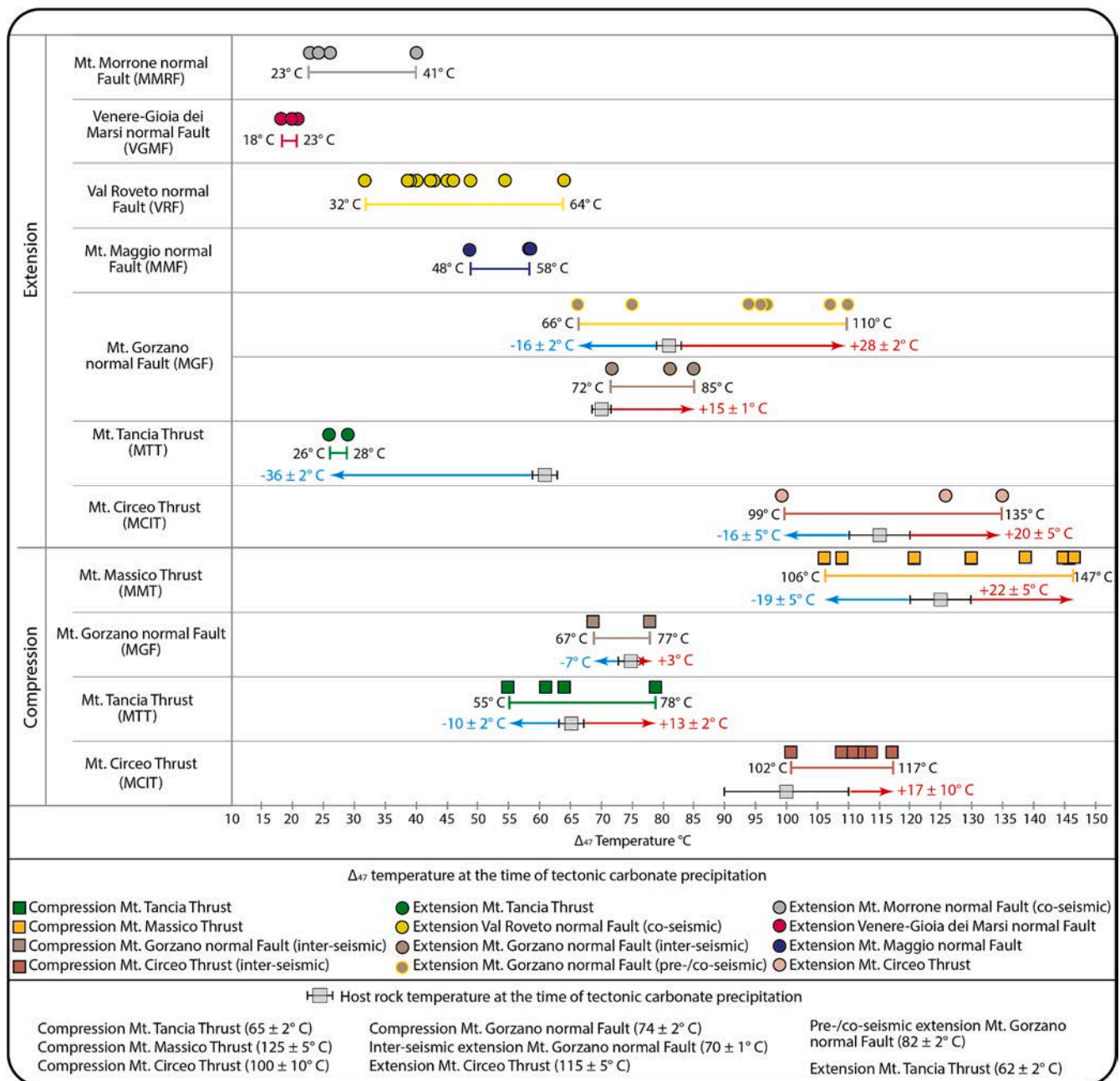


Fig. 14. Ranges of paleofluid (Δ_{47}) and host rock temperature. Segments and numbers indicate the differences between paleofluid and host rocks temperature at the time of tectonic calcite precipitation, thus showing thermal disequilibria (both positive and negative) in the fluid-rock systems at the time of tectonic calcite precipitation.

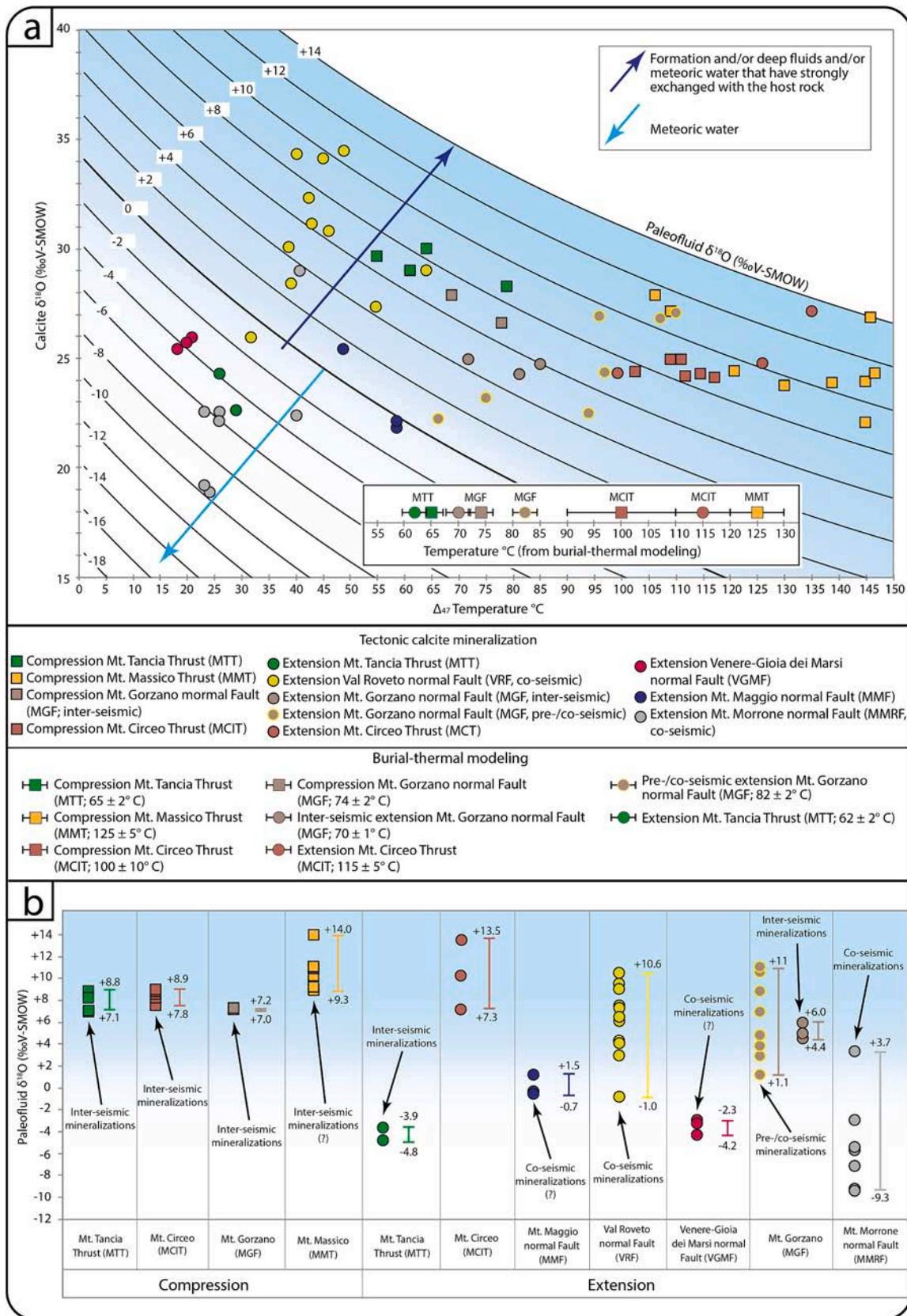
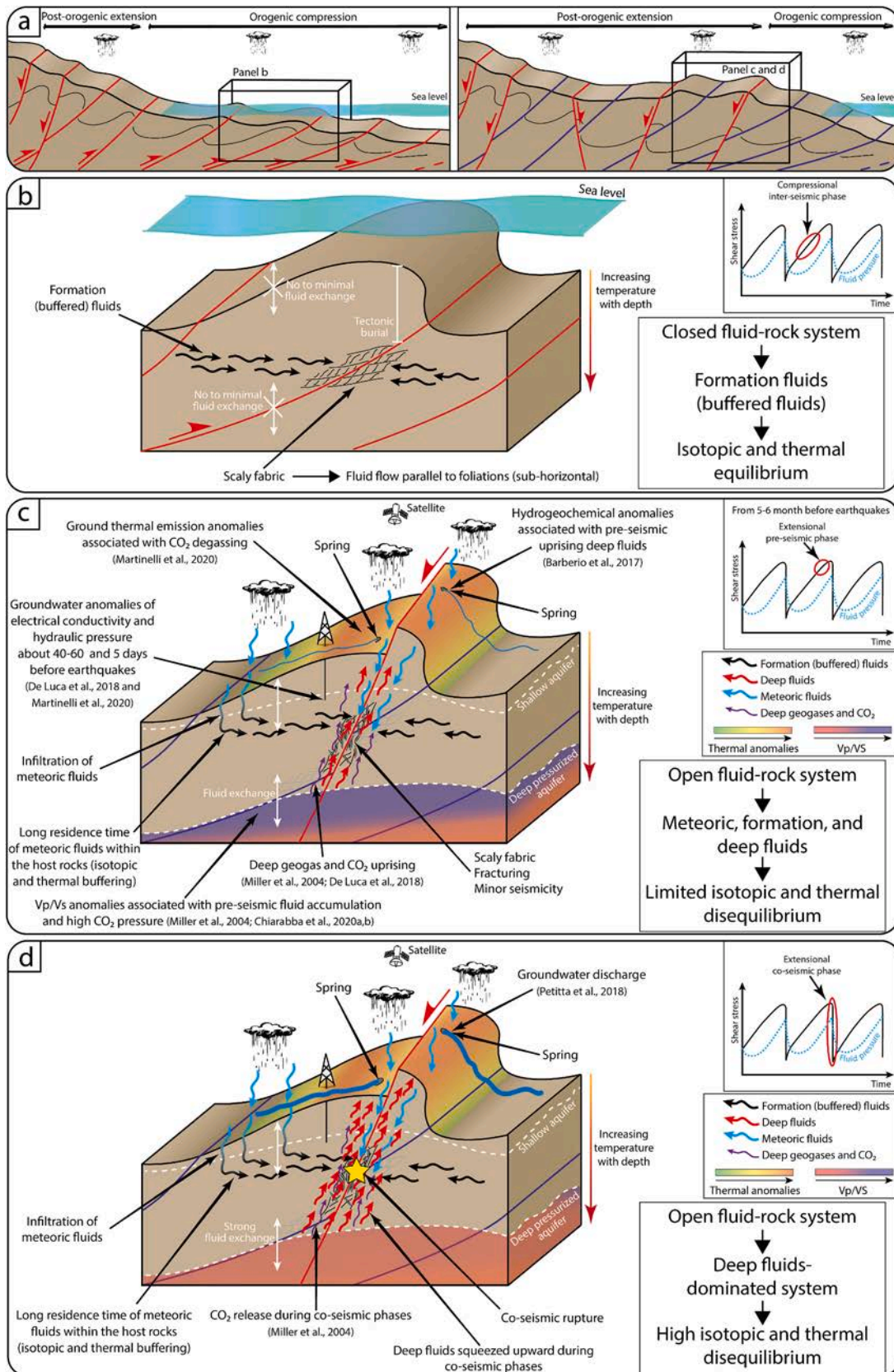


Fig. 15. (a) Oxygen isotope fractionation during equilibrium precipitation: $\delta^{18}\text{O}$ of tectonic calcite mineralization and paleofluid compositions (curves) as a function of temperature. Circles and squares in the inset represent the temperatures experienced by the host rocks at the time of calcite precipitation during extensional and compressional tectonics, respectively. (b) Paleofluid $\delta^{18}\text{O}$ composition of tectonic calcite mineralizations.



(caption on next page)

Fig. 16. Model of fluid circulation during compressional and post-compressional extensional deformation in the Apennines. (a) Schematic evolution of the Apennine wedge which developed under orogenic compressional deformation accommodated by thrusts and folds, followed by post-compressional extensional tectonics and associated normal faulting. (b) Thrust-related fluid circulation characterized by a closed fluid system, in which formation fluids do not (or limitedly) interact with external fluids. Scaly fabrics, associated with inter-seismic deformations, promote an along-foliation (sub-horizontal) fluid circulation, thus contributing to prevent the ingress of external fluids. (c) Fluid circulation during extensional pre-seismic phase in which the fluid system is open and meteoric and deep fluids mix with formation fluids. During pre-seismic phases (from 5 to 6 months before earthquakes; e.g. Skelton et al., 2014; Barberio et al., 2017; Chiarabba et al., 2020), deep fluids uprise and accumulate at depth, leading to fluid overpressure. Only some deep fluids (including CO₂, and anomalous elements such as As, V, and Fe) leak upward and give rise to the pre-seismic ground thermal emission anomalies, groundwater anomalies of electrical conductivity and hydraulic pressure, and hydrogeochemical anomalies in some springs (e.g., Wang and Manga, 2021). (d) During co-seismic extensional phases, pressurized fluids at depth trigger seismic extensional faulting so that fracture corridors permit rapid and abundant upward flow of fluids and associated groundwater discharge during the syn-/post-seismic phase. The model represented in panels c and d is a synthesis of structural and geochemical evidence from this review, hydrogeochemical evidence from Barberio et al. (2017), De Luca et al. (2018), Petitta et al. (2018), Boschetti et al. (2019), Barbieri et al. (2020), Chiodini et al. (2020), Martinelli et al. (2020), and Mastrorillo et al. (2020), and geophysical evidence from Miller et al. (2004), and Chiarabba et al. (2020, 2022).

5.4. Oxygen isotope composition of paleofluids

The fourth step derives the source(s) of fluids by calculating their $\delta^{18}\text{O}$ using the Δ_{47} -based temperatures (Fig. 7). Fig. 15a shows the $\delta^{18}\text{O}$ of calcite mineralizations plotted against the $\delta^{18}\text{O}$ of the fluid (black curves) calculated from Δ_{47} -based temperatures. Fig. 15b summarizes the calculated paleofluid $\delta^{18}\text{O}$. Calculated fluid compositions during compression range between +7‰ and +14‰ (MTT, MCIT, and MGF). Fluid $\delta^{18}\text{O}$ for extensional mineralizations ranges from -9.3‰ to +13.5‰. The broadest range of fluid $\delta^{18}\text{O}$ in extensional co-seismic mineralizations are from the VRF ranging from -1‰ to +10.6‰, pre-/co-seismic calcite mineralizations from the MGF ranging from +1.1‰ to +10.6‰, and co-seismic calcite mineralizations from the MMRF ranging from -9.3‰ to +3.7‰ (Fig. 15).

Our data indicate the involvement of formation and/or deep fluids ($\delta^{18}\text{O} > 7\text{‰}$) during compressional deformations. Alternatively, such a composition can arise from meteoric fluids with intensive fluid-rock interaction and low fluid-rock ratios. However, compressional deformations along the Apennine mostly occurred under the sea level. Therefore, it is likely that the fluids involved in compressional deformations were marine fluids trapped within the host rocks at the time of sedimentation below sea level. Hence, considering also the isotopic equilibria in compressional fluid-rock systems discussed in Section 5.3 and shown in Figs. 9 and 11, the analyzed mineralizations formed during compressional deformation precipitated from formation/pore fluids entrapped during the sedimentation and that have strongly interacted with the host rocks for a long time and were close to isotopic equilibrium with the host rock.

As shown in Fig. 15a, extensional mineralizations precipitated from both formation and/or deep fluids (with $\delta^{18}\text{O}$ values higher than 0‰) and meteoric water (with negative $\delta^{18}\text{O}$ values).

5.5. Tectonic processes, seismic cycling, and fluid-rock interaction

In the last step of our workflow (Fig. 7), the data are interpreted in the framework of the seismic cycle in compressional and extensional systems.

5.5.1. Compressional systems

The compressional calcite mineralizations with elongate blocky or fibrous textures presented in this study are associated with scaly fabrics and therefore can be interpreted as inter-seismic. In this study, we did not recognize any co-seismic compressional mineralization. This may be possibly due to their only partial preservation, likely caused by the long-lived tectonic activity of the studied faults, or alternatively by their less common formation compared to extensional tectonic settings. Inter-seismic compressional mineralizations associated with S—C fabrics exhibit limited variability of fluid $\delta^{18}\text{O}$ and limited thermal disequilibria between fluid and host rock (Figs. 9, 11, 14, 15, and 16a and b). For example, similar temperature values were obtained for fluid and host rock along the MTT and MGF, where 10 °C colder and 13 °C warmer fluids were involved in inter-seismic compressional deformations

(Figs. 13a, b, and 14). The same mineralizations show isotopic equilibrium with their host rock (Figs. 9a, b and 10a and b). This evidence suggests that inter-seismic compressional deformation, which was active when the rocks were still below the sea level, occurred in closed fluid systems or systems that were limitedly open to sea water and low fluid-rock ratios (Fig. 16b). This is consistent with the first studies of paleofluid circulation along faults in the Apennines (Conti et al., 2001; Ghisetti et al., 2001; Agosta and Kirschner, 2003; Fig. S1), which proposed a “semi-closed” fluid system during compression. A similar closed fluid system has also been documented during orogenic-related folding in the Northern Apennines (Beaudoin et al., 2020; Labeur et al., 2021).

The S—C tectonites are generally associated with low strain rates and are generally parallel to fault planes (Curzi et al., 2020a, 2021; Smeraglia et al., 2020a). Their geometric anisotropy tends to promote fluid flow parallel to the foliation rather than across it (e.g., Sibson and Scott, 1998; Curzi et al., 2023; Vannucchi, 2019; Cruset et al., 2023; Fig. 16b), as also recently documented by in situ outcrop permeability measurements along a thrust zone exposed in the Northern Apennines (Curzi et al., 2024). Lateral sub-horizontal fluid circulation implies limited isotopic and thermal disequilibria between fluid and rock and is consistent with the involvement of host rock derived fluids in a closed system, as indicated by homogeneous CL of mineralizations, similar to that of the host rock (MTT; Curzi et al., 2020a; Fig. 15b). Moreover, the low-permeability evaporites, which usually represent the regional basal decollement in the Apennines thrust-fault system, may have also contributed to prevent the upflow of deep fluids during thrusting (e.g., Beaudoin et al., 2020), as also documented in the Pyrenees (Cruset et al., 2023).

Our dataset highlights some differences with respect to the aforementioned fluid circulation model. A non-negligible difference in temperature between fluid and host rock is observed in the MMT, where up to 19 °C colder and 22 °C warmer fluids were involved (Figs. 13c and 14). For the same fault, isotopic disequilibrium between calcite mineralizations and host rock is also documented (Figs. 9c and 11c). Fluids involved in the MMT have been interpreted as pore fluids trapped within siliciclastic rocks (flysch) deposited about 5 Ma before thrusting (Fig. 13c) and mobilized in a closed fluid system (Smeraglia et al., 2020a). Hence, the relatively short residence time of fluids within the host rocks was proposed as a possible explanation for the apparent isotopic disequilibrium between tectonic mineralizations and host rocks (Figs. 9c and 11c; Smeraglia et al., 2020a). In other words, formation fluids were partially isotopically buffered and thermally equilibrated by a limited fluid-rock interaction before thrusting. Similar observations and interpretations have been proposed for the slight isotopic disequilibrium in flysch-hosted compressional tectonic mineralizations along the MCIT (Figs. 9f, 11f, and 13d; Tavani et al., 2023). If these interpretations are correct, then the residence time of fluids in closed systems is crucial in the determination of chemical (dis)equilibria.

Moreover, based on C, O, and Sr isotopes, Lucca et al. (2019) proposed the involvement of host rock-derived fluids together with meteoric fluids under out-of-sequence subaerial thrusting along the MCT (Figs. 9e and 11e). Such fluid mixing is also documented by the different

CL colors of the mineralizations (Lucca et al., 2019).

In summary, the Apennines thrust fault systems were typically characterized by the involvement of residential fluids that could be either completely or partially isotopically re-equilibrated with the host rock. Alternatively, thrust fault systems were characterized by mixing of residential fluids with (i) sea water in limitedly upward open system below the sea level or (ii) meteoric fluids in an upward open subaerial system.

5.5.2. Extensional systems

With the only exception of the VGMF, where fluids associated with fault activity had residence times long enough to equilibrate with host rock, along normal faults we observe a high variability of fluid $\delta^{18}\text{O}$ as well as isotopic and thermal disequilibria (both positive and negative) between mineralizations and host rock (Figs. 9a, b, 10, 11a, b, 12, 14, and 15). This indicates that extensional deformation tends to occur within open systems characterized by azimuthal/vertical infiltration of exotic fluids (Fig. 16a and c). More specifically, different degrees of fluid mixing, possibly related to different volumes of involved deep fluids (including meteoric fluids infiltrated and buffered at depth), are identified for distinct stages of the seismic cycle (Fig. 16c and d). Fibrous mineralizations associated with inter-seismic scaly fabrics along the extensionally-inverted MTT formed in an upward open fluid-rock system, where meteoric fluids were responsible for the decrease in $\delta^{18}\text{O}$ and the negative thermal disequilibrium with fluids 36 °C colder than the host rock (Figs. 11a, 14, and 15). Similarly, the involvement of meteoric fluids has been documented by the decrease of $\delta^{13}\text{C}$ and $\delta^{18}\text{O}$ of carbonates formed during the negative (extensional) inversion of the VFT (Fig. 9d) and MCT (Fig. 11e; Lucca et al., 2019).

Co-seismic extensional structures associated with the AFS formed in an upward open system. Indeed, as testified by $\delta^{13}\text{C}$ values from calcite mineralizations ranging between $\sim 0\text{‰}$ and -7‰ (Figs. 10d and 12d), meteoric fluids infiltrated during co-seismic surface ruptures (Vignaroli et al., 2020). In contrast, co-seismic extensional deformations along the MMRF occurred in an upward and downward open fluid system, in which dominant meteoric fluids mixed with deeper fluids in response to co-seismic rejuvenation of the structural permeability of the fault zone (Vignaroli et al., 2022). Mixing between meteoric and deep fluids is documented by the low $\delta^{13}\text{C}$ values of tectonic carbonates ranging from 0‰ to -11‰ (Figs. 10e and 12e), the calculated fluid $\delta^{18}\text{O}$ ranging between -9‰ to $+4\text{‰}$ (Fig. 15), the fluid temperatures ranging between $\sim 23^\circ\text{C}$ to $\sim 40^\circ\text{C}$ (Figs. 14 and 15a), and distinct CL colors of tectonic mineralizations (Vignaroli et al., 2022).

Along the MGF, extensional deformation occurred in an upward and downward open fluid system with a variable degree of mixing between formation, meteoric, and deep fluids in distinct phases of the seismic cycle (Curzi et al., 2021). The calculated paleofluid temperature ($72\text{--}85^\circ\text{C}$; Figs. 14 and 15a) for extensional inter-seismic deformation overlaps or is slightly warmer ($+15^\circ\text{C}$) than that experienced by the host rock at the time of precipitation (Fig. 14). This suggests only partial mixing with deeper and warmer fluids (Curzi et al., 2021). On the other hand, the consistently higher temperature recorded by pre-/co-seismic blocky mesh veins, up to 28°C warmer than that of the host rock (Fig. 14), calls for the involvement of deep fluids during pre-/co-seismic deformation (Fig. 16d). Based on the meso- and micro-structures of such veins and REE analyses, Curzi et al. (2021) proposed that pre-/co-seismic extensional deformation along the MGF was associated with impulsive events, in which deep and likely CO_2 -rich fluids were rapidly squeezed upward from a depth of about 3–4 km. Similarly, the variability of calculated fluid $\delta^{18}\text{O}$ of the VFR slip-parallel and comb veins testifies for the involvement of deep (and relatively warm) fluids during co-seismic deformation. These fluids, as documented by Sr isotopes and different CL colors within the same veins, were mixed with fluids that interacted with shallow crustal carbonates (Smeraglia et al., 2018).

The new insights discussed in this study on paleofluid circulation during normal fault activity in the Apennines represent a significant step

forward with respect to the “semi-open to open” definition proposed for the fluid-rock system by Ghisetti et al. (2001) and Agosta and Kirschner (2003); (Fig. S1). Indeed, the fluid-rock system associated with normal faulting in the Apennines seems to be often open both upward and downward with the involvement of exotic fluids in isotopic and thermal disequilibrium with the host rock. We interpret deep fluids as squeezed upward from deep structural levels during co-seismic events (Fig. 16c and d). The different degrees of disequilibrium observed in the analyzed fault systems can be explained by the different efficiency of the co-seismic pump effect or by the role played by the physical characteristics (mainly primary and secondary porosity and permeability) of the lithologies involved in faulting. Moreover, the depth reached by the faults may also affect the observed different degrees of disequilibrium. On this ground, the most remarkable evidence of seismic cycle-controlled fluid-rock system in the Apennines arises from the involvement of deep fluids during co-seismic rupturing along the seismically active MGF (this study; Curzi et al., 2021) and MMRF (Coppola et al., 2021). The involvement of deep fluids in the extensional co-seismic phases is of paramount importance as they represent suitable indicators for the active extensional seismic sequences and earthquakes in the Apennines, as discussed in the next section.

5.6. Implications on ongoing seismicity in the Apennines (and elsewhere)

The concept of fluid-rock chemical-physical (dis)equilibria linked with the seismic cycle derives from recent hydrogeochemical monitoring in seismic areas (e.g., Skelton et al., 2014, 2019; Barberio et al., 2017; Tamburello et al., 2018, 2022; Li et al., 2019; Franchini et al., 2021) and from studies on tectonic mineralizations in the Central Apennines (e.g., Coppola et al., 2021) and northern Iceland (Andr n et al., 2016), which validated chemical-physical anomalies identified before and during recent earthquakes (Skelton et al., 2014; Barberio et al., 2017).

Some recent extensional seismic sequences in the Apennines and elsewhere, with mainshocks up to Mw 6.5, have shown that the pre-seismic (up to about 5 months before the mainshock) and co-seismic phases can be characterized by chemical-physical disequilibria within the fluid-rock systems reflecting the involvement of exotic (deep) fluids flowing upward into the shallow groundwaters (e.g., Barberio et al., 2017; De Luca et al., 2018; Boschetti et al., 2022; Skelton et al., 2019; Barbieri et al., 2021; Franchini et al., 2021; Tamburello et al., 2022; Fig. 16c). In recent cases in the Apennines, the pre-/co-seismic injection of exotic fluids (and related exotic elements) into shallow groundwaters was preceded or accompanied by the ingress of deep CO_2 into the shallow crust (Chiodini et al., 2011, 2020; Miller et al., 2004; Boschetti et al., 2019; Barbieri et al., 2020; Martinelli et al., 2020; Di Luccio et al., 2022; Gori and Barberio, 2022; Fig. 16c). Moreover, Caracausi et al. (2022) recently showed that an increase of crustal ^4He in natural shallow crustal fluids often precedes or accompanies seismic events in the southern Apennines. The extensional seismic sequences in the Apennines (Fig. 5a) are often anticipated by upward migrating anomalies of Vp/Vs (the ratio of P to S wave velocities; Lucente et al., 2010; Savage, 2010; Chiarabba et al., 2020; Fig. 16c), which are usually the signal of pre-seismic dilatancy (Scholz et al., 1973) and related fluid ingress into the crust leading to post-seismic large (tens of millions of m^3) upward flow of fluids from the seismogenic depth to the surface. This was imaged by 4D tomography (Chiarabba et al., 2022) and matched by the consistent increase of discharge of groundwater measured in springs, streams and rivers (Petitta et al., 2018; Chiarabba et al., 2022). Based on these data, pre-seismic dilatancy and related upward ingress of water and deep CO_2 seem the main or one of the main factors driving pre-/co-seismic chemical-physical disequilibria, whereby CO_2 makes the crustal waters more acidic than normal and hence chemically aggressive toward the host rock. The dissolution of chemical elements from the host rock that are normally absent or nearly so in circulating shallow fluids would follow. Similar processes have been

recorded also elsewhere. For instance, in strike-slip environments in northern Iceland and China, increases of exotic elements and CO₂ in groundwaters have been documented before earthquakes (Claesson et al., 2004; Skelton et al., 2014, 2019; Barbieri et al., 2021; Li et al., 2021; Zhao et al., 2021; Yan et al., 2022) and, also in these cases, the input of deep CO₂ into the shallow system seems to be the main factor driving the pre-seismic disequilibria (Li et al., 2021; Boschetti et al., 2022; Yan et al., 2022).

In contrast, pre-seismic hydrogeochemical anomalies before earthquakes in compressional settings have been so far rarely recorded both in the Apennines and elsewhere. For instance, no significant anomalies of this kind were recorded before the 2012 Emilia compressional earthquakes (Mw mainshocks 6.1 and 5.8) in the northernmost buried front of the Apennines (e.g., Marcaccio and Martinelli, 2012; Cinti et al., 2023).

The picture of recently documented pre-seismic hydrogeochemical anomalies in the Apennines and elsewhere is consistent with our results from tectonic mineralizations and our inferences on the responsible paleofluids. Indeed, extensional tectonics is accompanied by pre-seismic dilatancy (e.g., Sibson, 1994; Doglioni et al., 2011, 2013) and circulation of fluids adding exotic chemical elements to the groundwaters leading to chemical-physical disequilibria (Barberio et al., 2017; Barbieri et al., 2020). Similar processes seem to occur also in seismic strike-slip environments (Skelton et al., 2014, 2019). On the contrary, compressional tectonics seem to inhibit upward-directed fluid circulation through the crust and hence significant chemical-physical disequilibria (e.g., Sibson, 1994; Doglioni et al., 2011, 2013; Marcaccio and Martinelli, 2012), although we feel that this matter, at least in the case of compressional tectonics, is still poorly investigated both in recent and in past seismic cycles and earthquakes. These differences may be related to the control exerted by the different stress field orientations on the evolution of seismic sequences developing in compressive and extensional regimes (Carminati et al., 2004).

In summary, while recent pre-seismic hydrogeochemical anomalies inspired our investigation of chemical-physical (dis)equilibria in tectonic mineralizations, our investigation, in particular for extensional tectonic mineralizations, contributes to build a consistent number of case studies necessary to validate the use of hydrogeochemical anomalies as valid seismic precursors.

5.7. Limits and caveats of the adopted methods and workflow

The proposed workflow (Fig. 7) and, in particular, the integration of different methods make it possible to determine (dis)equilibria in fluid-rock systems and link them to the phases of the seismic cycle. The main limitations of the proposed workflow (Fig. 7) are the errors associated with the calculated host rock and paleofluid temperatures and site-specific uncertainties. Such limits are discussed in the following.

5.7.1. Host rock temperature

The host rock temperature at the time of tectonic carbonate precipitation is calculated from burial-thermal modeling constrained by in situ radiometric dating on tectonic carbonates.

U—Pb and U—Th geochronology are among the most adopted methods for tectonic carbonates but it is not always possible to obtain geologically meaningful ages (Rasbury and Cole, 2009; Kylander-Clark, 2020; Hoareau et al., 2021; Roberts et al., 2021; Roberts and Holdsworth, 2022; Washburn et al., 2023). Moreover, the uncertainties associated with geochronological ages are often large and prevent the calculation of an unambiguous depth and temperature of tectonic carbonate precipitation. Alternatively, ages from multiple mineralizations can be so close in time to suggest a single event (e.g., Corrèa et al., 2022; Aubert et al., 2023), thus limiting the possibility to identify specific depth and temperature conditions for distinct phases of the seismic cycle. For these reasons, additional geochronological information from other datable minerals such as *syn*-kinematic fault-related authigenic

clays can help to improve the calculation of host rock temperatures (e.g., Fitz-Diaz et al., 2019; Curzi et al., 2020a).

The reconstruction of burial and thermal history of sedimentary successions in fold-and-thrust belts may be poorly constrained. This depends on the accuracy in the determination of stratigraphic age, thickness, burial rate and, on the number of paleothermal indicators (e.g., vitrinite reflectance, mixed layer illite-smectite, T_{max}) applied to constrain the maximum burial and temperature conditions experienced by the sedimentary succession. The greater the number of adopted paleothermal indicators, the more constrained the thermal reconstruction of the fold-and-thrust belt, especially if each thermal indicator has its own kinetically controlled response to the burial history (Aldega et al., 2007b; Corrado et al., 2020). Additionally, the poorly known value of the geothermal gradient or heat flow at the time of calcite precipitation increases the uncertainty of the calculation of the host rock temperature.

Clumped isotope thermometry on the carbonate host rock can represent an alternative thermal constraint for host rock temperature calculation if the rock has reached an equilibrium temperature during burial either through bond reordering or recrystallization. However, this is generally reached if the rocks have experienced temperatures >100–150 °C for millions of years (e.g., Passey and Henkes, 2012; Hemingway and Henkes, 2021; Looser et al., 2023). Thus, in most cases the temperature recorded by the host rock reflects a mixture of the original temperature of carbonate precipitation with some partial diagenetic resetting. For this reason, the host rock temperature rarely provides information on the maximum temperature reached by the host rock.

An alternative method to constrain the burial-thermal modeling of sedimentary successions and calculate the host rock temperature is offered by the recently applied paleopiezometry approach, which is based on the stylolite roughness inversion technique. Paleopiezometry provides the potential to calculate the maximum depth attained by the sedimentary succession and to infer the temperature experienced by the host rock during burial or during the occurrence of the first increment of compressional deformations, when the maximum horizontal stress is accommodated by folding (Labeur et al., 2021; Lacombe et al., 2021; Zeboudj et al., 2023). This method allows refining and validating the depth reached by the host rock, even though it does not provide information on the host rock temperature at the time of precipitation of tectonic carbonates directly associated with thrusting.

5.7.2. Paleofluid temperature reconstruction

Clumped isotope thermometry allows us to determine the temperature of tectonic carbonate precipitation and calculate the fluid δ¹⁸O (Ghosh et al., 2006; Swanson et al., 2012; Anderson et al., 2021; Hoareau et al., 2021). However, the uncertainties associated with the calculated temperatures can prevent an unambiguous identification of thermal disequilibria between fluid and host rock at the time of tectonic carbonate precipitation. Much effort has been invested in reducing uncertainties in carbonate clumped isotopes analysis through carbonate-based standardization (Bernasconi et al., 2018, 2021; Anderson et al., 2021) and in reducing the sample weight necessary for analysis to 80–130 μg of carbonate per replicate analysis (Schmid and Bernasconi, 2010; Meckler et al., 2015; Müller et al., 2019). However, many laboratories still use instrumentation requiring large sample amounts (2–10 mg per replicate). Thus, often the reported temperatures still have considerable uncertainties, limiting their accuracy. Clumped isotopes measurements can be coupled with other independent geothermometers to better constrain the crystallization temperature of carbonate minerals (Fig. 7). Microthermometry and Raman spectroscopy of fluid inclusions, allow to obtain not only the temperature but also information on the chemistry of the fluids (e.g., Roedder, 1984; Invernizzi et al., 1998; Ceriani et al., 2011; Bodnar et al., 2013; Manganot et al., 2017; Curzi et al., 2022). Unfortunately, fluid inclusions are not always present and their abundance in a given sample commonly increases with decrease in

size (Roedder, 1984) limiting their applicability. Moreover, tectonic carbonates can be deformed and twinned during the post-crystallization deformation histories. In these cases, fluid inclusions can be decrepitated after calcite precipitation, thus preventing their investigation.

5.7.3. Site specific conditions during deformation

Regional or local scale factors, including lithology, tectonic styles, paleoelevation of deforming zones, syn-tectonic erosion, and near-surface aquifers can control the involvement of meteoric and/or deep fluids during tectonic processes (Fig. 7; Dietrich et al., 1983; Uysal et al., 2007, 2009, 2011; Gébelin et al., 2012; Rossi and Rolland, 2014; Berardi et al., 2016; Smeraglia et al., 2019; Yıldırım et al., 2020; Looser et al., 2021). For instance, the involvement of deep derived fluids can be facilitated under thick-skinned tectonics, in which deeply rooted thrusts can act as conduits for deep fluids, as documented, for instance, along the Laramide province (USA; e.g., Beaudoin et al., 2014, 2022) and South Pyrenean fold-and-thrust belt (Spain; e.g., Beaudoin et al., 2022; Cruset et al., 2023). At the same time, although compressional deformations in the Apennines and in other orogens mostly develop below the sea level, the involvement of deep and/or meteoric fluids during compressional deformation can be locally promoted by (i) deformation in subaerial condition, such as documented along the Gran Sasso Massif in the Central Apennines (MCT; Fig. 5a; Lucca et al., 2019) and in the Jura fold-and-thrust belt (Looser et al., 2021; Berio et al., 2022), (ii) high-angle scaly fabric zones associated with high-angle reverse faults documented along the Internal Jura fold-and-thrust belt (France; Smeraglia et al., 2020b), and (iii) syn-tectonic uplift and subaerial exposure of thrust zones as documented in the Bornes Massif in France (Berio et al., 2022), Pyrenean (Spain; e.g., Travé et al., 2007; Lacroix et al., 2014, 2018a, 2018b; Hoareau et al., 2021; Cruset et al., 2023), Canadian Rockies (e.g., Garven, 1985), Mexican fold-and-thrust belt (e.g., Fitz-Diaz et al., 2011), and Albanides (e.g., Vilasi et al., 2009).

5.8. Future perspectives

The limits discussed above imply that the identification of (dis)equilibrium states in fluid-rock systems during the seismic cycle and earthquakes still requires further refinement. Future efforts aimed at advancing the understanding of the relationship between fluids and the seismic cycle in past events should include the following main lines of research (Fig. 7):

1. Improving the resolution of micro-analyses to investigate at even smaller scales the fluid-rock system during distinct phases of the seismic cycle. Tectonic mineralizations can, indeed, record tectonic events at the micro- or even nano- and atomic-scale. Through TEM analysis at the nano-scale, Tarling et al. (2018) documented the progressive formation of high-temperature reaction products formed by co-seismic amorphization and dehydration in a plate boundary-scale serpentinite shear zone. Lacroix et al. (2018a, 2018b), used detailed in-situ micron-scale $\delta^{18}\text{O}$ measured using Secondary Ion Mass Spectrometry (SIMS) combined with fluid inclusion and clumped isotope thermometry, to document the progressive evolution of a micron-scale fluid-rock system during fracture opening and vein growth related to the deformation along the Cotiella Thrust (Pyrenees, Spain). Fu and Espinosa-Marzal (2022), through nano-scale friction measurements performed by atomic force microscopy on calcite single crystals, showed that the origin of the velocity-weakening friction behavior is determined by contact aging resulting from atomic friction of the crystalline lattice. Therefore, the present and next frontier to advance our knowledge of fluid-rock relationships during the seismic cycle is the nano scale.
2. Instrumental improvements and integration of multiple radiometric dating techniques to reduce the uncertainties and limitations arising from post-crystallization chemical alteration of tectonic carbonates. Radiometric dating methods (including those treated in this paper)

may have large uncertainties. Although the largest part of the uncertainty is due to the type of material and not to the instrumentation, technical refinements in the ablation procedures and improvements in standardization could help to somewhat decrease the uncertainties (e.g. Guillong et al., 2020). Systematic integration of different geochronological methods such as U—Pb on tectonic carbonates with K—Ar and Ar—Ar on syn-kinematic clay minerals could also reduce the uncertainties. In addition, the uncertainties associated with paleofluid and host rock temperature calculation and the related thermal (dis)equilibria can be mitigated by the integration of other independent geothermometers such as clumped isotopes and fluid inclusions on tectonic mineralization (e.g., Manguet et al., 2019) and mixed layer illite-smectite and vitrinite reflectance on the faulted sedimentary succession.

3. Improving the knowledge of seismic cycle- and co-seismic-related geological structures. In the last 25 years much has been done to identify geological (micro)structures ascribable to earthquakes or seismic cycles. For instance, while Cowan (1999) asserted that pseudotachylytes were the only reliable indicator of fossil earthquakes, after 16 years, Rowe and Griffith (2015) presented a thorough review of geological markers of earthquakes including tens of new studies on this theme and many new potential markers. In this paper, we were inspired by Rowe and Griffith (2015) and attempted to integrate their co-seismic marker list with new potential markers (e.g., blocky stockwork veins). However, further studies on tectonic mineralizations (such as veins or cements in breccias) are necessary to improve our understanding of fossil seismic markers.
4. Improving the knowledge of site-specific markers and processes. As explained in this paper, the study of fossil fluid-rock (dis)equilibria is inspired by chemical-physical anomalies recently observed in seismic areas (e.g., Skelton et al., 2014; Barberio et al., 2017), which can be validated through paleofluid studies (e.g., Andrn et al., 2016; Coppola et al., 2021). For example, hydrogeochemical anomalies before the onset of the 2016–2017 Amatrice-Norcia seismic sequence in the Apennines consisted of increase and decrease of pH values and increase of As, V, and Fe concentrations (Barberio et al., 2017), whereas increases of Na, Si, Ca, and $\delta^2\text{H}$ were observed before earthquakes in northern Iceland (Skelton et al., 2014, 2019). Hence, earthquake-related geochemical anomalies and, therefore, chemical disequilibria strongly depend on site-specific conditions (e.g., lithology or pre-existing crustal discontinuities) and processes (e.g., thick vs. thin tectonics or deformation styles; Boschetti et al., 2019, 2022). Understanding these specific processes is one of the frontiers to reach in the study of fluid-earthquake relationships.

6. Conclusions

The proposed workflow (Fig. 7) aims at identifying chemical-physical (dis)equilibria in fluid-rock systems by merging an analytical approach that combines stable and clumped isotope analyses of tectonic mineralizations and 1D burial-thermal modeling of the sedimentary succession hosting such mineralizations. Specifically, for the Central Apennines we conclude that:

1. Fluid circulation during compressional deformation mainly occurs in closed fluid-rock systems, in which isotopic and thermal disequilibria are limited.
2. Fluid circulation in extensional deformation occurs in open fluid-rock systems where uprising (enriched in ^{18}O and warm) or downwelling (meteoric and cold) fluids can be involved.
3. Fluid circulation in extensional deformation settings may significantly change during fault activity and during the different phases of the seismic cycle. Different deformation phases can promote the opening of the fluid-rock system inducing (positive or negative) isotopic and thermal disequilibria. In this context, co-seismic

deformation provides the most obvious source to isotopic and thermal disequilibria between fluid and host rock.

The proposed approach still requires refinement and needs further data for finer tuning. At least, advances are necessary to reduce the uncertainties in the analytical methods adopted for temperature estimations, and to unequivocally identify geological (micro)structures (e.g., veins) connected with given phases of the seismic cycle (e.g., coseismic veins). Site specific condition of deformation is another field in which to progress. The integration of geological-structural constraints, geochemical tracers (e.g., REEs, Sr and He isotopes) and geothermometers (e.g., fluid inclusions) is therefore required for a more detailed identification of chemical-physical (dis)equilibrium states associated with seismic cycles and earthquakes. However, we emphasize the potential of the proposed workflow for understanding fluid-rock-earthquake relationships in the past and in the present-day seismic cycle. Indeed, the highlighted geological evidence is valuable for the identification of potential chemical-physical seismic precursors, that might be different in extensional and compressional settings.

CRediT authorship contribution statement

M. Curzi: Conceptualization, Data curation, Formal analysis, Funding acquisition, Investigation, Methodology, Supervision, Visualization, Writing – original draft, Writing – review & editing. **L. Aldega:** Data curation, Formal analysis, Investigation, Methodology, Funding acquisition, Resources, Supervision, Validation, Writing – original draft, Writing – review & editing. **A. Billi:** Conceptualization, Data curation, Formal analysis, Investigation, Methodology, Project administration, Supervision, Validation, Visualization, Writing – original draft, Writing – review & editing. **C. Boschi:** Data curation, Formal analysis, Methodology, Resources, Supervision, Writing – original draft, Writing – review & editing. **E. Carminati:** Conceptualization, Data curation, Formal analysis, Funding acquisition, Investigation, Methodology, Project administration, Supervision, Validation, Visualization, Writing – original draft, Writing – review & editing. **G. Vignaroli:** Investigation, Validation, Writing – original draft, Writing – review & editing. **G. Viola:** Investigation, Validation, Writing – original draft, Writing – review & editing. **S.M. Bernasconi:** Conceptualization, Data curation, Formal analysis, Investigation, Methodology, Project administration, Resources, Supervision, Validation, Writing – original draft, Writing – review & editing.

Declaration of competing interest

The authors declare that they have no known competing financial interests or personal relationships that could have appeared to influence the work reported in this paper.

Data availability

All the data used in this study are referenced in Table S1 of the Supplementary Material and Table 3 of the text.

Acknowledgments

This study was carried out within the RETURN Extended Partnership and received funding from the European Union Next-GenerationEU (National Recovery and Resilience Plan – NRRP, Mission 4, Component 2, Investment 1.3 – D.D. 1243 2/8/2022, PE0000005). The Editor (Gillian Foulger), Tonguç Uysal, and an anonymous reviewer are thanked for their comments and revisions. The work benefitted from interactions with F. Rossetti and S. Tavani. We thank M. Jaggi and S. Franchini for assistance with stable and clumped isotope analyses. We thank M. Coppola for providing original photos of ultracataclases. L. Smeraglia is thanked for providing original photos of fault rocks and

mineralizations of the Mt. Massico Thrust and Val Roveto normal Fault and for long-lasting common work.

Appendix A. Supplementary data

Supplementary data to this article can be found online at <https://doi.org/10.1016/j.earscirev.2024.104801>.

References

- Åberg, G., 1995. The use of natural strontium isotopes as tracers in environmental studies. *Water Air Soil Pollut.* 79, 309–322.
- Agosta, F., Kirschner, D.L., 2003. Fluid conduits in carbonate-hosted seismogenic normal faults of Central Italy. *J. Geophys. Res. Solid Earth* 108.
- Aldega, L., Botti, F., Corrado, S., 2007a. Clay mineral assemblages and vitrinite reflectance in the Laga Basin (Central Apennines, Italy): what do they record? *Clay Clay Miner.* 55, 504–518.
- Aldega, L., Corrado, S., Grasso, M., Maniscalco, R., 2007b. Correlation of diagenetic data from organic and inorganic studies in the Apenninic-Maghrebic fold-and-thrust belt: a case study from Eastern Sicily. *J. Geol.* 115 (3), 335–353.
- Anderson, N.T., Kelson, J.R., Kele, S., Daëron, M., Bonifacie, M., Horita, J., Mackey, T.J., John, C.M., Kluge, T., Petschnig, P., Jost, A.B., Huntington, K.W., Bernasconi, S.M., Bergmann, K.D., 2021. A unified clumped isotope thermometer calibration (0.5–1,100°C) using carbonate-based standardization. *Geophys. Res. Lett.* 48.
- Andrén, M., Stockmann, G., Skelton, A., Sturkell, E., Mörth, C.-M., Guðrúnardóttir, H.R., Keller, N.S., Odling, N., Dahrén, B., Broman, C., Balic-Zunic, T., Hjartarson, H., Siegmund, H., Freund, F., Kockum, I., 2016. Coupling between mineral reactions, chemical changes in groundwater, and earthquakes in Iceland. *J. Geophys. Res. Solid Earth* 121, 2315–2337.
- Asti, R., Saspiturry, N., Angrand, P., 2022. The Mesozoic Iberia-Eurasia diffuse plate boundary: A wide domain of distributed transtensional deformation progressively focusing along the North Pyrenean Zone. *Earth Sci. Rev.* 230, 104040.
- Aubert, I., Bitault, H., Léonide, P., Fournier, F., Godeau, N., Lamarche, J., Deschamps, P., Maia Correa, R.S., Marié, L., 2023. Effect of normal fault activity on carbonate reservoir diagenetic evolution (Urgonian facies, SE France). *Mar. Pet. Geol.* 158, 106546.
- Avigour, A., Magaritz, M., Issar, A., Dodson, M.H., 1990. Sr isotope study of vein and cave calcites from southern Israel. *Chem. Geol.* 82, 69–81.
- Baldermann, A., Mittermayr, F., Bernasconi, S.M., Dietzel, M., Grengg, C., Hippler, D., Kluge, T., Leis, A., Lin, K., Wang, X., Zünterli, A., Boch, R., 2020. Fracture dolomite as an archive of continental palaeo-environmental conditions. *Commun. Earth Environ.* 1 (1), 35.
- Ballentine, C.J., Burgess, R., Marty, B., 2002. Tracing fluid origin, transport and interaction in the crust. *Rev. Mineral. Geochem.* 47 (1), 539–614.
- Balsamo, F., Aldega, L., De Paola, N., Faoro, I., Storti, F., 2014. The signature and mechanics of earthquake ruptures along shallow creeping faults in poorly lithified sediments. *Geology* 42, 435–438.
- Barberio, M.D., Barbieri, M., Billi, A., Doglioni, C., Petitta, M., 2017. Hydrogeochemical changes before and during the 2016 Amatrice-Norcia seismic sequence (Central Italy). *Sci. Rep.* 7.
- Barberio, M.D., Gori, F., Barbieri, M., Boschetti, T., Caracausi, A., Cardello, G.L., Petitta, M., 2021. Understanding the origin and mixing of deep fluids in shallow aquifers and possible implications for crustal deformation studies: San vittorino plain, central apennines. *Appl. Sci. (Switzerland)* 11, 1–26.
- Barbieri, M., Boschetti, T., Barberio, M.D., Billi, A., Franchini, S., Iacumin, P., Selmo, E., Petitta, M., 2020. Tracing deep fluid source contribution to groundwater in an active seismic area (Central Italy): A combined geothermometric and isotopic ($\delta^{13}C$) perspective. *J. Hydrol.* 582, 124495.
- Barbieri, M., Franchini, S., Barberio, M.D., Billi, A., Boschetti, T., Giansante, L., Gori, F., Jónsson, S., Petitta, M., Skelton, A., Stockmann, G., 2021. Changes in groundwater trace element concentrations before seismic and volcanic activities in Iceland during 2010–2018. *Sci. Total Environ.* 793, 148635.
- Barker, S.L.L., Cox, S.F., 2011. Evolution of fluid chemistry and fluid-flow pathways during folding and faulting: an example from Taemas, NSW, Australia. *Geol. Soc. Lond. Spec. Publ.* 359, 203–227.
- Bau, M., 1991. Rare-earth element mobility during hydrothermal and metamorphic fluid-rock interaction and the significance of the oxidation state of europium. *Chem. Geol.* 93, 219–230.
- Bau, M., Moller, P., 1992. Rare earth element fractionation in metamorphic hydrothermal calcite, magnesite and siderite. *Mineral. Petrol.* 45, 231–246.
- Beaudoin, N., Bellahsen, N., Lacombe, O., Emmanuel, L., Pironon, J., 2014. Crustal-scale fluid flow during the tectonic evolution of the Bighorn Basin (Wyoming, USA). *Basin Res.* 26 (3), 403–435.
- Beaudoin, N.E., Labeur, A., Lacombe, O., Koehn, D., Billi, A., Hoareau, G., Boyce, A., John, C.M., Marchegiano, M., Roberts, N.M., Millar, I.L., Claverie, F., Pecheyran, C., Callot, J.P., 2020. Regional-scale paleofluid system across the Tuscan Nappe-Umbria-Marche Apennine Ridge (northern Apennines) as revealed by mesostructural and isotopic analyses of stylolite-vein networks. *Solid Earth* 11 (4), 1617–1641.
- Beaudoin, N.E., Lacombe, O., Hoareau, G., Callot, J.P., 2022. How the geochemistry of syn-kinematic calcite cement depicts past fluid flow and assists structural interpretations: a review of concepts and applications in orogenic forelands. *Geol. Mag.* 1–34.

- Ben-Zion, Y., Shi, Z., 2005. Dynamic rupture on a material interface with spontaneous generation of plastic strain in the bulk. *Earth Planet. Sci. Lett.* 236 (1–2), 486–496.
- Berardi, G., Vignaroli, G., Billi, A., Rossetti, F., Soligo, M., Kele, S., Baykara, M.O., Bernasconi, S.M., Castorina, F., Tecce, F., Shen, C.C., 2016. Growth of a Pleistocene giant carbonate vein and nearby thermogene travertine deposits at Semproniano, southern Tuscany, Italy: Estimate of CO₂ leakage. *Tectonophysics* 690, 219–239.
- Berio, L.R., Mittempergher, S., Storti, F., Bernasconi, S.M., Cipriani, A., Lugli, F., Balsamo, F., 2022. Open–closed–open palaeofluid system conditions recorded in the tectonic vein networks of the Parmelan anticline (Bornes Massif, France). *J. Geol. Soc. Lond.* 179.
- Bernasconi, S.M., Müller, I.A., Bergmann, K.D., Breitenbach, S.F.M., Fernandez, A., Hodell, D.A., Jaggi, M., Meckler, A.N., Millan, I., Ziegler, M., 2018. Reducing Uncertainties in Carbonate Clumped Isotope Analysis through Consistent Carbonate-based Standardization. *Geochem. Geophys. Geosyst.* 19, 2895–2914.
- Bernasconi, S.M., Daëron, M., Bergmann, K.D., Bonifacie, M., Meckler, A.N., Affek, H.P., Anderson, N., Bajnai, D., Barkan, E., Beverly, E., Blamart, D., Burgener, L., Calmels, D., Chaduteau, C., Clog, M., Davidheiser-Kroll, B., Davies, A., Dux, F., Eiler, J., Elliott, B., Fetrow, A.C., Fiebig, J., Goldberg, S., Hermoso, M., Huntington, K.W., Hyland, E., Ingalls, M., Jaggi, M., John, C.M., Jost, A.B., Katz, S., Kelson, J., Kluge, T., Kocken, I.J., Laskar, A., Leutert, T.J., Liang, D., Lucarelli, J., Mackey, T.J., Manganot, X., Meinicke, N., Modestou, S.E., Müller, I.A., Murray, S., Neary, A., Packard, N., Passey, B.H., Pelletier, E., Petersen, S., Piasecki, A., Schauer, A., Snell, K.E., Swart, P.K., Tripathi, A., Upadhyay, D., Vennemann, T., Winkelstern, I., Yarian, D., Yoshida, N., Zhang, N., Ziegler, M., 2021. InterCarb: A community effort to improve interlaboratory standardization of the carbonate clumped isotope thermometer using carbonate standards. *Geochem. Geophys. Geosyst.* 22 (5) e2020GC009588.
- Berthé, D., Choukroune, P., Jegouzo, P., 1979. Orthogneiss, mylonite and non coaxial deformation of granites: the example of the South Armorican Shear Zone. *J. Struct. Geol.* 1, 31–42.
- Billi, A., Di Toro, G., 2008. Fault-related carbonate rocks and earthquake indicators: recent advances and future trends. In: *Structural Geology: New Research*. Nova Science Publishers, New York, pp. 63–86.
- Billi, A., Tiberti, M.M., Cavinato, G.P., Cosentino, D., di Luzio, E., Keller, V.A., Kluth, C., Orlando, L., Parotto, M., Pratlurion, A., Romanelli, M., Storti, F., Wardell, N., 2006. First results from the CROP-11 deep seismic profile, central Apennines, Italy: evidence of mid-crustal folding. *J. Geol. Soc. Lond.* 163, 583–586.
- Billi, A., Smeraglia, L., Aldega, L., Balsamo, F., Barberio, M.D., Boschi, C., Caracausi, A., Carminati, E., Iannace, A., Mercuri, M., Pizzati, M., Tavani, S., 2023. Dolostone pulverization induced by coseismic rapid decompression of CO₂-rich gas in nature (Matese, Apennines, Italy). *Earth Planet. Sci. Lett.* 604, 117996.
- Bodnar, R.J., Lecumberri-Sanchez, P., Moncada, D., Steele-MacInnis, M., 2013. Fluid inclusions in hydrothermal ore deposits. In: *Treatise on Geochemistry*, Second edition. Elsevier Inc., pp. 119–142.
- Bolhar, R., Kamber, B.S., Moorbath, S., Fedo, C.M., Whitehouse, M.J., 2004. Characterisation of early Archaean chemical sediments by trace element signatures. *Earth Planet. Sci. Lett.* 222, 43–60.
- Bons, P.D., Elburg, M.A., Gomez-Rivas, E., 2012. A review of the formation of tectonic veins and their microstructures. *J. Struct. Geol.* 43, 33–62.
- Boschetti, T., Barbieri, M., Barberio, M.D., Billi, A., Franchini, S., Petitta, M., 2019. CO₂ inflow and elements desorption prior to a seismic sequence, Amatrice-Norcia 2016, Italy. *Geochem. Geophys. Geosyst.* 20 (5), 2303–2317.
- Boschetti, T., Barbieri, M., Barberio, M.D., Skelton, A., Stockmann, G., Toscani, L., 2022. Geothermometry and water–rock interaction modelling at Hafraalækur: possible implications of temperature and CO₂ on hydrogeochemical changes previously linked to earthquakes in northern Iceland. *Geothermics* 105, 102535.
- Braun, J.J., Pagel, M., Muller, J.-P., Bilong, P., Michard, A., Guillet, B., 1990. Cerium anomalies in lateritic profiles. *Geochim. Cosmochim. Acta* 54, 781–795.
- Breitenbach, S.F., Bernasconi, S.M., 2011. Carbon and oxygen isotope analysis of small carbonate samples (20 to 100 µg) with a GasBench II preparation device. *Rapid Commun. Mass Spectrom.* 25 (13), 1910–1914.
- Bullock, R.J., De Paola, N., Holdsworth, R.E., 2015. An experimental investigation into the role of phyllosilicate content on earthquake propagation during seismic slip in carbonate faults. *J. Geophys. Res. Solid Earth* 120, 3187–3207.
- Burnham, A.K., Sweeney, J.J., 1989. A chemical kinetic model of vitrinite maturation and reflectance. *Geochim. Cosmochim. Acta* 53, 2649–2657.
- Butler, R.W.H., 1992. Hydrocarbon maturation, migration and tectonic loading in the western Alps, 59. *Geological Society of London, Special Publications*, pp. 227–244.
- Cappa, F., Scuderi, M.M., Collettini, C., Guglielmi, Y., Avouac, J.-P., 2019. Stabilization of fault slip by fluid injection in the laboratory and in situ. *Sci. Adv.* 5 (3).
- Caracausi, A., Paternoster, M., 2015. Radiogenic helium degassing and rock fracturing: A case study of the southern Apennines active tectonic region. *J. Geophys. Res. Solid Earth* 120 (4), 2200–2211.
- Caracausi, A., Buttiitta, D., Picozzi, M., Paternoster, M., Stabile, T.A., 2022. Earthquakes control the impulsive nature of crustal helium degassing to the atmosphere. *Commun. Earth Environ.* 3 (1), 224.
- Carminati, E., Doglioni, C., Barba, S., 2004. Reverse migration of seismicity on thrusts and normal faults. *Earth Sci. Rev.* 65 (3–4), 195–222.
- Carminati, E., Lustrino, M., Cuffaro, M., Doglioni, C., 2010. Tectonics, magmatism and geodynamics of Italy: what we know and what we imagine. *J. Virtual Explor.* 36.
- Carminati, E., Lustrino, M., Doglioni, C., 2012. Geodynamic evolution of the central and western Mediterranean: Tectonics vs. igneous petrology constraints. *Tectonophysics* 579, 173–192.
- Cavinato, G.P., De Celles, P.G., 1999. Extensional basins in the tectonically bimodal central Apennines fold-and-thrust belt, Italy. Response to corner flow above a subducting slab in retrograde motion. *Geology* 27, 955–958.
- Cerchiari, A., Remitti, F., Mittempergher, S., Festa, A., Lugli, F., Cipriani, A., 2020. Cyclical variations of fluid sources and stress state in a shallow megathrust-zone mélange. *J. Geol. Soc. Lond.* 177 (3), 647–659.
- Ceriani, A., Calabrò, R., di Giulio, A., Buonaguro, R., 2011. Diagenetic and thermal history of the Jurassic-Tertiary succession of the Zagros Mountains in the Dezful Embayment (SW Iran): constraints from fluid inclusions. *Int. J. Earth Sci.* 100, 1265–1281.
- Chester, F.M., Chester, J.S., 1998. Ultracataclite structure and friction processes of the Punchbowl fault, San Andreas system, California. *Tectonophysics* 295, 199–221.
- Chiarabba, C., Amato, A., Anselmi, M., Baccheschi, P., Bianchi, I., Cattaneo, M., Cecere, G., Chiaraluca, L., Ciaccio, M.G., De Gori, P., De Luca, G., Di Bona, M., Di Stefano, R., Faenza, L., Govoni, A., Improta, L., Lucente, F.P., Marchetti, A., Margheriti, L., Mele, F., Michelini, A., Monachesi, G., Moretti, M., Pastori, M., Piana Agostinetti, N., Piccinini, D., Roselli, P., Seccia, D., Valoroso, L., 2009. The 2009 L'Aquila (central Italy) Mw6.3 earthquake: main shock and aftershocks. *Geophys. Res. Lett.* 36.
- Chiarabba, C., De Gori, P., Segou, M., Cattaneo, M., 2020. Seismic velocity precursors to the 2016 Mw 6.5 Norcia (Italy) earthquake. *Geology* 48, 924–928.
- Chiarabba, C., De Gori, P., Valoroso, L., Petitta, M., Carminati, E., 2022. Large extensional earthquakes push-up terrific amount of fluids. *Sci. Rep.* 12 (1), 14597.
- Chiaraluca, L., Di Stefano, R., Tinti, E., Scognamiglio, L., Michele, M., Casarotti, E., Cattaneo, M., De Gori, P., Chiarabba, C., Monachesi, G., Lombardi, A., Valoroso, L., Latorre, D., Marzorati, S., 2017. The 2016 Central Italy seismic sequence: A first look at the mainshocks, aftershocks, and source models. *Seismol. Res. Lett.* 88 (3), 757–771.
- Chiodini, G., Frondini, F., Cardellini, C., Parello, F., Peruzzi, L., 2000. Rate of diffuse carbon dioxide Earth degassing estimated from carbon balance of regional aquifers: the case of central Apennine, Italy. *J. Geophys. Res. Solid Earth* 105 (B4), 8423–8434.
- Chiodini, G., Caliro, S., Cardellini, C., Frondini, F., Inguaggiato, S., Matteucci, F., 2011. Geochemical evidence for and characterization of CO₂ rich gas sources in the epicentral area of the Abruzzo 2009 earthquakes. *Earth Planet. Sci. Lett.* 304 (3–4), 389–398.
- Chiodini, G., Cardellini, C., Luccio, F., Selva, J., Frondini, F., Caliro, S., Rosiello, A., Beldini, G., Ventura, G., 2020. Correlation between tectonic CO₂ Earth degassing and seismicity is revealed by a 10-year record in the Apennines, Italy. *Sci. Adv.* 6 (35).
- Cinti, D., Sciarra, A., Cantucci, B., Gallì, G., Pizzino, L., Procesi, M., Poncia, P.P., 2023. Hydrogeochemical investigation of shallow aquifers before and after the 2012 Emilia seismic sequence (northern Italy). *Appl. Geochem.* 105624.
- Cipollari, P., Cosentino, D., 1995. Miocene unconformities in the Central Apennines: geodynamic significance and sedimentary basin evolution. *Tectonophysics* 252, 375–389.
- Cipriani, A., 2016. Geology of the Mt. Cosce sector (Narni Ridge, Central Apennines, Italy). *J. Maps* 12, 328–340.
- Claesson, L., Skelton, A., Graham, C., Dietl, C., Mörth, M., Torrsander, P., Kockum, I., 2004. Hydrogeochemical changes before and after a major earthquake. *Geology* 32 (8), 641–644.
- Collettini, C., Viti, C., Tesi, T., Mollo, S., 2013. Thermal decomposition along natural carbonate faults during earthquakes. *Geology* 41, 927–930.
- Collettini, C., Carpenter, B.M., Viti, C., Cruciani, F., Mollo, S., Tesi, T., Trippetta, F., Valoroso, L., Chiaraluca, L., 2014. Fault structure and slip localization in carbonate-bearing normal faults: an example from the Northern Apennines of Italy. *J. Struct. Geol.* 67, 154–166.
- Conti, A., Turpin, L., Polino, R., Mattei, M., Zuppi, G.M., 2001. The relationship between evolution of fluid chemistry and the style of brittle deformation: examples from the Northern Apennines (Italy). *Tectonophysics* 330 (1–2), 103–117.
- Coppola, M., Correale, A., Barberio, M.D., Billi, A., Cavallo, A., Fondriest, M., Nazzari, M., Paonita, A., Romano, C., Stagno, V., Viti, C., Vona, A., 2021. Meso- to nano-scale evidence of fluid-assisted co-seismic slip along the normal Mt. Morrone Fault, Italy: Implications for earthquake hydrogeochemical precursors. *Earth Planet. Sci. Lett.* 568.
- Corrado, S., Aldega, L., Zattin, M., 2010. Sedimentary vs. tectonic burial and exhumation along the Apennines (Italy). *J. Virtual Explor.* 36.
- Corrado, S., Schito, A., Romano, C., Grigo, D., Poe, B.T., Aldega, L., Caricchi, C., Di Paolo, L., Zattin, M., 2020. An integrated platform for thermal maturity assessment of polyphase, long-lasting sedimentary basins, from classical to brand-new thermal parameters and models: an example from the on-shore Baltic Basin (Poland). *Mar. Pet. Geol.* 122, 104547.
- Corrèa, R.S., Ukar, E., Laubach, S.E., Aubert, I., Lamarche, J., Wang, Q., Stockli, D.F., Stockli, L.D., Larson, T.E., 2022. Episodic reactivation of carbonate fault zones with implications for permeability—an example from Provence, Southeast France. *Mar. Pet. Geol.* 145, 105905.
- Cosentino, D., Cipollari, P., Marsili, P., Scrocca, D., 2010. Geology of the central Apennines: a regional review. *J. Virtual Explor.* 36.
- Cosentino, D., Asti, R., Nocentini, M., Gliozzi, E., Kotsakis, T., Mattei, M., Esu, D., Spadi, M., Tallini, M., Cifelli, F., Pennacchioni, M., Cavuoto, G., Di Fiore, V., 2017. New insights into the onset and evolution of the central Apennine extensional intermontane basins based on the tectonically active L'Aquila Basin (Central Italy). *Geol. Soc. Am. Bull.* 129 (9–10), 1314–1336.
- Cowan, D.S., 1999. Do faults preserve a record of seismic slip? A field geologist's opinion. *J. Struct. Geol.* 8 (21), 995–1001.
- Cox, S.F., 2005. Coupling between Deformation, Fluid Pressures, and Fluid Flow in Ore-Producing Hydrothermal Systems at Depth in the Crust. *One Hundredth Anniversary Volume*. Society of Economic Geologists, pp. 39–76.

- Cox, S.F., 2010. The application of failure mode diagrams for exploring the roles of fluid pressure and stress states in controlling styles of fracture-controlled permeability enhancement in faults and shear zones. *Geofluids* 10 (1–2), 217–233.
- Cox, S.F., 2020. Chapter 2: The dynamics of permeability enhancement and fluid flow in overpressured, fracture-controlled hydrothermal systems. In: *Applied Structural Geology of Ore-forming Hydrothermal Systems*. Society of Economic Geologists, pp. 25–82.
- Cox, S.F., Knackstedt, M.A., Braun, J., 2001. Principles of structural control on permeability and fluid flow in hydrothermal systems. In: *Structural Controls on Ore Genesis*. Society of Economic Geologists, pp. 1–24.
- Cruset, D., Vergés, J., Muñoz-López, D., Moragas, M., Cantarero, L., Travé, A., 2023. Fluid evolution from extension to compression in the Pyrenean Fold Belt and Basque-Cantabrian Basin: A review. *Earth Sci. Rev.* 104494.
- Curzi, M., Aldega, L., Bernasconi, S.M., Berra, F., Billi, A., Boschi, C., Franchini, S., van der Lelij, R., Viola, G., Carminati, E., 2020a. Architecture and evolution of an extensionally-inverted thrust (Mt. Tancia Thrust, Central Apennines): Geological, structural, geochemical, and K–Ar geochronological constraints. *J. Struct. Geol.* 136.
- Curzi, M., Billi, A., Carminati, E., Rossetti, F., Albert, R., Aldega, L., Cardello, G.L., Conti, A., Gerdes, A., Smeraglia, L., van der Lelij, R., Vignaroli, G., Viola, G., 2020b. Disproving the Presence of Paleozoic-Triassic Metamorphic Rocks on the Island of Zannone (Central Italy): Implications for the Early Stages of the Tyrrhenian-Apennines Tectonic Evolution. *Tectonics* 39.
- Curzi, M., Bernasconi, S.M., Billi, A., Boschi, C., Aldega, L., Franchini, S., Albert, R., Gerdes, A., Barberio, M.D., Looser, N., Carminati, E., 2021. U–Pb age of the 2016 Amatrice earthquake causative fault (Mt. Gorzano, Italy) and paleo-fluid circulation during seismic cycles inferred from inter- and co-seismic calcite. *Tectonophysics* 819.
- Curzi, M., Caracausi, A., Rossetti, F., Rabiee, A., Billi, A., Carminati, E., Aldega, L., Bernasconi, S.M., Boschi, C., Drivenes, K., Rizzo, A.L., Sørensen, B.E., 2022. From Fossil to Active Hydrothermal Outflow in the Back-Arc of the Central Apennines (Zannone Island, Italy). *Geochem. Geophys. Geosyst.* 23.
- Curzi, M., Giuntoli, F., Vignaroli, G., Viola, G., 2023. Constraints on upper crustal fluid circulation and seismogenesis from in-situ outcrop quantification of complex fault zone permeability. *Sci. Rep.* 13 (1), 5548.
- Curzi, M., Cipriani, A., Aldega, L., Billi, A., Carminati, E., Van der Lelij, R., Vignaroli, G., Viola, G., 2024. Architecture and permeability structure of the Sibillini Mts. Thrust and influence upon recent, extension-related seismicity in the central Apennines (Italy) through fault-valve behavior. *Geol. Soc. Am. Bull.* 136 (1–2), 3–26. <https://doi.org/10.1130/B36616.1>.
- Czuppon, G., Ramsay, R.R., Özgenc, I., Demény, A., Gwalani, L.G., Rogers, K., Eves, A., Papp, L., Palcsu, L., Berkesi, M., Downes, P.J., 2014. Stable (H, O, C) and noble-gas (he and Ar) isotopic compositions from calcite and fluorite in the Speewah Dome, Kimberley Region, Western Australia: implications for the conditions of crystallization and evidence for the influence of crustal-mantle fluid mixing. *Mineral. Petrol.* 108, 759–775.
- Daëron, M., Drysdale, R.N., Peral, M., Huyghe, D., Blamart, D., Coplen, T.B., Lartaud, F., Zanchetta, G., 2019. Most Earth-surface calcites precipitate out of isotopic equilibrium. *Nat. Commun.* 10 (1), 429.
- De Luca, G., Di Carlo, G., Tallini, M., 2018. A record of changes in the Gran Sasso groundwater before, during and after the 2016 Amatrice earthquake, Central Italy. *Sci. Rep.* 8, 15982.
- De Paola, N., Chiodini, G., Hirose, T., Cardellini, C., Caliro, S., Shimamoto, T., 2011. The geochemical signature caused by earthquake propagation in carbonate-hosted faults. *Earth Planet. Sci. Lett.* 310, 225–232.
- Delle Piane, C., Clennell, M., Keller, J.V.A., Giwelli, A., Luzin, V., 2017. Carbonate hosted fault rocks: A review of structural and microstructural characteristic with implications for seismicity in the upper crust. *J. Struct. Geol.* 103, 17–36.
- Di Luccio, F., Chiodini, G., Caliro, S., Cardellini, C., Convertito, V., Pino, N.A., Tolomei, C., Ventura, G., 2018. Seismic signature of active intrusions in mountain chains. *Sci. Adv.* 4 (1), e1701825.
- Di Luccio, F., Palano, M., Chiodini, G., Cucci, L., Piromallo, C., Sparacino, F., Ventura, G., Improta, L., Cardellini, C., Persaud, P., Pizzino, L., Calderoni, G., Castellano, C., Cianchini, G., Scianetti, S., Cinti, D., Cusano, P., De Gori, P., De Santis, A., Del Gaudio, P., Zuccarello, L., 2022. Geodynamics, geophysical and geochemical observations, and the role of CO₂ degassing in the Apennines. *Earth Sci. Rev.* 104236.
- Dielforder, A., Villa, I.M., Berger, A., Herwegh, M., 2022. Tracing wedge-internal deformation by means of strontium isotope systematics of vein carbonates. *Geol. Mag.* 1–15.
- Dietrich, D., McKenzie, J.A., Song, H., 1983. Origin of calcite in syntectonic veins as determined from carbon-isotope ratios. *Geology* 11 (9), 547–551.
- Doan, M.L., Billi, A., 2011. High strain rate damage of Carrara marble. *Geophys. Res. Lett.* 38.
- Doan, M.L., d'Hour, V., 2012. Effect of initial damage on rock pulverization along faults. *J. Struct. Geol.* 45, 113–124.
- Doan, M.L., Gary, G., 2009. Rock pulverization at high strain rate near the San Andreas fault. *Nat. Geosci.* 2 (10), 709–712.
- Doblas, M., Mahecha, V., Hoyos, M., López-rui, J., 1997. Slickenside and fault surface kinematic indicators on active normal faults of the Alpine Betic Cordilleras, Granada, southern Spain. *J. Struct. Geol.* 19, 159–170.
- Doglioni, C., Barba, S., Carminati, E., Riguzzi, F., 2011. Role of the brittle-ductile transition on the fault activation. *Phys. Earth Planet. Inter.* 184, 160–171.
- Doglioni, C., Barba, S., Carminati, E., Riguzzi, F., 2013. Fault on-off versus coseismic fluids reaction. *Geosci. Front.* 5 (6), 767–780. <https://doi.org/10.1016/j.gsf.2013.08.004>.
- Dor, O., Ben-Zion, Y., Rockwell, T.K., Brune, J., 2006. Pulverized rocks in the Mojave section of the San Andreas Fault Zone. *Earth Planet. Sci. Lett.* 245 (3–4), 642–654.
- Drake, H., Kooijman, E., Kielman-Schmitt, M., 2020. Using ⁸⁷Sr/⁸⁶Sr LA-MC-ICP-MS transects within modern and ancient calcite crystals to determine fluid flow events in deep granite fractures. *Geosciences* 10 (9), 345.
- Dromgoole, E.L., Walter, L.M., 1990. Iron and manganese incorporation into calcite: Effects of growth kinetics, temperature and solution chemistry. *Chem. Geol.* 81 (4), 311–336.
- Ellsworth, W.L., Lindh, A.G., Prescott, W.H., Herd, D.G., 2013. The 1906 San Francisco Earthquake and the Seismic Cycle. In: *Earthquake Prediction: An International Review*, 4, pp. 126–140.
- Endignoux, L., Wolf, S., Letouzey, J., 1990. Thermal and kinematic evolution of thrust basins: A 2D numerical model. In: *Petroleum and Tectonics in Mobile Belts*. Editions Technip, Paris, pp. 181–192.
- Faccenna, C., Mattel, M., Funicello, R., Jolivet, L., 1997. Styles of back-arc extension in the Central Mediterranean. *Terra Nova* 9 (3), 126–130.
- Faccenna, C., Becker, T.W., Lucente, F.P., Jolivet, L., Rossetti, F., 2001. History of subduction and back arc extension in the Central Mediterranean. *Geophys. J. Int.* 145 (3), 809–820.
- Fagereng, Å., Harris, C., 2014. Interplay between fluid flow and fault-fracture mesh generation within underthrust sediments: Geochemical evidence from the Chrystalls Beach complex, New Zealand. *Tectonophysics* 612–613, 147–157.
- Fagereng, Å., Remitti, F., Sibson, R.H., 2010. Shear veins observed within anisotropic fabric at high angles to the maximum compressive stress. *Nat. Geosci.* 3, 482–485.
- Fagereng, Å., Remitti, F., Sibson, R.H., 2011. Incrementally developed slickenfibers - Geological record of repeating low stress-drop seismic events? *Tectonophysics* 510, 381–386.
- Fellin, M.G., Jose, M.S., Faccenna, C., Willett, S.D., Cosentino, D., Lanari, R., Gourbet, L., Maden, C., 2022. Transition from slab roll-back to slab break-off in the central Apennines, Italy: Constraints from the stratigraphic and thermochronologic record. *Bull. Geol. Soc. Am.* 134, 1916–1930.
- Ferraro, F., Agosta, F., Ukar, E., Grieco, D.S., Cavalcante, F., Belviso, C., Prosser, G., 2019. Structural diagenesis of carbonate fault rocks exhumed from shallow crustal depths: An example from the central-southern Apennines, Italy. *Journal of Structural Geology* 122, 58–80.
- Fiebig, J., Daëron, M., Bernecker, M., Guo, W., Schneider, G., Boch, R., Bernasconi, S., Jautzy, J., Dietzel, M., 2021. Calibration of the dual clumped isotope thermometer for carbonates. *Geochim. Cosmochim. Acta* 312, 235–256.
- Fisher, D.M., Hooker, J.N., Smye, A.J., Chen, T.W., 2021. Insights from the geological record of deformation along the subduction interface at depths of seismogenesis. *Geosphere* 17, 1686–1703.
- Fitz-Diaz, E., Hudleston, P., Siebenaller, L., Kirschner, D., Camprubí, A., Tolson, G., Puig, T.P., 2011. Insights into fluid flow and water-rock interaction during deformation of carbonate sequences in the Mexican fold-thrust belt. *J. Struct. Geol.* 33, 1237–1253.
- Fitz-Diaz, E., Cottle, J.M., Vidal-Reyes, M.I., Van der Pluijm, B., 2019. In situ Th/Pb dating of monazite in fibrous veins: Direct dating of veins and deformation in the shallow upper crust of the Mexican Orogen. *J. Struct. Geol.* 124, 136–142.
- Fondriest, M., Smith, S.A.F., Di Toro, G., Zampieri, D., Mittempergher, S., 2012. Fault zone structure and seismic slip localization in dolostones, an example from the Southern Alps, Italy. *J. Struct. Geol.* 45, 52–67.
- Fondriest, M., Smith, S.A.F., Candela, T., Nielsen, S.B., Mair, K., Di Toro, G., 2013. Mirror-like faults and power dissipation during earthquakes. *Geology* 41, 1175–1178.
- Franchini, S., Agostini, S., Barberio, M.D., Barbieri, M., Billi, A., Boschetti, T., Pennisi, M., Petitta, M., 2021. HydroQuakes, central Apennines, Italy: Towards a hydrogeochemical monitoring network for seismic precursors and the hydro-seismo-sensitivity of boron. *J. Hydrol.* 598, 125754.
- Fu, B., Espinosa-Marzal, R.M., 2022. Velocity-weakening and-strengthening friction at single and multiasperity contacts with calcite single crystals. *Proc. Natl. Acad. Sci.* 119 (22), e2112505119.
- Garven, G., 1985. The role of regional fluid flow in the genesis of the pine point deposit, Western Canada Sedimentary Basin. *Econ. Geol.* 80 (2), 307–324.
- Gautheron, C., Moreira, M., Allègre, C., 2005. He, Ne and Ar composition of the European lithospheric mantle. *Chem. Geol.* 217 (1–2), 97–112.
- Gébelin, A., Mulch, A., Teyssier, C., Page Chamberlain, C., Heizler, M., 2012. Coupled basin-detachment systems as paleoaltimetry archives of the western north American Cordillera. *Earth Planet. Sci. Lett.* 335–336, 36–47.
- Ghisetti, F., Kirschner, D.L., Vezzani, L., Agosta, F., 2001. Stable isotope evidence for contrasting paleofluid circulation in thrust faults and normal faults of the central Apennines, Italy. *J. Geophys. Res. Solid Earth* 106, 8811–8825.
- Ghosh, P., Adkins, J., Affek, H., Balta, B., Guo, W., Schauble, E.A., Schrag, D., Eiler, J.M., 2006. ¹³C–¹⁸O bonds in carbonate minerals: a new kind of paleothermometer. *Geochim. Cosmochim. Acta* 70 (6), 1439–1456.
- Goodfellow, B.W., Viola, G., Bingen, B., Nuriel, P., Kylander-Clark, A.R., 2017. Palaeocene faulting in SE Sweden from U–Pb dating of slickenfibres calcite. *Terra Nova* 29 (5), 321–328.
- Gori, F., Barberio, M.D., 2022. Hydrogeochemical changes before and during the 2019 Benevento seismic swarm in Central-Southern Italy. *J. Hydrol.* 604, 127250.
- Graham, D.W., 2002. Noble gas isotope geochemistry of mid-ocean ridge and ocean island basalts: Characterization of mantle source reservoirs. *Rev. Mineral. Geochim.* 47 (1), 247–319.
- Gratier, J.P., Gamond, J.F., 1990. Transition between seismic and aseismic deformation in the upper crust. *Geol. Soc. Lond.* 461–473.
- Gratier, J.-P., Richard, J., Renard, F., Mittempergher, S., Doan, M.-L., Di Toro, G., Hadizadeh, J., Boullier, A.-M., 2011. Aseismic sliding of active faults by pressure

- solution creep: evidence from the San Andreas Fault Observatory at Depth. *Geology* 39, 1131–1134.
- Griffith, W.A., St. Julien, R.C., Ghaffari, H.O., Barber, T.J., 2018. A tensile origin for fault rock pulverization. *J. Geophys. Res. Solid Earth* 123 (8), 7055–7073.
- Guillong, M., Wotzlaw, J.F., Looser, N., Laurent, O., 2020. Evaluating the reliability of U–Pb laser ablation inductively coupled plasma mass spectrometry (LA-ICP-MS) carbonate geochronology: matrix issues and a potential calcite validation reference material. *Geochronology* 2 (1), 155–167.
- Hajati, T., Langenbruch, C., Shapiro, S.A., 2015. A statistical model for seismic hazard assessment of hydraulic-fracturing-induced seismicity. *Geophys. Res. Lett.* 42, 10601–10606.
- Hancock, P.L., Barka, A.A., 1987. Kinematic indicators on active normal faults in western Turkey. *J. Struct. Geol.* 9 (5–6), 573–584.
- Hanks, C.L., Parris, T.M., Wallace, W.K., 2006. Fracture paragenesis and microthermometry in Lisburne Group detachment folds: implications for the thermal and structural evolution of the northeastern Brooks Range, Alaska. *Am. Assoc. Pet. Geol. Bull.* 90 (1), 1–20.
- Hayes, J.M., Valley, J.W., Cole, D.R., 2001. Stable Isotope Geochemistry. *Reviews in Mineralogy and Geochemistry*. Mineralogical Society of America, Washington, DC, p. 43.
- Hemingway, J.D., Henkes, G.A., 2021. A disordered kinetic model for clumped isotope bond reordering in carbonates. *Earth Planet. Sci. Lett.* 566, 116962.
- Hilgers, C., Urai, J.L., 2002. Microstructural observations on natural syntectonic fibrous veins: implications for the growth process. *Tectonophysics* 257–274.
- Hilgers, C., Koehn, D., Bons, P.D., Urai, J.L., 2001. Development of crystal morphology during uniaxial growth in a progressively widening vein: II. Numerical simulations of the evolution of antitaxial fibrous veins. *J. Struct. Geol.* 23, 873–885.
- Hilgers, C., Dilg-Gruschinski, K., Urai, J.L., 2004. Microstructural evolution of syntaxial veins formed by advective flow. *Geology* 32, 261.
- Hoareau, G., Crognier, N., Lacroix, B., Aubourg, C., Roberts, N.M.W., Niemi, N., Branellec, M., Beaudoin, N., Suárez Ruiz, I., 2021. Combination of $\Delta 47$ and U–Pb dating in tectonic calcite veins unravel the last pulses related to the Pyrenean Shortening (Spain). *Earth Planet. Sci. Lett.* 553, 116636.
- Hoefs, J., 1997. *Stable Isotope Geochemistry*, 201. Springer International Publishing.
- Horton, T.W., Blum, J.D., Craw, D., Koons, P.O., Chamberlain, C.P., 2003. Oxygen, carbon, and strontium isotopic constraints on timing and sources of crustal fluids in an active orogen: South Island, New Zealand. *N. Z. J. Geol. Geophys.* 46 (3), 457–471.
- Incel, S., Hiliret, N., Labrousse, L., John, T., Deldicque, D., Ferrand, T., Wang, Y., Renner, J., Morales, L., Schubnel, A., 2017. Laboratory earthquakes triggered during eclogitization of lawsonite-bearing blueschist. *Earth Planet. Sci. Lett.* 459, 320–331.
- Invernizzi, C., Vityk, M., Cello, G., Bodnar, R., 1998. Fluid inclusions in high pressure/low temperature rocks from the Calabrian Arc (Southern Italy): the burial and exhumation history of the subduction-related Diamante-Terranova unit. *J. Metamorph. Geol.* 16, 247–258.
- Italiano, F., Martinelli, G., Nuccio, P.M., 2001. Anomalies of mantle-derived helium during the 1997–1998 seismic swarm of Umbria-Marche, Italy. *Geophys. Res. Lett.* 28 (5), 839–842.
- Jautzy, J.J., Savard, M.M., Dhillon, R.S., Bernasconi, S.M., Smirnov, A., 2020. Clumped isotope temperature calibration for calcite: Bridging theory and experimentation. *Geochim. Perspect. Lett.* 14, 36–41.
- John, C.M., Bowen, D., 2016. Community software for challenging isotope analysis: first applications of “Easotope” to clumped isotopes. *Rapid Commun. Mass Spectrom.* 30, 2285–2300.
- Karabacak, V., Sançar, T., Yildirim, G., Uysal, I.T., 2022. When did the North Anatolian fault reach southern Marmara, Turkey? *Geology* 50 (4), 432–436.
- Kele, S., Breitenbach, S.F., Capezuoli, E., Meckler, A.N., Ziegler, M., Millán, I.M., Kluge, T., Deak, J., Hanselmann, K., John, C.M., Yan, H., Liu, Z., Bernasconi, S.M., 2015. Temperature dependence of oxygen-and clumped isotope fractionation in carbonates: A study of travertines and tufas in the 6–95 °C temperature range. *Geochim. Cosmochim. Acta* 168, 172–192.
- Kim, S.-T., O’Neil, J.R., 1997. Equilibrium and nonequilibrium oxygen isotope effects in synthetic carbonates. *Geochim. Cosmochim. Acta* 61, 3461–3475.
- Kolb, J., Rogers, A., Meyer, F.M., Siemes, H., 2005. Dominant coaxial deformation of veins during the interseismic stage of the fault-valve cycle: Microfabrics of laminated quartz veins of the Hutti gold mine, India. *J. Struct. Geol.* 27, 2043–2057.
- Kylander-Clark, A.R., 2020. Expanding the limits of laser-ablation U–Pb calcite geochronology. *Geochronology* 2 (2), 343–354.
- Labeur, A., Beaudoin, N.E., Lacombe, O., Emmanuel, L., Petracchini, L., Daëron, M., Klimowicz, S., Callot, J.P., 2021. Burial-deformation history of folded rocks unraveled by fracture analysis, stylolite paleoepiezometry and vein cement geochemistry: a case study in the Cingoli Anticline (Umbria-Marche, Northern Apennines). *Geosciences* 11 (3), 135.
- Lacombe, O., Beaudoin, N.E., Hoareau, G., Labeur, A., Pecheyran, C., Callot, J.P., 2021. Dating folding beyond folding, from layer-parallel shortening to fold tightening, using mesostructures: lessons from the Apennines, Pyrenees, and Rocky Mountains. *Solid Earth* 12 (10), 2145–2157.
- Lacroix, B., Travé, A., Buatier, M., Labaume, P., Vennemann, T., Dubois, M., 2014. Syntectonic fluid-flow along thrust faults: example of the South-Pyrenean fold-and-thrust belt. *Mar. Pet. Geol.* 49, 84–98.
- Lacroix, B., Baumgartner, L.P., Bouvier, A.S., Kempton, P.D., Vennemann, T., 2018a. Multi fluid-flow record during episodic mode I opening: A microstructural and SIMS study (Cotiella Thrust Fault, Pyrenees). *Earth Planet. Sci. Lett.* 503, 37–46.
- Lacroix, B., Baumgartner, L.P., Bouvier, A.S., Kempton, P.D., Vennemann, T., 2018b. Multi fluid-flow record during episodic mode I opening: A microstructural and SIMS study (Cotiella Thrust Fault, Pyrenees). *Earth Planet. Sci. Lett.* 503, 37–46.
- Li, B., Shi, Z., Wang, G., Liu, C., 2019. Earthquake-related hydrochemical changes in thermal springs in the Xianshuihe Fault zone, Western China. *J. Hydrol.* 579, 124175.
- Li, C., Zhou, X., Yan, Y., Ouyang, S., Liu, F., 2021. Hydrogeochemical Characteristics of Hot Springs and their Short-Term Seismic Precursor Anomalies along the Xiaojiang Fault Zone, Southeast Tibet Plateau. *Water* 13 (19), 2638.
- Lin, A., 2011. Seismic slip recorded by fluidized ultracataclastic veins formed in a coseismic shear zone during the 2008 MW 7.9 Wenchuan earthquake. *Geology* 39, 547–550.
- Lindh, A.G., 1990. The seismic cycle pursued. *Nature* 348, 580–581.
- Looser, N., Madritsch, H., Guillong, M., Laurent, O., Wohlwend, S., Bernasconi, S.M., 2021. Absolute age and temperature constraints on deformation along the basal décollement of the jura fold-and-thrust belt from carbonate U–Pb dating and clumped isotopes. *Tectonics* 40.
- Looser, N., Petschnig, P., Hemingway, J.D., Fernandez, A., Grafalua, L.M., Perez-Huerta, A., Vickers, M.L., Price, G.D., Schmidt, M.W., Bernasconi, S.M., 2023. Thermally-induced clumped isotope resetting in belemnite and optical calcites: Towards material-specific kinetics. *Geochim. Cosmochim. Acta* 350, 1–15.
- Lucca, A., Storti, F., Balsamo, F., Clemenzi, L., Fondriest, M., Burgess, R., Di Toro, G., 2019. From Submarine to Subaerial Out-of-Sequence Thrusting and Gravity-Driven Extensional Faulting: Gran Sasso Massif, Central Apennines, Italy. *Tectonics* 38, 4155–4184.
- Lucente, F., De Gori, P., Margheriti, L., Piccinini, D., Di Bona, M., Chiarabba, C., Piana, Agostinetti, N., 2010. Temporal variation of seismic velocity and anisotropy before the 2009 M W 6.3 L’Aquila earthquake, Italy. *Geology* 38, 1015–1018.
- Machel, H.G., 1985. Cathodoluminescence in calcite and dolomite and its chemical interpretation. *Geosci. Can.* 12, 139–147.
- Machel, H.G., 1997. Recrystallization versus neomorphism, and the concept of ‘significant recrystallization’ in dolomite research. *Sediment. Geol.* 113, 161–168.
- Machel, H.G., 2000. Application of cathodoluminescence to carbonate diagenesis. *Cathodolumin. Geosci.* 11, 271–301.
- Machel, H.G., Cavell, P.A., 1999. Low-flux, tectonically-induced squeegee fluid flow (“hot flash”) into the Rocky Mountain Foreland Basin. *Bull. Can. Petrol. Geol.* 47 (4), 510–533.
- Maiorani, A., Funicello, R., Mattei, M., Turi, B., 1992. Stable isotope geochemistry and structural elements of the Sabina region (Central Apennines, Italy). *Terra Nova* 4 (4), 484–488.
- Malinverno, A., Ryan, W.B.F., 1986. Extension in the Tyrrhenian Sea and shortening in the Apennines as result of arc migration driven by sinking of the lithosphere. *Tectonics* 5, 227–245.
- Mangenot, X., Bonifacie, M., Gasparrini, M., Götz, A., Chaduteau, C., Ader, M., Rouchon, V., 2017. Coupling $\Delta 47$ and fluid inclusion thermometry on carbonate cements to precisely reconstruct the temperature, salinity and $\delta 180$ of paleo-groundwater in sedimentary basins. *Chem. Geol.* 472, 44–57.
- Mangenot, X., Deçoninck, J.F., Bonifacie, M., Rouchon, V., Collin, P.Y., Quesne, D., Gasparrini, M., Sizun, J.P., 2019. Thermal and exhumation histories of the northern subalpine chains (Bauges and Bornes—France): evidence from forward thermal modeling coupling clay mineral diagenesis, organic maturity and carbonate clumped isotope ($\Delta 47$) data. *Basin Res.* 31 (2), 361–379.
- Marcaccio, M., Martinelli, G., 2012. Effects on the groundwater levels of the May–June 2012 Emilia seismic sequence. *Ann. Geophys.* 55 (4).
- Marchesini, B., Carminati, E., Aldega, L., Mirabella, F., Petrelli, M., Caracausi, A., Barchi, M.R., 2022. Chemical interaction driven by deep fluids in the damage zone of a seismogenic carbonate fault. *J. Struct. Geol.* 161, 104668.
- Mareschal, J.C., 1994. Thermal regime and post-orogenic extension in collision belts. *Tectonophysics* 238 (1–4), 471–484.
- Martinelli, G., Facca, G., Genzano, N., Gherardi, F., Lisi, M., Pierotti, L., Tramutoli, V., 2020. Earthquake-related signals in central Italy detected by hydrogeochemical and satellite techniques. *Front. Earth Sci. (Lausanne)* 8.
- Meckler, A.N., Ziegler, M., Millán, M.I., Breitenbach, S.F.M., Bernasconi, S.M., 2014. Long-term performance of the Kiel carbonate device with a new correction scheme for clumped isotope measurements. *Rapid Commun. Mass Spectrom.* 28, 1705–1715.
- Mastorillo, L., Saroli, M., Viaroli, S., Banzato, F., Valigi, D., Pettita, M., 2020. Sustained post-seismic effects on groundwater flow in fractured carbonate aquifers in Central Italy. *Hydrol. Process.* 34 (5), 1167–1181.
- Meckler, A.N., Affolter, S., Dublyansky, Y.V., Krüger, Y., Vogel, N., Bernasconi, S.M., Frenz, M., Kipfer, R., Leuenberger, M., Spoti, C., Carolin, S., Cobb, K.M., Moerman, J., Adkins, J.F., Fleitmann, D., 2015. Glacial–interglacial temperature change in the tropical West Pacific: A comparison of stalagmite-based paleothermometers. *Quat. Sci. Rev.* 127, 90–116.
- Meneghini, F., Moore, J.C., 2007. Deformation and hydrofracture in a subduction thrust at seismogenic depths: the Rodeo Cove thrust zone, Marin Headlands, California. *Geol. Soc. Am. Bull.* 119, 174–183.
- Menzies, C.D., Teagle, D.A.H., Craw, D., Cox, S.C., Boyce, A.J., Barrie, C.D., Roberts, S., 2014. IncurSION of meteoric waters into the ductile regime in an active orogen. *Earth Planet. Sci. Lett.* 399, 1–13.
- Micklethwaite, S., Cox, S.F., 2004. Fault-segment rupture, aftershock-zone fluid flow, and mineralization. *Geology* 32 (9), 813–816.
- Miller, S.A., Collettini, C., Chiaraluce, L., Cocco, M., Barchi, M., Kaus, B.J.P., 2004. Aftershocks driven by a high-pressure CO₂ source at depth. *Nature* 427, 724–727.
- Milli, S., Moscatelli, M., Stanzione, O., Falcini, F., 2007. Sedimentology and physical stratigraphy of the Messinian turbidite deposits of the Laga Basin (central Apennines, Italy). *Ital. J. Geosci.* 126, 255–281.
- Misra, K.C., 2012. *Introduction to Geochemistry: Principles and Applications*. John Wiley & Sons.

- Mort, K., Woodcock, N.H., 2008. Quantifying fault breccia geometry: Dent Fault, NW England. *J. Struct. Geol.* 30, 701–709.
- Müller, W., 2003. Strengthening the link between geochronology, textures and petrology. *Earth Planet. Sci. Lett.* 206 (3–4), 237–251.
- Müller, I.A., Fernandez, A., Radke, J., Van Dijk, J., Bowen, D., Schwieters, J., Bernasconi, S.M., 2017. Carbonate clumped isotope analyses with the long-integration dual-inlet (LIDI) workflow: Scratching at the lower sample weight boundaries. *Rapid Commun. Mass Spectrom.* 31 (12), 1057–1066.
- Müller, I.A., Rodriguez-Blanco, J.D., Storck, J.C., do Nascimento, G.S., Bontognali, T.R., Vasconcelos, C., Benning, L.G., Bernasconi, S.M., 2019. Calibration of the oxygen and clumped isotope thermometers for (proto-) dolomite based on synthetic and natural carbonates. *Chem. Geol.* 525, 1–17.
- Négrel, P., Guerrot, C., Cocherie, A., Azaroual, M., Brach, M., Fouillac, C., 2000. Rare earth elements, neodymium and strontium isotopic systematics in mineral waters: evidence from the Massif Central, France. *Appl. Geochem.* 15, 1345–1367.
- Nelson, C.S., Smith, A.M., 1996. Stable oxygen and carbon isotope compositional fields for skeletal and diagenetic components in New Zealand Cenozoic nontropical carbonate sediments and limestones: a synthesis and review. *N. Z. J. Geol. Geophys.* 39 (1), 93–107.
- Nuriel, P., Rosenbaum, G., Uysal, T.I., Zhao, J., Golding, S.D., Weinberger, R., Karabacak, V., Avni, Y., 2011. Formation of fault-related calcite precipitates and their implications for dating fault activity in the east Anatolian and dead sea fault zones. *Geol. Soc. Spec. Publ.* 359, 229–248.
- Nuriel, P., Rosenbaum, G., Zhao, J.X., Feng, Y., Golding, S.D., Villemant, B., Weinberger, R., 2012. U-Th dating of striated fault planes. *Geology* 40 (7), 647–650.
- O'Neil, J.R., Clayton, R.N., Mayeda, T.K., 1969. Oxygen isotope fractionation in divalent metal carbonates. *J. Chem. Phys.* 51 (12), 5547–5558.
- Özyurt, M., Ziya Kirmaci, M., Al-Aasm, I., Hollis, C., Taslı, K., Kandemir, R., 2020. REE characteristics of lower cretaceous limestone succession in gümişane, NE Turkey: Implications for ocean paleoredox conditions and diagenetic alteration. *Minerals* 10, 1–25.
- Palmer, M.R., Edmond, J.M., 1989. The strontium isotope budget of the modern ocean. *Earth Planet. Sci. Lett.* 92 (1), 11–26.
- Parotto, M., Praturlon, A., 1975. Geological summary of Central Apennines. *Quaderni della Ricerca Scientifica* 90, 257–311.
- Passchier, C.W., Trouw, R.A.J., 2005. *Microtectonics*. Springer Berlin Heidelberg, Berlin, Heidelberg.
- Passsey, B.H., Henkes, G.A., 2012. Carbonate clumped isotope bond reordering and geospeedometry. *Earth Planet. Sci. Lett.* 351–352, 223–236.
- Patacca, E., Sartori, R., Scandone, P., 1990. Tyrrhenian basin and Apenninic arcs: kinematic relations since late Tortonian times. *Mem. Soc. Geol. Ital.* 45, 425–451.
- Payne, R.M., Duan, B., 2017. Insights into pulverized rock formation from dynamic rupture models of earthquakes. *Geophys. J. Int.* 208 (2), 715–723.
- Peacock, D.C.P., Parfitt, E.A., 2002. Active relay ramps and normal fault propagation on Kilauea Volcano, Hawaii. *J. Struct. Geol.* 24 (4), 729–742.
- Petitta, M., Mastroiello, L., Preziosi, E., Banzato, F., Barberio, M.D., Billi, A., Cambi, C., De Luca, G., di Carlo, G., Di Curzio, D., Di Salvo, C., Nanni, T., Palpacelli, S., Rusi, S., Saroli, M., Tallini, M., Tazioli, A., Valigi, D., Vivalda, P., Doglioni, C., 2018. Water-table and discharge changes associated with the 2016–2017 seismic sequence in Central Italy: hydrogeological data and a conceptual model for fractured carbonate aquifers. *Hydrogeol. J.* 26, 1009–1026.
- Pili, E., Kennedy, B.M., Conrad, M.E., Gratier, J.P., 2011. Isotopic evidence for the infiltration of mantle and metamorphic CO₂–H₂O fluids from below in faulted rocks from the San Andreas Fault system. *Chem. Geol.* 281 (3–4), 242–252.
- Power, W.L., Tullis, T.E., 1989. The relationship between slickenside surfaces in fine-grained quartz and the seismic cycle. *J. Struct. Geol.* 11 (7), 879–893.
- Rasbury, E.T., Cole, J.M., 2009. Directly dating geologic events: U-Pb dating of carbonates. *Rev. Geophys.* 47 (3).
- Rielli, A., Boschi, C., Dini, A., 2022. Tectonically driven carbonation of serpentinite by mantle CO₂: genesis of the Castiglioncello magnesite deposit in the Ligurian ophiolite of Central Tuscany (Italy). *Ore Geol. Rev.* 149, 105022.
- Ring, U., Uysal, I.T., Yüce, G., Ünal-İmer, E., Italiano, F., İmer, A., Zhao, J., Xin, J., 2016. Recent mantle degassing recorded by carbonic spring deposits along sinistral strike-slip faults, south-Central Australia. *Earth Planet. Sci. Lett.* 454, 304–318.
- Roberts, N.M., Holdsworth, R.E., 2022. Timescales of faulting through calcite geochronology: A review. *J. Struct. Geol.* 104578.
- Roberts, N.M.W., Žák, J., Vacek, F., Sláma, J., 2021. No more blind dates with calcite: Fluid-flow vs. fault-slip along the Očkov thrust, Prague Basin. *Geosci. Front.* 12.
- Roedder, E., 1984. *Fluid Inclusions*, 12. Mineralogical Society of America, p. 644.
- Roedder, E., Bodnar, R.J., 1980. Geologic determinations from fluid inclusion studies. *Annu. Rev. Earth Planet. Sci.* 8 (1), 263–301.
- Rollinson, H.R., Pease, V., 1993. Using stable isotope data. In: *Using Geochemical Data: Evaluation, Presentation, Interpretation*. Geochemistry Series. Longman Scientific and Technical co-published with Wiley and Sons, New York, pp. 266–315.
- Rossi, M., Rolland, Y., 2014. Stable isotope and Ar/Ar evidence of prolonged multiscale fluid flow during exhumation of orogenic crust: example from the mont blanc and Aar Massifs (NW Alps). *Tectonics* 33, 1681–1709.
- Roure, F., Swennen, R., Schneider, F., Faure, J.L., Ferket, H., Guilhaumou, N., Osadetz, K., Robion, P., Vandeginste, V., 2005. Incidence and Importance of Tectonics and Natural Fluid Migration on Reservoir Evolution in Foreland Fold-and-Thrust Belts. *Oil Gas Sci. Technol.* 60 (1), 67–106.
- Rowe, C.D., Griffith, W.A., 2015. Do faults preserve a record of seismic slip: A second opinion. *J. Struct. Geol.* 78, 1–26.
- Rowe, C.D., Meneghini, F., Moore, J., 2011. Textural record of the seismic cycle: Strain-rate variation in an ancient subduction thrust. *Geol. Soc. Lond. Spec. Publ.* 359, 77–95.
- Santantonio, M., 1993. Facies associations and evolution of pelagic carbonate platform/basin systems: examples from the Italian Jurassic. *Sedimentology* 40, 1039–1067.
- Savage, M.K., 2010. The role of fluids in earthquake generation in the 2009 M_w 6.3 L'Aquila, Italy, earthquake and its foreshocks: figure 1. *Geology* 38, 1055–1056.
- Schauble, E.A., Ghosh, P., Eiler, J.M., 2006. Preferential formation of 13C–18O bonds in carbonate minerals, estimated using first-principles lattice dynamics. *Geochim. Cosmochim. Acta* 70 (10), 2510–2529.
- Schmid, T.W., Bernasconi, S.M., 2010. An automated method for 'clumped-isotope' measurements on small carbonate samples. *Rapid Commun. Mass Spectrom.* 24 (14), 1955–1963.
- Scholz, C.H., 1991. Earthquakes and faulting: self-organized critical phenomena with a characteristic dimension. In: *Spontaneous Formation of Space-Time Structures and Criticality*. Springer Netherlands, Dordrecht, pp. 41–56.
- Scholz, C.H., Sykes, L.R., Aggarwal, Y.P., 1973. Earthquake Prediction: A Physical Basis: Rock dilatancy and water diffusion may explain a large class of phenomena precursory to earthquakes. *Science* 181 (4102), 803–810.
- Slater, J.G., Christie, P.A.F., 1980. Continental stretching: an explanation of post-Mid cretaceous subsidence on the Central North Sea Basin. *J. Geophys. Res.* 85, 3711–3739.
- Shapiro, S.A., 2015. *Fluid-Induced Seismicity*. Cambridge University Press.
- Sharp, Z., 2017. *Principles of Stable Isotope Geochemistry*. Prentice Hall.
- Sibson, R.H., 1981. Fluid flow accompanying faulting: Field evidence and models. In: *Earthquake Prediction: An International Review*, 4, pp. 593–603.
- Sibson, R.H., 1986. Earthquakes and rock deformation in crustal fault zones. *Annu. Rev. Earth Planet. Sci.* 14 (1), 149–175.
- Sibson, R.H., 1994. Crustal stress, faulting and fluid flow. *Geol. Soc. Lond. Spec. Publ.* 78, 69–84.
- Sibson, R.H., 2000. Fluid involvement in normal faulting. *J. Geodyn.* 29, 469–499.
- Sibson, R.H., 2004. Frictional Mechanics of Seismogenic Thrust Systems in the Upper Continental Crust—Implications for Fluid Overpressures and Redistribution, 82. American Association of Petroleum Geology, pp. 1–17.
- Sibson, R.H., Scott, J., 1998. Stress/fault controls on the containment and release of overpressured fluids: examples from gold-quartz vein systems in Juneau, Alaska; Victoria, Australia and Otago, New Zealand. *Ore Geol. Rev.* 13, 293–306.
- Skelton, A., Andrén, M., Kristmannsdóttir, H., Stockmann, G., Mörth, C.M., Sveinbjörnsdóttir, Á., Jónsson, S., Sturkell, E., Guðrúnardóttir, H.R., Hjartarson, H., Siegmund, H., Kockum, I., 2014. Changes in groundwater chemistry before two consecutive earthquakes in Iceland. *Nat. Geosci.* 7, 752–756.
- Skelton, A., Liljedahl-Claesson, L., Wästeby, N., Andrén, M., Stockmann, G., Sturkell, E., Mörth, C.-M., Stefansson, A., Tollefsen, E., Siegmund, H., Keller, H., Kjartansdóttir, E., Hjartarson, H., Kockum, I., 2019. Hydrochemical changes before and after earthquakes based on long-term measurements of multiple parameters at two sites in northern Iceland—a review. *J. Geophys. Res. Solid Earth* 124 (3), 2702–2720.
- Smeraglia, L., Berra, F., Billi, A., Boschi, C., Carminati, E., Doglioni, C., 2016. Origin and role of fluids involved in the seismic cycle of extensional faults in carbonate rocks. *Earth Planet. Sci. Lett.* 450, 292–305.
- Smeraglia, L., Bernasconi, S.M., Berra, F., Billi, A., Boschi, C., Caracausi, A., Carminati, E., Castorina, F., Doglioni, C., Italiano, F., Rizzo, A.L., Uysal, I.T., Zhao, J., 2018. Crustal-scale fluid circulation and co-seismic shallow comb-veining along the longest normal fault of the central Apennines, Italy. *Earth Planet. Sci. Lett.* 498, 152–168.
- Smeraglia, L., Aldega, L., Billi, A., Carminati, E., di Fiore, F., Gerdes, A., Albert, R., Rossetti, F., Vignaroli, G., 2019. Development of an Intrawedge Tectonic Mélange by Out-of-Sequence Thrusting, Buttressing, and Intraformational Rheological Contrast, Mt. Massico Ridge, Apennines, Italy. *Tectonics* 38, 1223–1249.
- Smeraglia, L., Aldega, L., Bernasconi, S.M., Billi, A., Boschi, C., Caracausi, A., Carminati, E., Franchini, S., Rizzo, A.L., Rossetti, F., Vignaroli, G., 2020a. The role of trapped fluids during the development and deformation of a carbonate/shale intrawedge tectonic mélange (Mt. Massico, Southern Apennines, Italy). *J. Struct. Geol.* 138.
- Smeraglia, L., Fabbri, O., Choulet, F., Buatier, M., Boulvais, P., Bernasconi, S.M., Castorina, F., 2020b. Syntectonic fluid flow and deformation mechanisms within the frontal thrust of a foreland fold-and-thrust belt: Example from the Internal Jura, Eastern France. *Tectonophysics* 778.
- Smith, Z.D., Griffith, W.A., 2022. Evolution of pulverized fault zone rocks by dynamic tensile loading during successive earthquakes. *Geophys. Res. Lett.* 49 (19) e2022GL099971.
- Smith, Steven A.F., Billi, A., Di Toro, G., Spiess, R., 2011. Principal Slip zones in Limestone: Microstructural Characterization and Implications for the Seismic Cycle (Tre Monti Fault, Central Apennines, Italy). *Pure Appl. Geophys.* 168, 2365–2393.
- Snell, T., De Paola, N., van Hunen, J., Nielsen, S., Collettini, C., 2020. Modelling fluid flow in complex natural fault zones: Implications for natural and human-induced earthquake nucleation. *Earth Planet. Sci. Lett.* 530, 115869.
- Sommer, S.E., 1972. Cathodoluminescence of carbonates, 1. Characterization of cathodoluminescence from carbonate solid solutions. *Chem. Geol.* 9, 257–273.
- Stewart, I.S., Hancock, P.L., 1990. Brecciation and fracturing within neotectonic normal fault zones in the Aegean region. *Geol. Soc. Lond. Spec. Publ.* 54, 105–110.
- Sturrock, C.P., Catlos, E.J., Miller, N.R., Akgun, A., Fall, A., Gabitov, R.I., Yilmaz, I.O., Larson, T., Black, K.N., 2017. Fluids along the North Anatolian Fault, Niksar basin, north Central Turkey: Insight from stable isotopic and geochemical analysis of calcite veins. *J. Struct. Geol.* 101, 58–79.
- Swanson, E.M., Wernicke, B.P., Eiler, J.M., Losh, S., 2012. Temperatures and fluids on faults based on carbonate clumped-isotope thermometry. *Am. J. Sci.* 312, 1–21.
- Sweeney, J.J., Burnham, A.K., 1990. Evaluation of a simple model of vitrinite reflectance based on chemical kinetics (1). *Am. Assoc. Pet. Geol. Bull.* 74 (10), 1559–1570.

- Tamburello, G., Pondrelli, S., Chiodini, G., Rouwet, D., 2018. Global-scale control of extensional tectonics on CO₂ earth degassing. *Nat. Commun.* 9 (1), 4608.
- Tamburello, G., Chiodini, G., Ciotoli, G., Procesi, M., Rouwet, D., Sandri, L., Carbonara, N., Masciantonio, C., 2022. Global thermal spring distribution and relationship to endogenous and exogenous factors. *Nat. Commun.* 13 (1), 6378.
- Tarling, M.S., Smith, S.A., Viti, C., Scott, J.M., 2018. Dynamic earthquake rupture preserved in a creeping serpentinite shear zone. *Nat. Commun.* 9 (1), 3552.
- Tavani, S., Smeraglia, L., Fabbri, S., Aldega, L., Sabbatino, M., Cardello, G.L., Maresca, A., Schirripa Spagnolo, G., Kylander-Clark, A., Billi, A., Bernasconi, S.M., Carminati, E., 2023. Timing thrusting mode, and negative inversion along the Circeo thrust, Apennines, Italy: how the accretion-to-extension transition operated during slab rollback. *Tectonics*, 42(6), e2022TC007679.
- Tesei, T., Collettini, C., Viti, C., Barchi, M.R., 2013. Fault architecture and deformation mechanisms in exhumed analogues of seismogenic carbonate-bearing thrusts. *J. Struct. Geol.* 55, 167–181.
- Tesei, T., Collettini, C., Barchi, M.R., Carpenter, B.M., Di Stefano, G., 2014. Heterogeneous strength and fault zone complexity of carbonate-bearing thrusts with possible implications for seismicity. *Earth Planet. Sci. Lett.* 408, 307–318.
- Travé, A., Labaume, P., Vergés, J., 2007. Fluid systems in foreland fold-and-thrust belts: an overview from the Southern Pyrenees. In: *Thrust Belts and Foreland Basins: From Fold Kinematics to Hydrocarbon Systems*, pp. 93–115.
- Turrini, C., Angeloni, P., Lacombe, O., Ponton, M., Roure, F., 2015. Three-dimensional seismo-tectonics in the Po Valley basin, Northern Italy. *Tectonophysics* 661, 156–179.
- Ünal-Imer, E., Uysal, I.T., Zhao, J.X., Işık, V., Shulmeister, J., Imer, A., Feng, Y.X., 2016. CO₂ outburst events in relation to seismicity: Constraints from microscale geochronology, geochemistry of late Quaternary vein carbonates, SW Turkey. *Geochim. Cosmochim. Acta* 187, 21–40.
- Uysal, I.T., Feng, Y., Zhao, J., Altunel, E., Weatherley, D., Karabacak, V., Cengiz, O., Golding, S.D., Lawrence, M.G., Collerson, K.D., 2007. U-series dating and geochemical tracing of late Quaternary travertine in co-seismic fissures. *Earth Planet. Sci. Lett.* 257, 450–462.
- Uysal, I.T., Feng, Y., Zhao, J., Isik, V., Nuriel, P., Golding, S.D., 2009. Hydrothermal CO₂ degassing in seismically active zones during the late Quaternary. *Chem. Geol.* 265, 442–454.
- Uysal, I.T., Feng, Y., Zhao, J., Xin, Bolhar, R., Işık, V., Baubly, K.A., Yago, A., Golding, S.D., 2011. Seismic cycles recorded in late Quaternary calcite veins: Geochronological, geochemical and microstructural evidence. *Earth Planet. Sci. Lett.* 303, 84–96.
- Valley, J.W., Lackey, J.S., Cavosie, A.J., Clechenko, C.C., Spicuzza, M.J., Basei, M.A.S., Bindeman, I.N., Ferreira, V.P., Sial, A.N., King, E.M., Peck, W.H., Sinha, A.K., Wei, C.S., 2005. 4.4 billion years of crustal maturation: oxygen isotope ratios of magmatic zircon. *Contrib. Mineral. Petrol.* 150, 561–580.
- Vannucchi, P., 2019. Scaly fabric and slip within fault zones. *Geosphere* 15, 342–356.
- Vignaroli, Gianluca, Mancini, M., Brilli, M., Bucci, F., Cardinali, M., Giustini, F., Voltaggio, M., Yu, T.L., Shen, C.C., 2020. Spatial-Temporal Evolution of Extensional Faulting and Fluid Circulation in the Amatrice Basin (Central Apennines, Italy) during the Pleistocene. *Front. Earth Sci.* 8, 130.
- Vignaroli, G., Rossetti, F., Petracchini, L., Argante, V., Bernasconi, S.M., Brilli, M., Giustini, F., Yu, T.L., Shen, C.C., Soligo, M., 2022. Middle Pleistocene fluid infiltration with 10–15 ka recurrence within the seismic cycle of the active Monte Morrone Fault System (central Apennines, Italy). *Tectonophysics* 827.
- Vilasi, N., Malandain, J., Barrier, L., Callot, J.-P., Amrouch, K., Guilhaumou, N., Lacombe, O., Muska, K., Roure, F., Swennen, R., 2009. From outcrop and petrographic studies to basin-scale fluid flow modelling: the use of the Albanian natural laboratory for carbonate reservoir characterisation. *Tectonophysics* 474, 367–392.
- Wang, C.Y., Manga, M., 2021. *Water and Earthquakes*. Springer Nature, p. 387.
- Wang, X.L., Shu, L.S., Xing, G.F., Zhou, J.C., Tang, M., Shu, X.J., Qi, L., Hu, Y.H., 2012. Post-orogenic extension in the eastern part of the Jiangnan orogen: evidence from ca 800–760 Ma volcanic rocks. *Precambrian Res.* 222, 404–423.
- Wang, Y., Chen, J., Li, S., Wang, S., Shi, D., Shen, W., 2022. Coseismic fluid–rock interactions in the Yingxiu–Beichuan surface rupture zone of the Mw 7.9 Wenchuan earthquake and their implications for the structural diagenesis of fault rocks. *J. Struct. Geol.* 159.
- Washburn, A.M., Sylvester, P.J., Snell, K.E., 2023. A record of overpressure and Sevier tectonics within beef calcite of the Heath Formation, Central Montana Trough. *Geochemistry* 126073.
- Webb, G.E., Kamber, B.S., 2000. Rare earth elements in Holocene reefal microbialites: A new shallow seawater proxy. *Geochim. Cosmochim. Acta* 64 (9), 1557–1565.
- Wechsler, N., Allen, E.E., Rockwell, T.K., Girty, G., Chester, J.S., Ben-Zion, Y., 2011. Characterization of pulverized granitoids in a shallow core along the San Andreas Fault, Little Rock, CA. *Geophys. J. Int.* 186 (2), 401–417.
- Woodcock, N.H., Mort, K., 2008. Classification of fault breccias and related fault rocks. *Geol. Mag.* 145, 435–440.
- Woodcock, N.H., Dickson, J.A.D., Tarasewicz, J.P.T., 2007. Transient permeability and reseat hardening in fault zones: evidence from dilation breccia textures. *Geol. Soc. Lond. Spec. Publ.* 270, 43–53.
- Xu, S., Ben-Zion, Y., 2017. Theoretical constraints on dynamic pulverization of fault zone rocks. *Geophys. J. Int.* 209 (1), 282–296.
- Yan, Y., Zhou, X., Liao, L., Tian, J., Li, Y., Shi, Z., Liu, F., Ouyang, S., 2022. Hydrogeochemical characteristic of geothermal water and precursory anomalies along the Xianshuihe Fault Zone, Southwestern China. *Water* 14 (4), 550.
- Yildirm, G., Mutlu, H., Karabacak, V., Uysal, I.T., Dirik, K., Temel, A., Yuce, G., Zhao, J.X., 2020. Temporal changes in geochemical-isotopic systematics of the late Pleistocene Akkaya travertines (Turkey)—Implications for fluid flow circulation and seismicity. *Geochemistry* 80 (4), 125630.
- Yuan, F., Prakash, V., Tullis, T., 2011. Origin of pulverized rocks during earthquake fault rupture. *J. Geophys. Res. Solid Earth* 116 (B6).
- Zeboudj, A., Bah, B., Lacombe, O., Beaudoin, N.E., Gout, C., Godeau, N., Girard, J.P., Deschamps, P., 2023. Depicting past stress history at passive margins: A combination of calcite twinning and stylolite roughness paleopiezometry in supra-salt Sendji deep carbonates, lower Congo Basin, West Africa. *Mar. Pet. Geol.* 152, 106219.
- Zhao, Y., Liu, Z., Li, Y., Hu, L., Chen, Z., Sun, F., Lu, C., 2021. A case study of 10 years groundwater radon monitoring along the eastern margin of the Tibetan Plateau and in its adjacent regions: Implications for earthquake surveillance. *Appl. Geochem.* 131, 105014.
- Zhu, J.B., Kang, J.Q., Elsworth, D., Xie, H.P., Ju, Y., Zhao, J., 2021. Controlling Induced Earthquake Magnitude by Cycled Fluid Injection. *Geophys. Res. Lett.* 48.
- Zwiessler, R., Kenkmann, T., Poelchau, M.H., Nau, S., Hess, S., 2017. On the use of a split Hopkinson pressure bar in structural geology: High strain rate deformation of Seiberger sandstone and Carrara marble under uniaxial compression. *J. Struct. Geol.* 97, 225–236.